Epigenetic targeting of metabolic and lineage abnormality in cancer

Dimitrios Karagiannis

Submitted in partial fulfillment of the
requirements for the degree of
Doctor of Philosophy
under the Executive Committee
of the Graduate School of Arts and Sciences

COLUMBIA UNIVERSITY

2023

Abstract

Epigenetic targeting of metabolic and lineage abnormality in cancer

Dimitrios Karagiannis

Chromatin regulation is a major aspect of cancer development, progression, and treatment. Several small molecule inhibitors of chromatin regulators are currently used for treatment of certain hematological malignancies. However, there is still opportunity for many more patients to benefit from therapeutic approaches that target chromatin regulation, especially in the context of solid tumors. A critical unmet need is the identification of robust biomarkers that can guide the application of epigenetic inhibitors in a precise and personalized manner. In my dissertation, I aim to address this important knowledge gap by studying how perturbation of chromatin can target metabolic and lineage abnormalities in solid tumors for therapeutic benefit. To do this, I have focused on genetic and pharmacological perturbations of chromatin pathways in two cancer models: (1) lung adenocarcinoma (LUAD) with NRF2 activation and (2) neuroendocrine esophageal carcinoma (NEC).

In the study on NRF2-active LUAD, we found that histone deacetylase (HDAC) inhibitors can be repurposed to reprogram the epigenomic and metabolic landscape, which leads to specific and potent anti-tumor effects in the context of NRF2 activation. Specifically, we employed a chromatin-focused genetic screen to identify dependencies on chromatin regulators. The screen revealed an NRF2-specific dependency on class I histone deacetylases. Experiments in mouse and human LUAD cell lines *in vitro* and *in vivo* indicated an NRF2-specific sensitivity to the class I HDAC inhibitor Romidepsin. Mechanistically, profiling of histone acetylation and

gene expression upon Romidepsin treatment revealed a relative loss of histone H4 acetylation at promoters which was associated with reduced gene expression. Many downregulated genes were more essential for the survival of NRF2 hyperactive cancer cells, including genes involved in glutamine and serine metabolism, c-Myc and several of its targets involved in purine and pyrimidine synthesis. These transcriptional changes had corresponding effects on altering the metabolic pathways that NRF2-active cells selectively require for survival.

In the study on neuroendocrine esophageal carcinoma (NEC), we identified a crucial role for epigenetic regulation of lineage fate through transcriptional control of the key epidermal transcription factor p63. This project originated from data from my collaborators that indicates a role for p63 in the suppression of basal-to-neuroendocrine identity transition in the developing esophagus. Consistently, I found that p63 is silenced in NEC through a non-genetic mechanism. Reintroducing p63 isoforms in a human NEC cell line showed that ΔNp63α was sufficient to restore squamous marker expression. An epigenetic drug screen assessing p63 gene expression and subsequent validation experiments revealed that inhibition of EZH2, a histone methyltransferase, induced expression of ΔNp63α and genes related to the squamous identity. Analysis of the chromatin state in the *TP63* locus showed that EZH2 inhibition led to a loss histone H3 methylation and a gain of histone H3 acetylation and its reader BRD4. These results support the hypothesis that the squamous identity can be reactivated epigenetically in NEC through de-repression of ΔNp63α as a potential therapeutic strategy.

Together, these studies contribute to our understanding of the transcriptional response to chromatin perturbation and show that this can be leveraged to modulate cell metabolism and identity, as well as to achieve therapeutic benefit in new contexts of cancer.

Table of Contents

iii

List of Figures

Chapter 3: Epigenetic regulation of p63 controls basal to neuroendocrine cell fate transition during esophagus development and malignancy.

Acknowledgments

Firstly, I would like to thank my thesis advisor Dr. Chao Lu, for his continuous support through professional and personal difficulties. From the very beginning of joining his lab, I was strongly encouraged to pursue my scientific interests and under his mentorship I grew greatly as a scientist. He is a great mentor and supervisor.

Secondly, I would like to thank my mentor Dr. Thales Papagiannakopoulos, for putting his trust in me when I joined his lab and guiding me for many years since. He gave me the means and direction to be independent in a new professional environment, which set my career on a new trajectory.

I would like to thank many faculty of the university who guided me through rotations, qualifying exams, and training committee meetings, including Drs Zhiguo Zhang, Christine Chio, Mimi Shirasu-Hiza, Michael Shen, Peter Canoll, Wellington Cardoso, and Alberto Ciccia.

I would like to thank my collaborators Warren Wu and Makiko Hayashi, Albert Li and Jiangbin Ye, and Yongchun Zhang, Helu Liu and Jianwen Que for their help and expertise.

I would also like to thank many past and present members of the Lu lab for their help, including Xiao 'Sean' Chen, Yinglu Li, Xinjing Xu, and Varun Sahu. All lab members contributed to a friendly and productive work environment.

Finally, I would like to thank my wife Pinelopi for always supporting me.

Dedication

I dedicate this work to my family.

Chapter 1: Introduction

1.1 Preface

In this introductory chapter, I highlight current knowledge and literature on chromatin regulation, specifically in relation to cell metabolism, lineage identity and cancer treatment, which were focal points of my thesis research. My work on targeted epigenetic therapy for NRF2-active LUAD led me to study HDAC inhibitors and co-author a review article in 2021 titled "HDAC Inhibitors: Dissecting Mechanisms of Action to Counter Tumor Heterogeneity"[1]. At the final part of this introduction, I include a portion of this article that I wrote that discusses literature on the effects of HDAC inhibitors in cell identity and metabolism in respect to therapeutic targeting of tumor heterogeneity, as well as a portion that discusses variables that create limitations and challenges to HDAC inhibitor research, such as dose, duration, and primary vs secondary effects.

1.2 Chromatin regulation in normal and cancer cells

1.2.1 Organization and regulation of chromatin in mammalian cells

In eukaryotic cells, genetic information encoded as DNA is packaged into the nucleus in the form of chromatin. The nucleosome, the fundamental unit of chromatin, consists of 147 base pairs of DNA wrapped around an octamer of four core histone protein dimers: two H2A-H2B dimers and one histone H3-H4 tetramer[2]. Nucleosomes are linked by a short stretch of linker DNA that is bound by H1 histones at the nucleosome DNA start and end sites, stabilizing the complex. Nucleosomes fold up into 30-nm fibers which are further packaged into larger fiber structures to ultimately form chromosomes[3]. In general, chromatin is organized either as

heterochromatin, a compact state that usually suppresses DNA-binding and gene transcription, or euchromatin, a more 'open', accessible conformation that supports transcription.

All cellular processes that involve genomic DNA, such as DNA replication, DNA damage repair, DNA recombination and gene transcription require tight control of chromatin organization. This is accomplished primarily through remodeling of nucleosomes and epigenetic marks. Nucleosome remodeling, the rearrangement, exchange and displacement of nucleosomes as well as the incorporation of histone variants is mediated by ATP-dependent chromatin remodeling complexes[4]. Epigenetic marks, which are post-translational modifications on histones and chemical modifications on DNA, are deposited and removed by specialized enzymes ('writers' and 'erasers'), and facilitate recruitment of scaffolding and effector proteins with specific functions ('readers')[5].

1.2.2 Chromatin regulation of transcription

Gene transcription is regulated by multiple aspects of chromatin organization, including nuclear localization, higher order structure, nucleosome organization, distal and proximal interactions with regulatory elements, recruitment of transcription factors and chemical modifications on DNA and histones. For example, the location of a gene locus in relation to nuclear elements, such as pores, speckles, nucleoli, and the lamina, is strongly correlated with key features of transcription regulation such as chromatin accessibility and transcription factor binding[6,7]. In addition, higher order structures such as topologically associating domains (TADs) and chromatin loops can limit the potential interactions of a gene locus with distal regulatory elements and promote or suppress formation of heterochromatin[8]. Finally, the chromatin state of proximal and distal genomic regulatory sequences, such as the presence of histone and DNA

modifications, and nucleosome composition and organization, regulates the recruitment of transcription factors and activation of RNA pol II[9,10].

1.2.3 Chromatin regulation in cancer

Chromatin homeostasis is disrupted frequently in cancer, and is implicated in tumor initiation, progression and treatment[11]. Many cellular pathways involved in the establishment of cancer hallmarks are under the control of the chromatin state. For example, epigenetic alterations in cancer cells have been demonstrated to enable activation or suppression of oncogenes and tumor suppressors, respectively[12]. The prevalence of these alterations is often attributed to stochastic events that propagate through natural selection. However, it should be noted that chromatin dysregulation, such redistribution of DNA methylation[13], likely contributes to these occurrences.

Chromatin regulators are mutated frequently in cancer and some enzymes have been shown to drive tumorigenesis as oncogenes or tumor suppressors themselves[14–16]. In most cases, the underlying mechanism of tumorigenesis by chromatin enzyme mutations is not well understood due to the broad and complex effects of such mutations in chromatin homeostasis. Notably, extensive alteration of the epigenomic landscape is widespread in cancer even in the absence of mutations in the chromatin regulatory machinery[17,18]. Together, these points highlight the strong connection between chromatin regulation and tumorigenesis.

1.3 Crosstalk between chromatin regulation and cell metabolism

1.3.1 Metabolism in normal and cancer cells

Cells rely on an extensive and complex network of interconnecting metabolic pathways of enzymatic reactions in order to perform their physiological functions. Firstly, cells utilize

catabolic pathways that break down complex organic molecules to generate energy and primary building blocks for biosynthesis. Energetic demands are primarily met through glycolysis and oxidative phosphorylation. Anabolic pathways use building blocks such as amino acids, nucleotides, and sugars for macromolecule synthesis such as proteins, nucleic acids, and fatty acids. All metabolic pathways are tightly regulated by signaling pathways and feedback loops to achieve homeostasis and meet the cell's metabolic demands.

In cancer cells, metabolism is rewired to promote uptake of necessary nutrients from the microenvironment and utilization of these nutrients to support cell survival and proliferation[19,20]. Cancer cells require key nutrients from the microenvironment such as glucose and amino acids, but also utilize all types of available nutrition that may be available, such as nucleotides and lipids. Nutrients are utilized by pathways such as glycolysis, tricarboxylic acid (TCA) cycle and one-carbon metabolism to support protein, lipid and nucleic acid synthesis as well as to generate energy in the form ATP and NADPH.

Reprogramming of cellular metabolism in tumorigenesis can result directly or indirectly from genetic mutations. It has become evident that cancer-associated metabolic alterations occur at all stages of metabolism regulation, including increased uptake of nutrients from the microenvironment, activation of catabolic and anabolic pathways, and metabolic rewiring that favors utilization of metabolites in tumor-promoting pathways. Such metabolic alterations often occur as a result of oncogenic signaling, such as Kras oncogenic mutations[21] and c-Myc overexpression[22]. In addition, cancer cells frequently activate stress response pathways that directly or indirectly affect metabolic pathways, such as the KEAP1/NRF2 pathway antioxidant response pathway[23], the hypoxia-inducible factors (HIFs)[24], and the unfolded protein response to endoplasmic reticulum (ER) stress[25].

Another important regulator of cancer cell metabolism is the tumor microenvironment. Environmental factors such as the surrounding tissue, proximity to blood vessels, presence of immune and stromal cells can dictate the availability of nutrients and oxygen, pH, growth signals and more[26]. The combination of unique environmental and cell-autonomous influences on cancer cell metabolism creates context-specific metabolic demands and vulnerabilities that have incited intense scientific interest on therapeutic approaches targeting metabolism[27].

1.3.2 Crosstalk of metabolism and chromatin

There is an intricate crosstalk between chromatin regulation and metabolism (**Figure 1.1**). On one hand, changes in metabolism often cause widespread changes in chromatin landscape [28,29]. This is in part because many enzymes that catalyze histones and DNA modifications depend on metabolites such as SAM, α-KG and acetyl-CoA that are present in limiting concentrations in the cells. Fluctuations in metabolite concentrations can affect chromatin modifying activity, an event that has been demonstrated in the context of cancer. For example, TET and KDM dioxygenases, enzymes that utilize α-KG and O_2 to demethylate DNA and histones respectively, were shown to be affected by changes in the concentration of O_2 and TCA cycle metabolites, disrupting gene expression and cell fate[30–32].

On the other hand, expression of metabolic genes is regulated by the chromatin state of their genetic locus. For example, several metabolic genes have been reported to be silenced by DNA methylation in cancer, including *FBP2*[33], *ASS1* and *SAT1*[34], and *ZDHHC1*[35]. Furthermore, several studies have shown a link between histone acetylation and regulation of metabolic genes, such as suppression of glycolysis genes by the histone deacetylase SIRT6[36], amino acid metabolism and nucleotide synthesis by histone deacetylase HDAC11[37], and branch chain amino acid metabolism by EZH2[38].

Evidence for the control of metabolic genes by chromatin is also found in the context of cancer treatment, such as suppression of glycolysis by HDAC inhibitors in glioblastoma[39]. Furthermore, several studies have found therapeutic potential in combining of epigenetic and metabolic perturbation, such as a preclinical study on inhibition of HDACs and fatty acid oxidation[39], and a clinical study on inhibition of glutaminase and DNA methyltransferases[40] (NCT03047993).
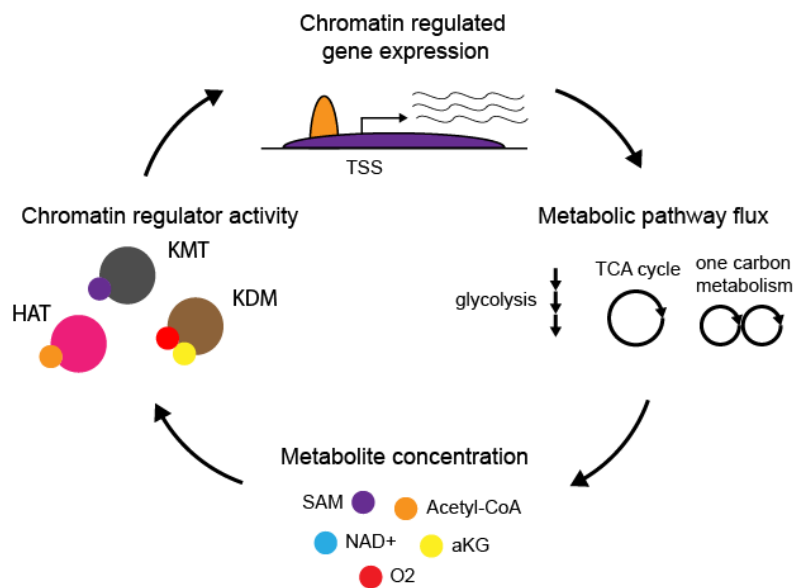
Figure 1.1. Crosstalk between chromatin regulation and metabolism. Schematic illustrating how chromatin regulates transcription of metabolic genes has an impact on metabolic pathway activity. As a result, there is fluctuation in the concentration of metabolites that act as cofactors in enzymatic reactions of chromatin regulators, which in turn affects regulation of chromatin state.

1.4 Crosstalk between chromatin regulation and cell identity

1.4.1 Cell fate transitions in normal and cancer cells

Cell differentiation is an essential process for the development, growth, reproduction, and longevity of multicellular organisms. Differentiation is a multi-step process that begins from pluripotent stem cells or progenitors with the ability to self-replicate, which generate progeny that gradually acquire lineage characteristics until a terminal differentiation cell state with distinct physiology and functions. During this process cells turn on cell-type-specific gene expression programs in response to extracellular and intracellular signals, cell-cell interactions, and stochastic events.

Despite its name, terminal differentiation can be reversed or altered in normal, disease and laboratory conditions. Depending on the directionality of cell fate change, three types of changes have been described: reprogramming, dedifferentiation and transdifferentiation[41,42]. Reprogramming occurs when cells lose their differentiation characteristics and return to pluripotency, effectively becoming stem cells. In dedifferentiation, differentiated cells lose parts of their identity and gain progenitor characteristics. In transdifferentiation, cells lose aspects of their identity and acquire characteristics of another differentiated cell type. These cell fate transitions are considered reversible and not exclusive, for example transdifferentiation can be preceded by dedifferentiation[43]. The ability of cells to switch cell identity characteristics, termed cell plasticity, is an intensely studied topic of cancer research as it represents a significant obstacle to cancer treatment.

In cancer, cell identity is subjected to multiple alterations during initiation, progression and treatment[44]. Studies indicating the expression of embryonic and stem-cell identity genes support the hypothesis that transformation is associated with loss of differentiation[45,46].

7

Moreover, studies have shown that cancer cells can undergo all types of cell fate changes, such as transdifferentiation of castration-resistant prostate cancer (CRPC) from adenocarcinoma to neuroendocrine CRPC[47], acquirement of stem cell characteristics by squamous cell carcinoma (SCC) cells[48] and glioblastoma[49], and epithelial-to-mesenchymal (EMT) transition by many solid tumors[50].

1.4.2 Crosstalk between chromatin and cell identity

Precise chromatin regulation is vital for coordination of gene expression programs during cell fate determination and as a result plays a crucial role during cell fate transition[51,52]. A popular illustration of this is the Waddington's epigenetic landscape, where the undifferentiated cell is depicted as a ball rolling down splitting valleys which represent states of differentiation[53] (**Figure 1.2**). In order for the ball to be transferred to a new valley, more energy is needed the further away the new valley is (vertically or horizontally). Similarly, the extent of epigenetic reprogramming needed for a cell to switch to a new differentiation state is proportional to the 'distance' between the two cell fates. Although oversimplified[54], this model facilitates comprehension of the interconnection between cell fate and the epigenetic state.

Waddington's epigenetic landscape

Pluripotent

Differentiated

Dynamic regulation of chromatin
Pluripotency super-enhancers
Bivalent marked genes
DNA hypomethylation

Selective activation and silencing
of enhancers and developmental genes
Cell type-dependent chromatin state
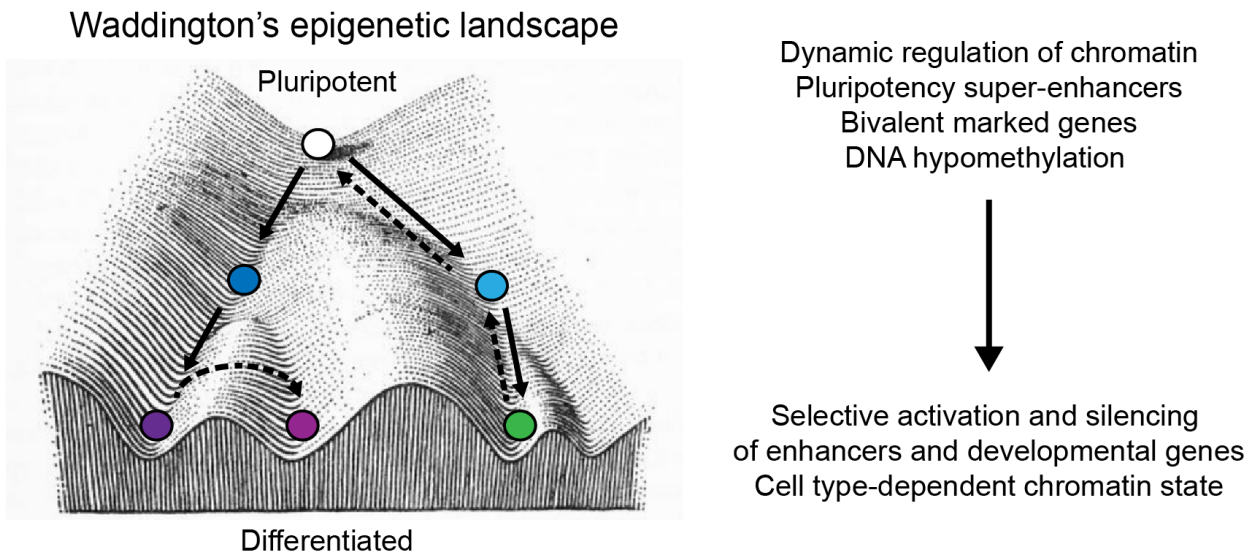
Figure 1.2. Epigenetic regulation during cell fate transition. Schematic showing an adaptation of Waddington's landscape[53], the potential cell fate transitions between pluripotent and differentiated cells, as well as the associated chromatin changes.

The interplay between chromatin and cell fate has been extensively studied in the context of cell reprogramming. During induction of pluripotency, there is extensive rewiring of the epigenetic landscape, which is influenced by the presence of both pluripotency transcription factors and chromatin regulators[55]. In embryonic stem cells (ESCs), studies have shown that chromatin is regulated in a highly dynamic manner[56] and allows for globally hyperactive transcription[57]. Furthermore, expression of genes associated with cell identity is regulated by specific chromatin elements. During development, enhancers are differentially utilized[58] and form super-enhancers to accommodate master transcription factor activity[59]. In addition, developmental genes in ESCs are marked by a bivalent chromatin state that is poised for activation or repression, characterized by the co-localization of activating and repressive histone marks[60]. These examples highlight the major role of chromatin for cell fate determination.

In cancer, cell fate transition is closely linked to epigenetic reprogramming. For example, localized epigenetic alterations at the *SOX2* and *SOX9* gene loci regulates EMT in lung adenocarcinoma[61]. At the global chromatin level, the tissue of origin and subtype is often linked to distinct chromatin landscape. For example, SCC cells with hair follicle, epidermal, and stem cell identity characteristics showed differences in chromatin accessibility landscape[48]. In a study using 60 human cancer cell lines representing nine types of cancer, profiling of histone modifications revealed significant differences between tissue types[62]. At the same time, there are

common patterns of chromatin alterations that occur in the majority of cancer types, such as genome-wide DNA hypomethylation, that is associated with normal cell transformation[63]. As a result, alteration of the epigenetic landscape in cancer cells is tightly linked to retainment or loss of their original identity.

1.5 Targeting chromatin in cancer

1.5.1 Drug resistance and current epigenetic therapies in cancer

Treatment resistance remains a major obstacle in cancer therapy. Drug resistant cancer cells display various adaptations that enable them to survive treatment, including metabolic reprogramming and cell plasticity[64]. Regarding metabolism, several pathways have been found to be involved in drug resistance, including drug efflux and neutralization, oxidative stress adaptation, lipid metabolism and glycolysis[65]. Plasticity of tumor cells drives the generation of heterogeneous populations, which promotes the emergence of populations with a phenotypic state that no longer depends on the drug-targeted pathway[66]. As a result, the crosstalk between chromatin with cell metabolism and plasticity underlines the therapeutic potential of epigenetic therapy to overcome tumor resistance to conventional cancer treatment.

Despite years of development, drugs targeting chromatin regulation are approved for treatment of only a handful of malignancies, in part reflecting our limited understanding of their mechanisms of action[67]. Currently, there are multiple therapeutic regimens that target chromatin regulation in cancer. The most prominent ones are histone deacetylase (HDAC) inhibitors, such as Romidepsin and Vorinostat which are used for treatment of refractory T-cell lymphoma[68,69], as well as DNA methyltransferase inhibitors which are used as first-line treatment of myeloid malignancies[70]. Importantly, the efficacy of these agents was determined through phenotypic

observations and analogue-based drug discovery[71]. As a result, the precise mechanism of cell killing is not well understood. In addition, these agents display several clinical adverse effects at high doses, such as myelosuppresion[72,73]. Together, these issues have limited their application to only specific hematologic cancer types, despite years of intense investigation.

Histone acetylation and DNA methylation are epigenetic marks that are closely linked to regulation of gene transcription. Studies in preclinical models have indicated various mechanisms to explain their anti-cancer effects, including re-activation of tumor suppressor gene expression, induction of retrotransposon expression and DNA damage[1,74–77]. However, the causal relationship between these effects and cancer cell death is often found to be context dependent. As a result, a better understanding of the underlying biology would allow identification of new biomarkers and broaden the number of cancer patients who could benefit from these epigenetic drugs.

In the following section, I will focus on HDAC inhibitors, which is the topic of investigation in Chapter 2, as an example to highlight our current knowledge of the mechanism and limitation of epigenetic therapies.

1.5.2 Perspective on HDAC inhibitors (HDACi) in cancer treatment

Extensive research on HDACi has found that they impact most cancer-related pathways. To date, HDACi have been implicated in the regulation of numerous cellular processes, including chromatin regulation, gene expression, apoptosis, cell cycle progression, genome maintenance, DNA repair, metabolism, phenotypic plasticity, and aspects of the tumor micro-environment. This is due to the broad and complex functions of the HDAC enzymes. Through deacetylation of histones and proteins, these enzymes regulate gene expression, chromatin structure, genome replication and maintenance, and several other cellular pathways.

Understanding how HDACi mediate each of their effects will be important for clinical application of these inhibitors. Rational use of HDAC inhibitors, such as in conjunction with other treatments or in selected patients, could be leveraged to reduce tumor heterogeneity and thus mitigate tumor resistance and recurrence mechanisms (**Figure 1.3, Table 1**).
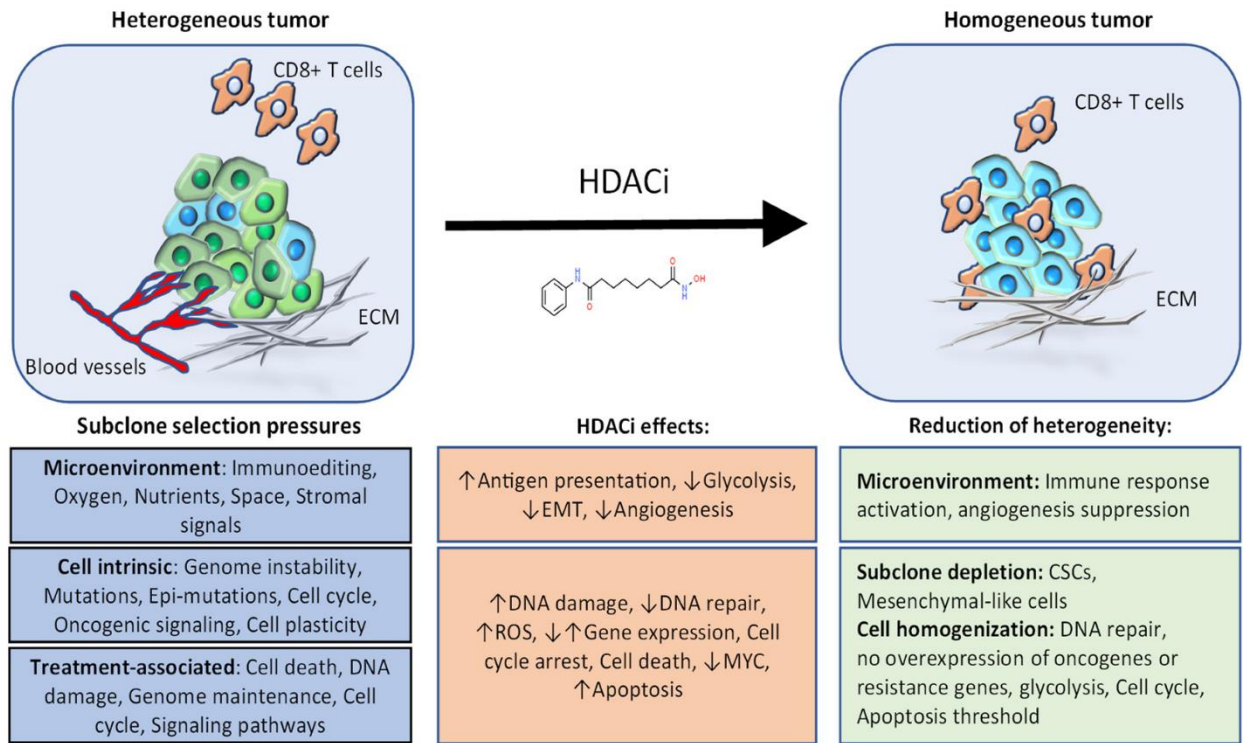
Figure 1.3. HDAC inhibitors can counteract tumor heterogeneity. A schematic illustrating how HDAC inhibitors could be utilized to reduce heterogeneity in cancer. During cancer progression, subclone selection pressures from the microenvironment, intrinsic cellular properties and selection pressures during treatment generate tumor heterogeneity. The effects of HDACi can be utilized rationally to counter these sources of heterogeneity. Through this approach, the tumor becomes more homogeneous in certain aspects of tumor cell biology and the microenvironment, and thus responds better to cytotoxic and/or targeted therapy. EMT:

Epithelial-Mesenchymal Transition; ROS: Reactive Oxygen Species; CSCs: Cancer Stem Cells;

ECM: Extracellular Matrix.

Table 1. Examples of how HDAC inhibitors can be utilized to mitigate specific resistance mechanisms in several types of treatment and cancer settings.

Treatment	Cancer Type	Resistance Mechanism that Can Be Suppressed by HDACi
Chemotherapy	Solid tumor without targeted therapy option	Clonal transcriptional heterogeneity
		Glycolysis induction[78]
PARP inhibition	HRR-deficient cancer	HRR activation[79]
Checkpoint blockade inhibition	Lung, Bladder and more	Immune surveillance evasion[80]
Tyrosine kinase inhibitor	EGFR+ Lung cancer	MET overexpression; EMT [81]
Anti-estrogens	ER+ Breast cancer	Transcriptional Heterogeneity [82]

Metabolism. HDAC inhibitors have been shown to have a strong effect on cell

metabolism. Several studies have reported reduction in glycolysis upon HDAC inhibition, and in

one the pentose phosphate pathway was shown to be reduced as well [39,83–85]. Importantly, this

effect was observed by several HDAC inhibitors in several types of cancer. It is possible that it is

driven by inhibition of HDAC3, which represents a major regulator of glucose metabolism and

fatty acid oxidation in muscle and adipose tissue[86,87]. In another study, authors identified

synergistic interaction between HDAC inhibition and inhibition of glycolysis[88,89], although the

reason for this is not known. The link between HDAC inhibition and perturbation of metabolism

could be related to regulation of enhancers. In glioblastoma, inhibition of glycolysis by HDACi

was attributed to MYC super-enhancer disruption and glycolysis gene downregulation[39].

Notably, in a proteomics approach using a Vorinostat affinity probe, Vorinostat was found to

directly interact with Enolase 1 (ENO1) and could therefore potentially inhibit its enzymatic role in glycolysis[90].

Therapeutic implications: Metabolic reprogramming is known to introduce metabolic liabilities in cancer cells[91]. Therefore, dysregulation of metabolism by HDAC inhibition presents an opportunity for design of combinatorial or targeted therapeutic strategies to achieve enhanced responses. Notably, several studies have identified synergistic interactions between HDACi and inhibitors of metabolic pathways such as glycolysis, fatty acid β-oxidation and oxidative phosphorylation in glioma[88,39]. It would be interesting to see whether tumors with inherent defects in these pathways due to specific mutations or limited nutrient availability would be more sensitive to HDAC inhibition.

Cell metabolism responds dynamically to intracellular and extracellular cues present in tumor cells, such as nutrient availability, signalling pathway activation, and gene expression. These stimuli constitute a considerable source of tumor heterogeneity that affects response[92]. Therefore, HDACi could be applied to counter this heterogeneity, by forcing cells to conform to a certain metabolic phenotype. For example, glucose levels generate heterogeneity in cell glycolysis[93], which could be countered by using HDACi to inhibit glycolysis in all cells. This could be a way to introduce a bottleneck that limits cancer cell adaptability and resistance. In addition, induction of glycolysis after chemotherapy has been found to support cell survival and resistance in ovarian cancer[78]. As a result, HDACi-mediated inhibition of glycolysis could be leveraged to inhibit this resistance mechanism.

Phenotypic Plasticity. The plasticity of tumor cells in phenotypic states, such as epithelial–mesenchymal transition (EMT) and cancer stemness, contributes significantly to

tumor heterogeneity[94]. EMT refers to the reversible shift of cells from an epithelial state, characterized by strong cell-to-cell adhesion, to a mesenchymal state, where cells become more migratory and invasive[95,96]. This transition affects several cellular processes and components, including the cytoskeleton, metabolism, innate immunity, proliferation, and apoptosis. In cancer this process is usually partial and is associated with metastatic disease and chemoresistance[97]. Several groups have demonstrated that HDAC inhibitors suppress the EMT transcriptional program in several cancer types, including breast, biliary tract, bladder, and others[98–102]. Importantly, this suppression was evident in cell lines that were predominantly mesenchymal-like, either intrinsically or due to exogenous signals such as TGFβ. This may explain why the opposite effect has also been reported in epithelial-like cancer cell lines[103,104]. Therefore, it is likely that the influence of HDAC inhibitors in EMT is context dependent, specifically on the initial phenotypic state of the cancer cells.

It is well accepted that epigenetic heterogeneity leads to transcriptional plasticity and adaptive responses to chemoresistance in cancer. Cancer stem cells (CSCs) and poorly differentiated cancer cells represent sources of cellular heterogeneity within tumors, and there is strong clinical evidence that these subpopulations are critical to conferring drug resistance[105–108]. CSCs have the potential to self-renew with symmetric or asymmetric division and are characterized by high tumor-initiating capacity[109]. Moreover, their divisions can generate differentiated progeny and transient amplifying cells, increasing the tumor's heterogeneity. In addition, CSCs can enter a quiescent state that protects them upon treatment, since chemotherapy is more effective against proliferating cells[110]. Targeted pharmaceutical inhibition of stem cell-related signaling pathways, such as Wnt, Notch, and Hedgehog, causes high levels of toxicity, as

15

normal tissue homeostasis also relies on these pathways[111]. Moreover, compensatory activation

of other signaling pathways often confers resistance[112].

Just as in normal cells, self-renewal of cancer stem cells or proliferation of cells with

undifferentiated phenotypes is highly dependent on key transcriptional programs that are

regulated by specific epigenetic patterns in their chromatin [113,114]. For instance, differential DNA

methylation is associated with the expression of stem cell marker genes such as CD44, CD133,

and Musashi-1 (MSI1). More specifically, hypomethylation can activate these CSC genes in

aggressive tumors [115,116]. Other studies in glioblastomas (GBM) have demonstrated that

chromatin in CSCs is characterized by reduced levels of the silencing histone mark, H3K27me3,

and possesses a more open conformation compared to non-CSCs, which together allow genes

that maintain the stem cell phenotype to be expressed [117]. The overexpression of several HDACs

has been associated with cancer stem cell identity, regulation of the Sonic-Hedgehog pathway,

and poor survival in GBM, NSCLC, and breast and ovarian cancers [118–121]. In addition, in acute

myeloid leukemia (AML), CSCs were characterized by higher H3K4me3 levels on genes

involved in stem cell identity, proliferation, and metabolic reprogramming compared to non-

CSCs, indicating that differentiation processes were associated with epigenetic silencing of stem

cell identity genes[122].

Therapeutic Implications. Phenotypic plasticity such as that in the form of EMT state

contributes significantly to tumor heterogeneity[94], and is considered an important mechanism of

therapy resistance because it is accompanied by anti-apoptotic signaling and drug efflux[97,123].

The EMT-suppressive effect of HDACi in mesenchymal-like cells can be employed in tumors

where EMT occurs and mediates resistance, such as patient subsets in breast and pancreatic

cancer[124,125]. In this setting, EMT inhibition could confer several beneficial effects, including

enhancements of the effects of other therapeutics, and suppression of mesenchymal subclone emergence and metastasis.

The importance of epigenetic regulation in CSCs suggests a dependence that could be exploited for cancer treatment. Specifically, disruption of chromatin states and the expression of genes required to maintain cancer stemness could be a way to target CSC populations and reduce heterogeneity[113]. Interestingly, recent studies have demonstrated that targeting the epigenetic state of the CSC pool in tumors via HDAC inhibitors can suppress the growth of cancer stem cells without impairing the functions of normal stem cells [126]. For instance, in triple-negative breast cancer, the Class I HDAC inhibitor Entinostat was reported to decrease the CSC population [127]. Similarly, HDAC inhibition has been shown to reduce the cancer stem cell burden in GBM tumors[119,128,129] and NSCLC[121].

Dissecting the variables of HDAC inhibition. Thus far we explored the application of HDACi in cancer treatment to counter tumor heterogeneity and achieve greater response by targeting specific cellular processes (**Figure 1.3**, **Table 1**). However, targeted therapeutic approaches require deep understanding of the effects and mechanisms of action of the candidate drug. At first glance, the widespread effects of HDAC inhibitors in cell biology do not suggest a unifying mechanism of action. Several questions arise when considering how HDAC inhibitors act: Which HDACs are relevant for the effects of HDACi? Why are HDACi only effective in hematological malignancies? Which effects of HDACi are primary and which are secondary? How does HDACi dosage affect the phenotypes observed? Answering these questions is vital for comprehending why HDAC inhibition is successful or not in cancer treatment, as well as for development of effective therapeutic strategies, such as countering tumor heterogeneity.

Target selectivity. Firstly, we must consider if the selectivity of HDAC inhibitors influences their biological activity. Despite their name, histone deacetylases have diverse targets, which are often not histones. Moreover, HDAC inhibitors often target more than one HDAC protein, and the target specificity varies between compounds. The drugs used in clinical and pre-clinical settings of cancer treatment vary in their target specificity (**Table 1**). Some are selective for Class I HDACs, such as Romidepsin and Entinostat while others inhibit Class I, II and IV to various degree, such as Vorinostat and its derivatives[130]. Despite their differences in targeting selectivity, HDAC inhibitors are used in similar clinical settings and seem to have similar phenotypic effects. In addition, they invariably inhibit HDAC family members 1, 2 and 3, which suggests that inhibition of these proteins is what mediates their anti-cancer activity.

This notion is challenged by the fact that several Class II and HDAC6-specific inhibitors have shown promise as anticancer agents as well. HDAC6 deacetylates cytoplasmic proteins such as tubulin and HSP90 and has important functions in tumorigenesis, such as modulation of protein homeostasis through regulation of HSP90 and proteasomal degradation[131–133], p53 apoptotic activity[134] and tyrosine kinase signaling[135]. As a result several groups have contributed to the development of HDAC6-selective inhibitors [136–138]. Ricolinostat, an HDAC6-selective inhibitor, was effective in models of multiple myeloma and lymphoma in vitro and in vivo [139,140]. As a result, several clinical trials are currently assessing its efficacy in multiple myeloma and lymphoma[141](NCT01997840, NCT02091063). Notably, Ricolinostat was recently reported to mediate cell death through off-target toxicity[142], which could be attributed to its low selectivity to HDAC6 compared to class I HDACs[139]. Another HDAC6-specific inhibitor Citarinostat has also displayed anti-cancer activity and are being investigated in the clinic[143] (NCT02886065).

To our knowledge few studies have directly compared how HDACi with different selectivity affect various cellular processes. In a study of p53 and NFκB signalling, the Class I/IIa selective inhibitor VPA had distinct effects from the HDAC6-selective inhibitor Marbostat [144]. Vorinostat and Romidepsin similarly induced expression of pro-apoptotic genes [145], as well as cytokine expression in CTCL[146]. Sonnemann et al. reported a partial difference in p53 dependency[147]. Overall, Class I and Class I/II/IV HDACi have mostly similar effects in cells, but it is probably best that HDAC6-specific HDACi are considered as distinct agents. Finally, it should be noted that several effects of HDACi have been reproduced by genetic knock-down or knock-out of Class I HDACs[39,148–150]. Therefore, it is likely that many or most effects of HDAC inhibitors stem from inhibition of Class I HDAC.

Tissue specificity. Secondly, we must consider if the activity of HDAC inhibitors is tissue specific. So far, HDACi are being employed in the clinic only for treatment of a few hematological cancers, which could point to a tissue specific effect. Class I and Class II HDACs have important roles in T-cell development and differentiation, which could underlie the effectiveness of HDAC inhibitors in T-cell lymphoma[151]. In addition, HDACi have been shown to target blood cancer-specific pathways such as BCL6 overexpression in B-cell lymphoma[152], aggresome dependency in multiple myeloma[153,154], and HDAC6 overexpression in lymphoma[136].

Therefore, it is possible that HDACi have not achieved the desired efficacy as monotherapy in solid tumors because of tissue specificity, as well as due to inter- and intra-tumoral heterogeneity. Nevertheless, HDAC inhibitors exhibit useful biological effects in both solid and hematological cancers that can be leveraged to target specific cancer alterations and improve the efficacy of other therapies. Additionally, HDACs are found overexpressed in solid cancers as well [155], which also supports the use of HDACi in solid tumor treatment.

Dose-dependent effects. Thirdly, we need to consider how HDACi dosage influences the manifestation of their phenotypic effects. Several studies have indicated differences in concentration thresholds between effects such as DNA damage and histone hyperacetylation. ROS generation and apoptosis is generally observed at high-concentrations of HDACi [156,157]. In a study of dose-dependent effects of class I HDACi Largazole, cell cycle block was observed only in higher concentrations of the inhibitor[158]. In contrast, changes in H3K9ac and H3K27ac abundance and genomic distribution were observed even at the lowest concentrations. Moreover, there was marked difference between high and low dose HDACi in the subsets of enhancers and transcripts that are affected. In line with this, in a concentration gradient of Vorinostat treatments, histone acetylation induction was observed at lower doses than DNA damage, assessed by γH2A.X[159].

In summary, the current evidence suggests that lower levels of HDACi are sufficient to disrupt epigenetic regulation such as enhancer acetylation, but more severe phenotypic effects such as genomic instability, cell cycle block and apoptosis occur only by extensive HDAC inhibition. In the clinic, HDACi are administered at sufficiently high concentrations that tumor cells should display severe phenotypic effects[130]. However, it is likely that poorly vascularized regions of solid tumors are exposed to lower concentrations of HDACi, which likely impairs their cell killing effects. This might explain their success in the treatment of hematological cancers, where drug diffusion is unobstructed. Moreover, this is an additional incentive to look for combinatorial or targeted therapeutic approaches where a low dose of HDACi is sufficient. The disruption of epigenomic and transcriptional regulation observed even at low concentrations of HDACi most likely confers vulnerabilities that could be exploited for therapeutic benefit.

Primary and Secondary effects. Finally, we need to identify which of the effects of HDAC inhibition are primary and which are secondary. Ideally, this could be achieved by construction of a time-course for all observed effects, but only few studies have assessed phenotypic effects earlier than 16 hours after HDACi treatment. The earliest events are most likely histone acetylation and DNA damage, which were observed to increase in just 3 minutes of exposure to TSA[160]. The kinetics of DNA damage generation suggest that it is likely caused by genome instability and not by indirect means such as downregulation of DNA repair components. Generation of ROS was shown to happen as early as 2 hours post-treatment[156], but earlier timepoints have not been assessed and it is thus not clear whether this is the underlying cause of DNA damage. TSA primed cells for enhanced induction of NFκB signaling after 1 hour of treatment[161]. Effects on transcription were found as early as 1 hour post-treatment, when vorinostat was shown to significantly reduce MYC mRNA levels and cause widespread gene expression changes[162]. Two studies reported effects of HDACi on gene expression as early as 4 hours and 10 minutes after treatment respectively, which stemmed from modulation of transcriptional elongation[163,164]. Apoptosis is generally observed after 17 hours of treatment, so it is likely a secondary event.

Based on these findings and our knowledge so far, we can speculate on the order of events after HDAC inhibition (**Figure 1.4**). Under low dose of HDACi, histone acetylation increase modulates enhancer and promoter chromatin structure and activity which leads to transcriptional changes. This could underlie transcription priming observed in immune response genes. Subsequently, gene downregulation impairs metabolic and DNA repair pathways. Under high dose of HDACi additional effects are observed. Initially, strong HDAC inhibition disrupts DNA replication and/or DNA repair by histone and/or protein hyperacetylation. This leads to

DNA damage, H2A.X phosphorylation, and activation of the DNA damage response and cell cycle checkpoints. Subsequently, excessive DNA damage and inability to resolve it, due to functional and transcriptional compromisation of DNA repair, leads to apoptosis and possibly to activation of innate immunity pathways such as antigen presentation.
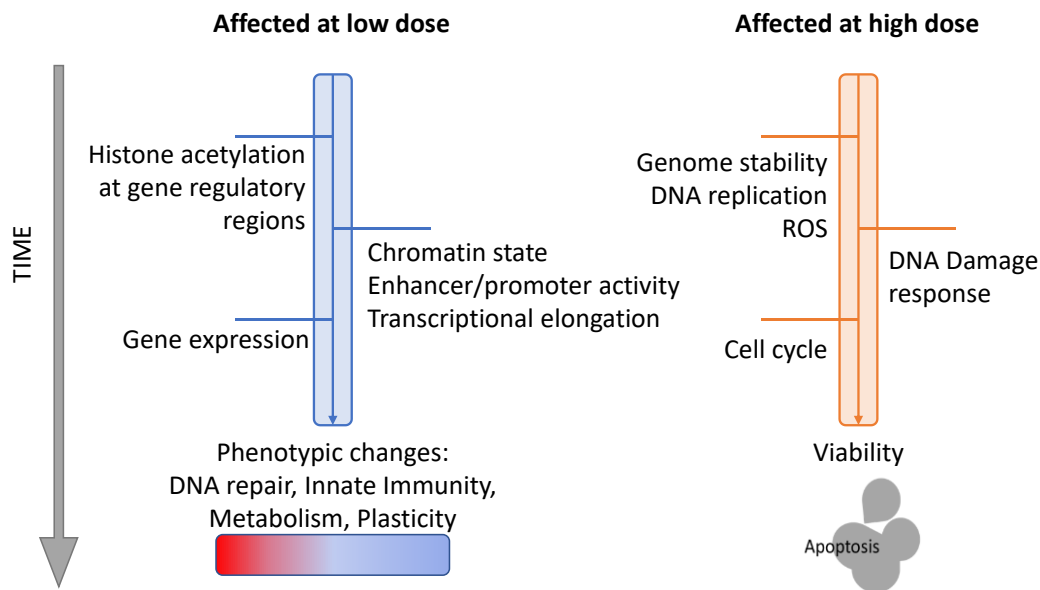
Figure 1.4. HDAC inhibitors have variable effects. Perspective on how prominent effects of HDAC inhibitors take place in a time- and dose-dependent manner based on current literature.

References

1. Karagiannis, D. & Rampias, T. HDAC Inhibitors: Dissecting Mechanisms of Action to Counter Tumor Heterogeneity. *Cancers* **13**, 3575 (2021).
2. Cutter, A. R. & Hayes, J. J. A brief review of nucleosome structure. *FEBS Letters* **589**, 2914–2922 (2015).
3. Annunziato, A. (2008) DNA Packaging: Nucleosomes and Chromatin. Nature Education 1(1):26.
4. Saha, A., Wittmeyer, J. & Cairns, B. R. Chromatin remodelling: the industrial revolution of DNA around histones. *Nat Rev Mol Cell Biol* **7**, 437–447 (2006).

5. Allis, C. D. & Jenuwein, T. The molecular hallmarks of epigenetic control. *Nat Rev Genet* **17**, 487–500 (2016).

6. Morimoto, M. & Boerkoel, C. F. The Role of Nuclear Bodies in Gene Expression and Disease. *Biology (Basel)* **2**, 976–1033 (2013).

7. Kalverda, B., Röling, M. D. & Fornerod, M. Chromatin organization in relation to the nuclear periphery. *FEBS Letters* **582**, 2017–2022 (2008).

8. Szabo, Q., Bantignies, F. & Cavalli, G. Principles of genome folding into topologically associating domains. *Science Advances* **5**, eaaw1668 (2019).

9. Li, B., Carey, M. & Workman, J. L. The Role of Chromatin during Transcription. *Cell* **128**, 707–719 (2007).

10. Cramer, P. Organization and regulation of gene transcription. *Nature* **573**, 45–54 (2019).

11. Flavahan, W. A., Gaskell, E. & Bernstein, B. E. Epigenetic plasticity and the hallmarks of cancer. *Science* **357**, eaal2380 (2017).

12. Baylin, S. B. & Jones, P. A. Epigenetic Determinants of Cancer. *Cold Spring Harb Perspect Biol* **8**, a019505 (2016).

13. Kulis, M. *et al.* Epigenomic analysis detects widespread gene-body DNA hypomethylation in chronic lymphocytic leukemia. *Nat Genet* **44**, 1236–1242 (2012).

14. Shen, H. & Laird, P. W. Interplay between the Cancer Genome and Epigenome. *Cell* **153**, 38–55 (2013).

15. Chen, C. *et al.* MLL3 Is a Haploinsufficient 7q Tumor Suppressor in Acute Myeloid Leukemia. *Cancer Cell* **25**, 652–665 (2014).

16. Yap, D. B. *et al.* Somatic mutations at EZH2 Y641 act dominantly through a mechanism of selectively altered PRC2 catalytic activity, to increase H3K27 trimethylation. *Blood* **117**, 2451–2459 (2011).

17. Jones, P. A. & Baylin, S. B. The epigenomics of cancer. *Cell* **128**, 683–692 (2007).

18. Baylin, S. B. & Jones, P. A. A decade of exploring the cancer epigenome — biological and translational implications. *Nat Rev Cancer* **11**, 726–734 (2011).

19. Pavlova, N. N. & Thompson, C. B. The Emerging Hallmarks of Cancer Metabolism. *Cell Metabolism* **23**, 27–47 (2016).

20. Martínez-Reyes, I. & Chandel, N. S. Cancer metabolism: looking forward. *Nat Rev Cancer* **21**, 669–680 (2021).

21. Ying, H. *et al.* Oncogenic Kras Maintains Pancreatic Tumors through Regulation of Anabolic Glucose Metabolism. *Cell* **149**, 656–670 (2012).

22. Miller, D. M., Thomas, S. D., Islam, A., Muench, D. & Sedoris, K. c-Myc and Cancer Metabolism. *Clin Cancer Res* **18**, 5546–5553 (2012).

23. Itoh, K. *et al.* Keap1 represses nuclear activation of antioxidant responsive elements by Nrf2 through binding to the amino-terminal Neh2 domain. *Genes Dev.* **13**, 76–86 (1999).

24. Luo, Z. *et al.* Hypoxia signaling in human health and diseases: implications and prospects for therapeutics. *Sig Transduct Target Ther* **7**, 1–30 (2022).

25. Hetz, C., Zhang, K. & Kaufman, R. J. Mechanisms, regulation and functions of the unfolded protein response. *Nat Rev Mol Cell Biol* **21**, 421–438 (2020).

26. Lyssiotis, C. A. & Kimmelman, A. C. Metabolic Interactions in the Tumor Microenvironment. *Trends in Cell Biology* **27**, 863–875 (2017).

27. Cai, L.-Y. *et al.* Targeting p300/CBP Attenuates Hepatocellular Carcinoma Progression through Epigenetic Regulation of Metabolism. *Cancer Research* **81**, 860–872 (2021).

28. Janke, R., Dodson, A. E. & Rine, J. Metabolism and Epigenetics. *Annu. Rev. Cell Dev. Biol.* **31**, 473–496 (2015).
29. Lu, C. & Thompson, C. B. Metabolic regulation of epigenetics. *Cell Metab* **16**, 9–17 (2012).
30. Thienpont, B. *et al.* Tumour hypoxia causes DNA hypermethylation by reducing TET activity. *Nature* **537**, 63 (2016).
31. Chakraborty, A. A. *et al.* Histone demethylase KDM6A directly senses oxygen to control chromatin and cell fate. *Science* **363**, 1217–1222 (2019).
32. Xiao, M. *et al.* Inhibition of α-KG-dependent histone and DNA demethylases by fumarate and succinate that are accumulated in mutations of FH and SDH tumor suppressors. *Genes & Development* **26**, 1326–1338 (2012).
33. Li, H. *et al.* Decreased fructose-1,6-bisphosphatase-2 expression promotes glycolysis and growth in gastric cancer cells. *Mol Cancer* **12**, 110 (2013).
34. Yeon, A. *et al.* Rewiring of cisplatin-resistant bladder cancer cells through epigenetic regulation of genes involved in amino acid metabolism. *Theranostics* **8**, 4520–4534 (2018).
35. Le, X. *et al.* DNA methylation downregulated ZDHHC1 suppresses tumor growth by altering cellular metabolism and inducing oxidative/ER stress-mediated apoptosis and pyroptosis. *Theranostics* **10**, 9495–9511 (2020).
36. Zhong, L. *et al.* The histone deacetylase Sirt6 regulates glucose homeostasis via Hif1alpha. *Cell* **140**, 280–293 (2010).
37. Bi, L. *et al.* HDAC11 Regulates Glycolysis through the LKB1/AMPK Signaling Pathway to Maintain Hepatocellular Carcinoma Stemness. *Cancer Research* **81**, 2015–2028 (2021).
38. Gu, Z. *et al.* Loss of EZH2 Reprograms BCAA Metabolism to Drive Leukemic Transformation. *Cancer Discovery* **9**, 1228–1247 (2019).
39. Nguyen, T. T. T. *et al.* HDAC inhibitors elicit metabolic reprogramming by targeting super-enhancers in glioblastoma models. *J Clin Invest* **130**, 3699–3716 (2020).
40. Guerra, V. *et al.* Interim results from a phase Ib/II clinical study of the glutaminase inhibitor telaglenastat (CB-839) in combination with azacitidine in patients with advanced myelodysplastic syndrome (MDS). *JCO* **37**, 7037–7037 (2019).
41. Jopling, C., Boue, S. & Belmonte, J. C. I. Dedifferentiation, transdifferentiation and reprogramming: three routes to regeneration. *Nat Rev Mol Cell Biol* **12**, 79–89 (2011).
42. Xiong, S., Feng, Y. & Cheng, L. Cellular Reprogramming as a Therapeutic Target in Cancer. *Trends in Cell Biology* **29**, 623–634 (2019).
43. Puri, S., Folias, A. E. & Hebrok, M. Plasticity and dedifferentiation within the pancreas: development, homeostasis, and disease. *Cell Stem Cell* **16**, 18–31 (2015).
44. Le Magnen, C., Shen, M. M. & Abate-Shen, C. Lineage Plasticity in Cancer Progression and Treatment. *Annual Review of Cancer Biology* **2**, 271–289 (2018).
45. Kim, J. & Orkin, S. H. Embryonic stem cell-specific signatures in cancer: insights into genomic regulatory networks and implications for medicine. *Genome Med* **3**, 75 (2011).
46. Monk, M. & Holding, C. Human embryonic genes re-expressed in cancer cells. *Oncogene* **20**, 8085–8091 (2001).
47. Zou, M. *et al.* Transdifferentiation as a Mechanism of Treatment Resistance in a Mouse Model of Castration-Resistant Prostate Cancer. *Cancer Discov* **7**, 736–749 (2017).
48. Ge, Y. *et al.* Stem Cell Lineage Infidelity Drives Wound Repair and Cancer. *Cell* **169**, 636-650.e14 (2017).
49. Dirkse, A. *et al.* Stem cell-associated heterogeneity in Glioblastoma results from intrinsic tumor plasticity shaped by the microenvironment. *Nat Commun* **10**, 1787 (2019).

50. Dongre, A. & Weinberg, R. A. New insights into the mechanisms of epithelial–mesenchymal transition and implications for cancer. *Nat Rev Mol Cell Biol* **20**, 69–84 (2019).

51. Tee, W.-W. & Reinberg, D. Chromatin features and the epigenetic regulation of pluripotency states in ESCs. *Development* **141**, 2376–2390 (2014).

52. Watanabe, A., Yamada, Y. & Yamanaka, S. Epigenetic regulation in pluripotent stem cells: a key to breaking the epigenetic barrier. *Philosophical Transactions of the Royal Society B: Biological Sciences* **368**, 20120292 (2013).

53. Waddington, C. H. *The Strategy of the Genes*. (Routledge, 2014).

54. Ferrell, J. E. Bistability, bifurcations, and Waddington's epigenetic landscape. *Curr Biol* **22**, R458–R466 (2012).

55. Apostolou, E. & Hochedlinger, K. Chromatin dynamics during cellular reprogramming. *Nature* **502**, 462–471 (2013).

56. Meshorer, E. *et al.* Hyperdynamic plasticity of chromatin proteins in pluripotent embryonic stem cells. *Dev Cell* **10**, 105–116 (2006).

57. Efroni, S. *et al.* Global transcription in pluripotent embryonic stem cells. *Cell Stem Cell* **2**, 437–447 (2008).

58. Nord, A. S. *et al.* Rapid and pervasive changes in genome-wide enhancer usage during mammalian development. *Cell* **155**, 1521–1531 (2013).

59. Whyte, W. A. *et al.* Master transcription factors and mediator establish super-enhancers at key cell identity genes. *Cell* **153**, 307–319 (2013).

60. Bernstein, B. E. *et al.* A bivalent chromatin structure marks key developmental genes in embryonic stem cells. *Cell* **125**, 315–326 (2006).

61. Lin, S.-C. *et al.* Epigenetic Switch between SOX2 and SOX9 Regulates Cancer Cell Plasticity. *Cancer Research* **76**, 7036–7048 (2016).

62. Gopi, L. K. & Kidder, B. L. Integrative pan cancer analysis reveals epigenomic variation in cancer type and cell specific chromatin domains. *Nat Commun* **12**, 1419 (2021).

63. Berdasco, M. & Esteller, M. Aberrant Epigenetic Landscape in Cancer: How Cellular Identity Goes Awry. *Developmental Cell* **19**, 698–711 (2010).

64. Aleksakhina, S. N., Kashyap, A. & Imyanitov, E. N. Mechanisms of acquired tumor drug resistance. *Biochimica et Biophysica Acta (BBA) - Reviews on Cancer* **1872**, 188310 (2019).

65. Chen, X., Chen, S. & Yu, D. Metabolic Reprogramming of Chemoresistant Cancer Cells and the Potential Significance of Metabolic Regulation in the Reversal of Cancer Chemoresistance. *Metabolites* **10**, 289 (2020).

66. Boumahdi, S. & de Sauvage, F. J. The great escape: tumour cell plasticity in resistance to targeted therapy. *Nat Rev Drug Discov* **19**, 39–56 (2020).

67. Pfister, S. X. & Ashworth, A. Marked for death: targeting epigenetic changes in cancer. *Nat Rev Drug Discov* **16**, 241–263 (2017).

68. Iyer, S. P. & Foss, F. F. Romidepsin for the Treatment of Peripheral T-Cell Lymphoma. *The Oncologist* **20**, 1084–1091 (2015).

69. Mann, B. S., Johnson, J. R., Cohen, M. H., Justice, R. & Pazdur, R. FDA Approval Summary: Vorinostat for Treatment of Advanced Primary Cutaneous T-Cell Lymphoma. *The Oncologist* **12**, 1247–1252 (2007).

70. Diesch, J. *et al.* A clinical-molecular update on azanucleoside-based therapy for the treatment of hematologic cancers. *Clinical Epigenetics* **8**, 71 (2016).

71. Ganesan, A., Arimondo, P. B., Rots, M. G., Jeronimo, C. & Berdasco, M. The timeline of epigenetic drug discovery: from reality to dreams. *Clinical Epigenetics* **11**, 174 (2019).

72. Subramanian, S., Bates, S. E., Wright, J. J., Espinoza-Delgado, I. & Piekarz, R. L. Clinical Toxicities of Histone Deacetylase Inhibitors. *Pharmaceuticals (Basel)* **3**, 2751–2767 (2010).

73. Lyko, F. & Brown, R. DNA Methyltransferase Inhibitors and the Development of Epigenetic Cancer Therapies. *JNCI: Journal of the National Cancer Institute* **97**, 1498–1506 (2005).

74. Ramaiah, M. J., Tangutur, A. D. & Manyam, R. R. Epigenetic modulation and understanding of HDAC inhibitors in cancer therapy. *Life Sciences* **277**, 119504 (2021).

75. Bender, C. M., Pao, M. M. & Jones, P. A. Inhibition of DNA methylation by 5-aza-2'-deoxycytidine suppresses the growth of human tumor cell lines. *Cancer Res* **58**, 95–101 (1998).

76. Jin, B. & Robertson, K. D. DNA methyltransferases, DNA damage repair, and cancer. *Adv Exp Med Biol* **754**, 3–29 (2013).

77. Chiappinelli, K. B. *et al.* Inhibiting DNA Methylation Causes an Interferon Response in Cancer via dsRNA Including Endogenous Retroviruses. *Cell* **162**, 974–986 (2015).

78. Han, C. Y., Patten, D. A., Richardson, R. B., Harper, M.-E. & Tsang, B. K. Tumor metabolism regulating chemosensitivity in ovarian cancer. *Genes Cancer* **9**, 155–175 (2018).

79. Gogola, E., Rottenberg, S. & Jonkers, J. Resistance to PARP Inhibitors: Lessons from Preclinical Models of BRCA-Associated Cancer. *Annual Review of Cancer Biology* **3**, 235–254 (2019).

80. Binnewies, M. *et al.* Understanding the tumor immune microenvironment (TIME) for effective therapy. *Nature Medicine* **24**, 541–550 (2018).

81. Tomasello, C. *et al.* Resistance to EGFR inhibitors in non-small cell lung cancer: Clinical management and future perspectives. *Critical Reviews in Oncology/Hematology* **123**, 149–161 (2018).

82. Hinohara, K. *et al.* KDM5 Histone Demethylase Activity Links Cellular Transcriptomic Heterogeneity to Therapeutic Resistance. *Cancer Cell* **34**, 939-953.e9 (2018).

83. Alcarraz-Vizán, G., Boren, J., Lee, W.-N. P. & Cascante, M. Histone deacetylase inhibition results in a common metabolic profile associated with HT29 differentiation. *Metabolomics* **6**, 229–237 (2010).

84. Yang, J. *et al.* Inhibiting histone deacetylases suppresses glucose metabolism and hepatocellular carcinoma growth by restoring FBP1 expression. *Sci Rep* **7**, (2017).

85. Wardell, S. E. *et al.* Glucose Metabolism as a Target of Histone Deacetylase Inhibitors. *Mol Endocrinol* **23**, 388–401 (2009).

86. Ferrari, A. *et al.* HDAC3 is a molecular brake of the metabolic switch supporting white adipose tissue browning. *Nature Communications* **8**, 93 (2017).

87. Song, S. *et al.* The HDAC3 enzymatic activity regulates skeletal muscle fuel metabolism. *J Mol Cell Biol* **11**, 133–143 (2019).

88. Egler, V. *et al.* Histone Deacetylase Inhibition and Blockade of the Glycolytic Pathway Synergistically Induce Glioblastoma Cell Death. *Clin Cancer Res* **14**, 3132–3140 (2008).

89. Faubert, B., Solmonson, A. & DeBerardinis, R. J. Metabolic reprogramming and cancer progression. *Science* **368**, (2020).

90. Lu, C. *et al.* Preparation and characterization of vorinostat-coated beads for profiling of novel target proteins. *Journal of Chromatography A* **1372**, 34–41 (2014).

91. Luengo, A., Gui, D. Y. & Vander Heiden, M. G. Targeting Metabolism for Cancer Therapy. *Cell Chem Biol* **24**, 1161–1180 (2017).

92. Kim, J. & DeBerardinis, R. J. Mechanisms and Implications of Metabolic Heterogeneity in Cancer. *Cell Metabolism* **30**, 434–446 (2019).

93. Kondo, H. *et al.* Single-cell resolved imaging reveals intra-tumor heterogeneity in glycolysis, transitions between metabolic states, and their regulatory mechanisms. *Cell Reports* **34**, 108750 (2021).

94. Jolly, M. K. & Celià-Terrassa, T. Dynamics of Phenotypic Heterogeneity Associated with EMT and Stemness during Cancer Progression. *J Clin Med* **8**, (2019).

95. Craene, B. D. & Berx, G. Regulatory networks defining EMT during cancer initiation and progression. *Nat Rev Cancer* **13**, 97–110 (2013).

96. Nieto, M. A., Huang, R. Y.-J., Jackson, R. A. & Thiery, J. P. EMT: 2016. *Cell* **166**, 21–45 (2016).

97. Shibue, T. & Weinberg, R. A. EMT, CSCs, and drug resistance: the mechanistic link and clinical implications. *Nat Rev Clin Oncol* **14**, 611–629 (2017).

98. Shah, P., Gau, Y. & Sabnis, G. Histone deacetylase inhibitor entinostat reverses epithelial to mesenchymal transition of breast cancer cells by reversing the repression of E-cadherin. *Breast Cancer Res Treat* **143**, 99–111 (2014).

99. Su, Y. *et al.* Epigenetic reprogramming of epithelial mesenchymal transition in triple negative breast cancer cells with DNA methyltransferase and histone deacetylase inhibitors. *Journal of Experimental & Clinical Cancer Research* **37**, 314 (2018).

100. Tang, H. M. *et al.* An epithelial marker promoter induction screen identifies histone deacetylase inhibitors to restore epithelial differentiation and abolishes anchorage independence growth in cancers. *Cell Death Discovery* **2**, 1–10 (2016).

101. Hu, Y., Nie, Q., Dai, M., Chen, F. & Wu, H. Histone Deacetylases Inhibit the Snail2-Mediated EMT During Metastasis of Hepatocellular Carcinoma Cells. *Front. Cell Dev. Biol.* **8**, (2020).

102. Rahimian, A., Barati, G., Mehrandish, R. & Mellati, A. A. Inhibition of Histone Deacetylases Reverses Epithelial-Mesenchymal Transition in Triple-Negative Breast Cancer Cells through a Slug Mediated Mechanism. *Mol Biol* **52**, 406–413 (2018).

103. Xiao, Q. *et al.* Histone deacetylase inhibitors promote epithelial-mesenchymal transition in Hepatocellular Carcinoma via AMPK-FOXO1-ULK1 signaling axis-mediated autophagy. *Theranostics* **10**, 10245–10261 (2020).

104. Jiang, G.-M. *et al.* Histone deacetylase inhibitor induction of epithelial–mesenchymal transitions via up-regulation of Snail facilitates cancer progression. *Biochimica et Biophysica Acta (BBA) - Molecular Cell Research* **1833**, 663–671 (2013).

105. Li, X. *et al.* Intrinsic resistance of tumorigenic breast cancer cells to chemotherapy. *J Natl Cancer Inst* **100**, 672–679 (2008).

106. Yu, F. *et al.* let-7 regulates self renewal and tumorigenicity of breast cancer cells. *Cell* **131**, 1109–1123 (2007).

107. Creighton, C. J. *et al.* Residual breast cancers after conventional therapy display mesenchymal as well as tumor-initiating features. *Proc Natl Acad Sci U S A* **106**, 13820–13825 (2009).

108. Tehranchi, R. *et al.* Persistent Malignant Stem Cells in del(5q) Myelodysplasia in Remission. *New England Journal of Medicine* **363**, 1025–1037 (2010).

109. Plaks, V., Kong, N. & Werb, Z. The Cancer Stem Cell Niche: How Essential Is the Niche in Regulating Stemness of Tumor Cells? *Cell Stem Cell* **16**, 225–238 (2015).

110. Carnero, A. *et al.* The cancer stem-cell signaling network and resistance to therapy. *Cancer Treat Rev* **49**, 25–36 (2016).

111.   Saygin, C., Matei, D., Majeti, R., Reizes, O. & Lathia, J. D. Targeting Cancer Stemness in the Clinic: From Hype to Hope. *Cell Stem Cell* **24**, 25–40 (2019).

112.   Takebe, N. *et al.* Targeting Notch, Hedgehog, and Wnt pathways in cancer stem cells: clinical update. *Nat Rev Clin Oncol* **12**, 445–464 (2015).

113.   Wainwright, E. N. & Scaffidi, P. Epigenetics and Cancer Stem Cells: Unleashing, Hijacking, and Restricting Cellular Plasticity. *Trends Cancer* **3**, 372–386 (2017).

114.   Dawson, M. A. The cancer epigenome: Concepts, challenges, and therapeutic opportunities. *Science* **355**, 1147–1152 (2017).

115.   Baba, T. *et al.* Epigenetic regulation of CD133 and tumorigenicity of CD133+ ovarian cancer cells. *Oncogene* **28**, 209–218 (2009).

116.   Yi, J. M. *et al.* Abnormal DNA methylation of CD133 in colorectal and glioblastoma tumors. *Cancer Res* **68**, 8094–8103 (2008).

117.   Lin, B. *et al.* Global analysis of H3K4me3 and H3K27me3 profiles in glioblastoma stem cells and identification of SLC17A7 as a bivalent tumor suppressor gene. *Oncotarget* **6**, 5369–5381 (2015).

118.   Marampon, F. *et al.* HDAC4 and HDAC6 sustain DNA double strand break repair and stem-like phenotype by promoting radioresistance in glioblastoma cells. *Cancer Lett* **397**, 1–11 (2017).

119.   Yang, W., Liu, Y., Gao, R., Yu, H. & Sun, T. HDAC6 inhibition induces glioma stem cells differentiation and enhances cellular radiation sensitivity through the SHH/Gli1 signaling pathway. *Cancer Lett* **415**, 164–176 (2018).

120.   Witt, A. E. *et al.* Identification of a cancer stem cell-specific function for the histone deacetylases, HDAC1 and HDAC7, in breast and ovarian cancer. *Oncogene* **36**, 1707–1720 (2017).

121.   Bora-Singhal, N. *et al.* Novel HDAC11 inhibitors suppress lung adenocarcinoma stem cell self-renewal and overcome drug resistance by suppressing Sox2. *Sci Rep* **10**, 4722 (2020).

122.   Yamazaki, J. *et al.* The epigenome of AML stem and progenitor cells. *Epigenetics* **8**, 92–104 (2013).

123.   Easwaran, H., Tsai, H.-C. & Baylin, S. B. Cancer epigenetics: tumor heterogeneity, plasticity of stem-like states, and drug resistance. *Mol Cell* **54**, 716–727 (2014).

124.   Hennessy, B. T. *et al.* Characterization of a naturally occurring breast cancer subset enriched in epithelial-to-mesenchymal transition and stem cell characteristics. *Cancer Res* **69**, 4116–4124 (2009).

125.   Wellner, U. *et al.* The EMT-activator ZEB1 promotes tumorigenicity by repressing stemness-inhibiting microRNAs. *Nat Cell Biol* **11**, 1487–1495 (2009).

126.   Keyvani-Ghamsari, S., Khorsandi, K., Rasul, A. & Zaman, M. K. Current understanding of epigenetics mechanism as a novel target in reducing cancer stem cells resistance. *Clinical Epigenetics* **13**, 120 (2021).

127.   Schech, A., Kazi, A., Yu, S., Shah, P. & Sabnis, G. Histone Deacetylase Inhibitor Entinostat Inhibits Tumor-Initiating Cells in Triple-Negative Breast Cancer Cells. *Mol Cancer Ther* **14**, 1848–1857 (2015).

128.   Hsu, C.-C. *et al.* Suberoylanilide hydroxamic acid represses glioma stem-like cells. *Journal of Biomedical Science* **23**, 81 (2016).

129.   Pastorino, O. *et al.* Histone Deacetylase Inhibitors Impair Vasculogenic Mimicry from Glioblastoma Cells. *Cancers (Basel)* **11**, (2019).

130.   McClure, J. J., Li, X. & Chou, C. J. Chapter Six - Advances and Challenges of HDAC Inhibitors in Cancer Therapeutics. in *Advances in Cancer Research* (eds. Tew, K. D. & Fisher, P. B.) vol. 138 183–211 (Academic Press, 2018).

131.   Kawaguchi, Y. *et al.* The deacetylase HDAC6 regulates aggresome formation and cell viability in response to misfolded protein stress. *Cell* **115**, 727–738 (2003).

132.   Kovacs, J. J. *et al.* HDAC6 regulates Hsp90 acetylation and chaperone-dependent activation of glucocorticoid receptor. *Mol Cell* **18**, 601–607 (2005).

133.   Krämer, O. H., Mahboobi, S. & Sellmer, A. Drugging the HDAC6-HSP90 interplay in malignant cells. *Trends Pharmacol Sci* **35**, 501–509 (2014).

134.   Ryu, H.-W. *et al.* HDAC6 deacetylates p53 at lysines 381/382 and differentially coordinates p53-induced apoptosis. *Cancer Lett* **391**, 162–171 (2017).

135.   Tien, S.-C. & Chang, Z.-F. Oncogenic Shp2 disturbs microtubule regulation to cause HDAC6-dependent ERK hyperactivation. *Oncogene* **33**, 2938–2946 (2014).

136.   Cosenza, M. & Pozzi, S. The Therapeutic Strategy of HDAC6 Inhibitors in Lymphoproliferative Disease. *Int J Mol Sci* **19**, (2018).

137.   Hai, Y. & Christianson, D. W. Histone deacetylase 6 structure and molecular basis of catalysis and inhibition. *Nature Chemical Biology* **12**, 741–747 (2016).

138.   Gawel, J. M. *et al.* PTG-0861: A novel HDAC6-selective inhibitor as a therapeutic strategy in acute myeloid leukaemia. *Eur J Med Chem* **201**, 112411 (2020).

139.   Santo, L. *et al.* Preclinical activity, pharmacodynamic, and pharmacokinetic properties of a selective HDAC6 inhibitor, ACY-1215, in combination with bortezomib in multiple myeloma. *Blood* **119**, 2579–2589 (2012).

140.   Amengual, J. E. *et al.* Dual Targeting of Protein Degradation Pathways with the Selective HDAC6 Inhibitor ACY-1215 and Bortezomib Is Synergistic in Lymphoma. *Clin Cancer Res* **21**, 4663–4675 (2015).

141.   Yee, A. J. *et al.* Ricolinostat plus lenalidomide, and dexamethasone in relapsed or refractory multiple myeloma: a multicentre phase 1b trial. *Lancet Oncol* **17**, 1569–1578 (2016).

142.   Lin, A. *et al.* Off-target toxicity is a common mechanism of action of cancer drugs undergoing clinical trials. *Science Translational Medicine* **11**, (2019).

143.   Huang, P. *et al.* Selective HDAC inhibition by ACY-241 enhances the activity of paclitaxel in solid tumor models. *Oncotarget* **8**, 2694–2707 (2016).

144.   Schäfer, C. *et al.* Class I histone deacetylases regulate p53/NF-κB crosstalk in cancer cells. *Cell Signal* **29**, 218–225 (2017).

145.   Bolden, J. E. *et al.* HDAC inhibitors induce tumor-cell-selective pro-apoptotic transcriptional responses. *Cell Death & Disease* **4**, e519–e519 (2013).

146.   Tiffon, C. E. *et al.* The histone deacetylase inhibitors vorinostat and romidepsin downmodulate IL-10 expression in cutaneous T-cell lymphoma cells. *British Journal of Pharmacology* **162**, 1590–1602 (2011).

147.   Sonnemann, J. *et al.* p53-dependent and p53-independent anticancer effects of different histone deacetylase inhibitors. *British Journal of Cancer* **110**, 656–667 (2014).

148.   Gryder, B. E. *et al.* Chemical genomics reveals histone deacetylases are required for core regulatory transcription. *Nature Communications* **10**, 3004 (2019).

149.   Thurn, K. T., Thomas, S., Raha, P., Qureshi, I. & Munster, P. N. Histone Deacetylase Regulation of ATM-Mediated DNA Damage Signaling. *Mol Cancer Ther* **12**, 2078–2087 (2013).

150. Yan, W. *et al.* Histone deacetylase inhibitors suppress mutant p53 transcription via histone deacetylase 8. *Oncogene* **32**, 599–609 (2013).
151. Chen, I.-C., Sethy, B. & Liou, J.-P. Recent Update of HDAC Inhibitors in Lymphoma. *Front. Cell Dev. Biol.* **8**, (2020).
152. Cortiguera, M. G. *et al.* Suppression of BCL6 function by HDAC inhibitor mediated acetylation and chromatin modification enhances BET inhibitor effects in B-cell lymphoma cells. *Sci Rep* **9**, 16495 (2019).
153. Hideshima, T. *et al.* Small-molecule inhibition of proteasome and aggresome function induces synergistic antitumor activity in multiple myeloma. *PNAS* **102**, 8567–8572 (2005).
154. Simms-Waldrip, T. *et al.* Targeting the Aggresome Pathway in Hematologic Malignancies. *Mol Genet Metab* **94**, 283–286 (2008).
155. Chun, P. Histone deacetylase inhibitors in hematological malignancies and solid tumors. *Arch Pharm Res* **38**, 933–949 (2015).
156. Rosato, R. R., Almenara, J. A. & Grant, S. The Histone Deacetylase Inhibitor MS-275 Promotes Differentiation or Apoptosis in Human Leukemia Cells through a Process Regulated by Generation of Reactive Oxygen Species and Induction of p21CIP1/WAF1 1. *Cancer Res* **63**, 3637–3645 (2003).
157. Jing, B. *et al.* Vorinostat and quinacrine have synergistic effects in T-cell acute lymphoblastic leukemia through reactive oxygen species increase and mitophagy inhibition. *Cell Death & Disease* **9**, 1–11 (2018).
158. Sanchez, G. J. *et al.* Genome-wide dose-dependent inhibition of histone deacetylases studies reveal their roles in enhancer remodeling and suppression of oncogenic super-enhancers. *Nucleic Acids Res* **46**, 1756–1776 (2018).
159. Conti, C. *et al.* Inhibition of histone deacetylase in cancer cells slows down replication forks, activates dormant origins, and induces DNA damage. *Cancer Res* **70**, 4470–4480 (2010).
160. Gaymes, T. J. *et al.* Histone Deacetylase Inhibitors (HDI) Cause DNA Damage in Leukemia Cells: A Mechanism for Leukemia-Specific HDI-Dependent Apoptosis? *Mol Cancer Res* **4**, 563–573 (2006).
161. Chen, L., Fischle, W., Verdin, E. & Greene, W. C. Duration of Nuclear NF-κB Action Regulated by Reversible Acetylation. *Science* **293**, 1653–1657 (2001).
162. Slaughter, M. J. *et al.* HDAC inhibition results in widespread alteration of the histone acetylation landscape and BRD4 targeting to gene bodies. *Cell Reports* **34**, 108638 (2021).
163. Kim, Y. J. *et al.* HDAC inhibitors induce transcriptional repression of high copy number genes in breast cancer through elongation blockade. *Oncogene* **32**, 2828–2835 (2013).
164. Vaid, R., Wen, J. & Mannervik, M. Release of promoter–proximal paused Pol II in response to histone deacetylase inhibition. *Nucleic Acids Research* **48**, 4877–4890 (2020).

Chapter 2: Metabolic Reprogramming by Histone Deacetylase Inhibition Selectively Targets NRF2-activated tumors.

2.1 Preface and Respective Contributions

This chapter consists of a manuscript that was recently submitted to *Cell Reports* and revisions are currently underway. I include this manuscript as part of my thesis as it represents the main part of my doctoral work. Many researchers contributed to this manuscript from various laboratories, including the Lu, Papagiannakopoulos and Ye laboratories. With guidance from my advisor and senior collaborators, I designed, performed and visualized all the experiments and analyses in this study, with the following exceptions: (1) the CRISPR/Cas9 genetic screen was designed by Franscisco Sånchez-Rivera and Yadira Soto-Feliciano and performed by Warren Wu of the Thales Papagiannakopoulos laboratory, (2) the LC-MS experiment was performed by Albert Li of the Ye laboratory and (3) the patient-derived xenografts were performed by Makiko Hayashi of the Thales Papagiannakopoulos laboratory. The manuscript was written by me and my advisor Chao Lu, with feedback from all listed authors.

2.2 Authorships and affiliations

Metabolic Reprogramming by Histone Deacetylase Inhibition Selectively Targets NRF2-activated tumors.

Dimitris Karagiannis[1], Warren Wu[2,*], Albert Li[3,*], Makiko Hayashi[2,*], Xiao Chen[1], Michaela Yip[1], Vaibhav Mangipudy[1], Xinjing Xu[1], Francisco J. Sánchez-Rivera[4,5], Yadira M. Soto-Feliciano[4,5], Jiangbin Ye[3], Thales Papagiannakopoulos[2,6], Chao Lu[1,7,#]

[1]Department of Genetics and Development, Columbia University Irving Medical Center, New York, NY 10032, USA.
[2]Department of Pathology, New York University Grossman School of Medicine, New York, NY 10016, USA.
[3]Department of Radiation Oncology, Stanford University School of Medicine, Stanford, CA 94305, USA.
[4]David H. Koch Institute for Integrative Cancer Research, Massachusetts Institute of Technology, Cambridge, MA 02142, USA.
[5]Department of Biology, Massachusetts Institute of Technology, Cambridge, MA 02142, USA.
[6]Laura and Isaac Perlmutter NYU Cancer Center, New York University Grossman School of Medicine, New York, NY 10016, USA.
[7]Herbert Irving Comprehensive Cancer Center, Columbia University Irving Medical Center, New York, NY 10032, USA.

* Equal contribution
# Corresponding Author: Chao Lu, PhD, Email: cl3684@cumc.columbia.edu

2.3 Abstract

Interplay between metabolism and chromatin signaling have been implicated in cancer initiation and progression. However, whether and how metabolic reprogramming in tumors generates specific epigenetic vulnerabilities remain unclear. Lung adenocarcinoma (LUAD) tumors frequently harbor mutations that cause aberrant activation of the NRF2 antioxidant pathway and

drive aggressive and chemo-resistant disease. We performed a chromatin-focused CRISPR screen and report that NRF2 activation sensitized LUAD cells to genetic and chemical inhibition of class I histone deacetylases (HDAC). This association was consistently observed across cultured cells, syngeneic mouse models and patient-derived xenografts. HDAC inhibition causes widespread increases in histone H4 acetylation (H4ac) at intergenic regions, but also drives re-targeting of H4ac reader protein BRD4 away from promoters with high H4ac levels and transcriptional downregulation of corresponding genes. Integrative epigenomic, transcriptomic and metabolomic analysis demonstrates that these chromatin changes are associated with reduced flux into amino acid metabolism and *de novo* nucleotide synthesis pathways that are preferentially required for the survival of NRF2-active cancer cells. Together, our findings suggest that metabolic alterations such as NRF2 activation could serve as biomarkers for effective repurposing of HDAC inhibitors to treat solid tumors.

2.4 Introduction

Eukaryotic cells have evolved sophisticated mechanisms to sense and integrate extracellular information into an intrinsic signaling system that regulates transcription so that environmental fluctuations can be delivered and responded to in a timely and accurate manner. A key player in the process is chromatin, as many chromatin-modifying reactions require not only the proteinaceous enzymes, but also small-molecule substrates/co-factors that are intermediates of central carbon metabolism. Indeed, it has been well-documented that chemical modifications of DNA and histones can act as sensors for fluctuations in cellular metabolic flux and in turn mediate the transcriptional response to maintain metabolic homeostasis[1]. Importantly, we and others have reported that these mechanisms can be hijacked by cancer cells to reprogram gene

expression and facilitate tumor progression[2–4]. It is less clear, however, if distinct metabolic

abnormalities also render cancer cells vulnerable to perturbations of chromatin regulatory

mechanisms. As a result, the therapeutic potential of targeting the crosstalk between chromatin

and metabolism remains under-explored.

Nearly 20% of lung adenocarcinoma (LUAD) tumors carry loss-of-function mutations in KEAP1

or gain-of-function mutations in NFE2L2 genes, both of which lead to activation of the NRF2

antioxidant response pathway5. Activation of this pathway conveys several tumor-promoting

properties to cells, including an increase in anabolic processes, production of antioxidants and

detoxifying enzymes5–7. These effects promote aggressive disease and drug resistance, which

makes NRF2-active tumors particularly hard to treat. Aberrant NRF2 activation also occurs in

other cancer contexts, such as head and neck squamous cell carcinoma and hepatocellular

carcinoma, through genetic and non-genetic mechanisms8,9. It has been reported that metabolic

reprogramming upon NRF2 activation confers sensitivity to glutaminase inhibition10,11.

However, the KEAPSAKE clinical trial (NCT04265534), which evaluated the efficacy of

glutaminase inhibitor CB-839 in patients with *KEAP1* mutation, was discontinued due to lack of

clinical benefit. As a result, identifying selective vulnerabilities of NRF2-active cancers that can

be exploited for more effective treatment remains a key challenge.

Similar to many cancer-associated metabolic alterations, previous reports have linked NRF2

activation to dysregulated chromatin state[12,13]. However, little is known about the underlying

mechanisms and their importance for therapy. In this study, we sought to test if metabolic

reprogramming by NRF2 activation confers potential chromatin-based vulnerabilities. Through a

chromatin-focused CRISPR-Cas9 genetic screen, we uncovered an NRF2-driven sensitivity to

Class I histone deacetylase (HDAC) inhibition and defined the underlying molecular basis using

integrative epigenomic, transcriptomic and metabolomics analysis. Our findings suggest that cancer cells harboring metabolic alterations may exhibit strong and specific dependencies on chromatin regulators that can be therapeutically exploited and highlight the potential of combinatorial targeting of metabolism and chromatin – two emerging and intimately linked cancer molecular hallmarks.

2.5 Results

2.5.1 NRF2 activation confers preferential vulnerability to loss of Class I HDACs.

To model and study NRF2 activation in LUAD, we used mouse lung adenocarcinoma cell lines derived from tumors generated through a genetically engineered mouse model (GEMM) of $Kras^{G12D/+}$;$p53^{-/-}$ driven lung adenocarcinoma. This system also enables CRISPR-Cas9 mediated knockout (KO) of a gene of interest such as $Keap1$[14]. As previously described, $Kras^{G12D/+}$;$p53^{-/-}$ (KP) and $Kras^{G12D/+}$;$p53^{-/-}$;$Keap1^{-/-}$ (KPK) tumors were generated using sgRNAs against $tdTomato$ (non-targeting control) or $Keap1$, respectively[10]. Thus, KPK cell lines represent tumor-derived cells with constitutively activated NRF2 pathway and KP cell lines serve as control cells with normal NRF2 activity.
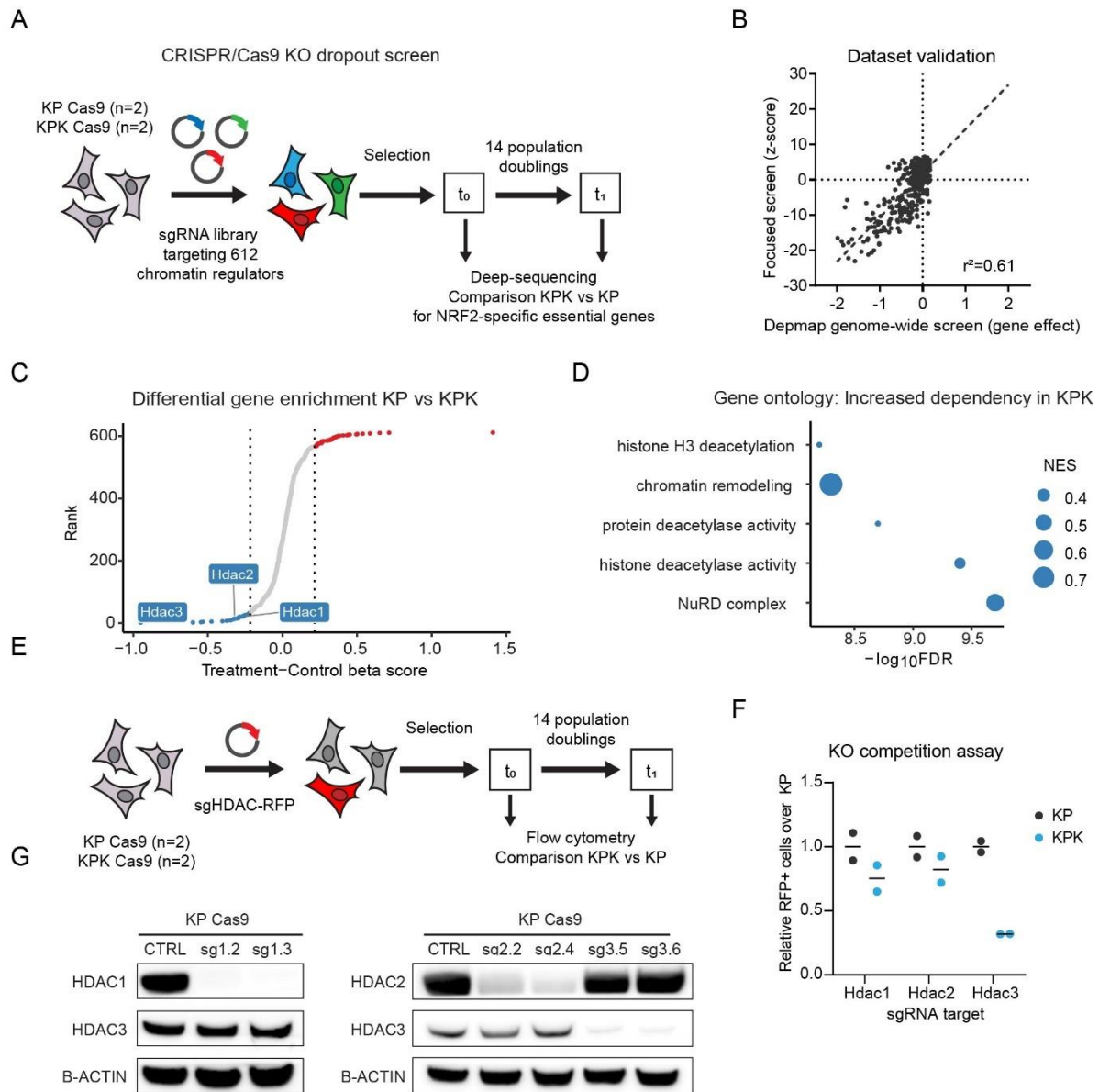
Figure 2.1. NRF2 activation confers preferential vulnerability to loss of Class I HDACs. A. Schematic of chromatin focused CRISPR/Cas9 genetic screen. **B.** Pearson correlation of gene z-score (KP cells t1 vs t0) of focused CRISPR/Cas9 screen to gene effect score of NSCLC cell lines (n=94) from CERES 21Q3 DepMap dataset. **C.** Scatter plot of genes ranked by beta-score (KPK-KP) and ontology analysis **(D)** of genes more essential in KPK cells. **E.** Schematic of competition assay employed to validate hits from the CRIPSR screen. **F**. Competition assay in KP (n=2) and KPK (n=2) cells to CRISPR/Cas9-mediated KO of HDAC genes and HDAC protein levels upon KO (**G**).

To identify novel chromatin vulnerabilities associated with NRF2 activation, we performed a targeted CRISPR-Cas9 genetic screen. KP and KPK cells were infected with a pool of single-guide RNAs (sgRNAs) targeting 612 chromatin regulators[15] and passaged for 14 population doublings (**Figure 2.1A**) . To confirm the quality of the screen, we compared the gene effect scores determined in this screen with that from genome-wide CRISPR-Cas9 screens in non-small cell lung cancer (NSCLC) cell lines from the DepMap database[16,17] and found strong correlation between the two datasets (**Figure 2.1B**). Genes more essential in the context of activated NRF2 were identified by comparing the decreases in the abundance of sgRNAs in KP vs. KPK cells over time. Notably, among genes that were essential in KP but not KPK cells the top hit was *Ube2m* (**Figure 2.S1A**), which is known to interact with the KEAP1 and Cullin-RING ligase (CRL) E3 ligase complex, and thus served as a positive control in our screen. Analysis of significantly depleted genes revealed multiple differential dependencies, including genes encoding Class I HDACs *Hdac1*, *Hdac2* and *Hdac3* which were synthetic lethal with *Keap1* loss (**Figures 2.1C-D, 2.S1B**). Consistent with this result, in a competition assay assessing the fitness of cell populations carrying various sgRNAs targeting HDAC genes, KPK cells were more sensitive than KP cells to the loss of HDAC1-3 (**Figures 2.1E-G**). Taken together, our results suggest that Class I HDAC genes are preferentially required for KPK cell viability and represent candidate therapeutic targets in the context of NRF2 activation.

2.5.2 NRF2 activation confers HDAC inhibitor sensitivity.

To To further validate the genetic screen results and investigate the therapeutic potential, we used another isogenic system with the overexpression of NRF2ΔNeh2, a gain-of-function truncated NRF2 mutant lacking the KEAP1 interacting domain[18] (**Figure 2.2A**). NRF2ΔNeh2

robustly induced NRF2 activation in KP cells (henceforth referred to as NRF2 overexpression), as indicated by stabilization of NRF2 protein levels and induction of NRF2 target gene expression (**Figures 2.2B-C**). In Cas9 expressing cells carrying empty (EV) or NRF2 overexpression introduction of sgRNA targeting Hdac3 showed significant difference in cell fitness as determined by a competition assay (**Figure 2.S2A**). This difference is in agreement with the comparison of KP to KPK but less pronounced, likely due to incomplete knock-out of Hdac3 (**Figure 2.S2B**).

Next we examined the effect of pharmacologic inhibition of HDACs on the viability of cells with activated NRF2. Consistent with the association between NRF2 activation and genetic dependency on Class I HDACs, NRF2ΔNeh2-expressing KP cells were more sensitive to several HDAC inhibitors with high specificity against class I HDACs[19] (**Figure 2.2D-E**). Notably, NRF2 activation did not alter sensitivity to pan-HDAC inhibitors (**Figure 2.2F**). Moreover, analysis of Depmap datasets indicated that *KEAP1*-mutant non-small cell lung cancer (NCLC) cell lines were on average more sensitive to class I HDAC inhibitors compared to wild-type cell lines, albeit not significantly (**Figure 2.S2C**), and not to pan-HDAC inhibitors (**Figure 2.S2D**). In further experiments we focused on the FDA-approved Class I HDAC inhibitor Romidepsin[20]. To ensure that this finding is not due to selective pressures of long-term NRF2 activation, we employed three additional experimental systems. To induce transient NRF2 activation, we either used KI696, a small molecule that disrupts the interaction between KEAP1 and NRF2, or a dox-inducible system of NRF2ΔNeh2 overexpression (**Figure 2.2G**). In both cases, we observed increased sensitivity to Romidepsin treatment. Moreover, we overexpressed KEAP1 in KPK cells and observed reduced NRF2 protein levels and resistance to Romidepsin
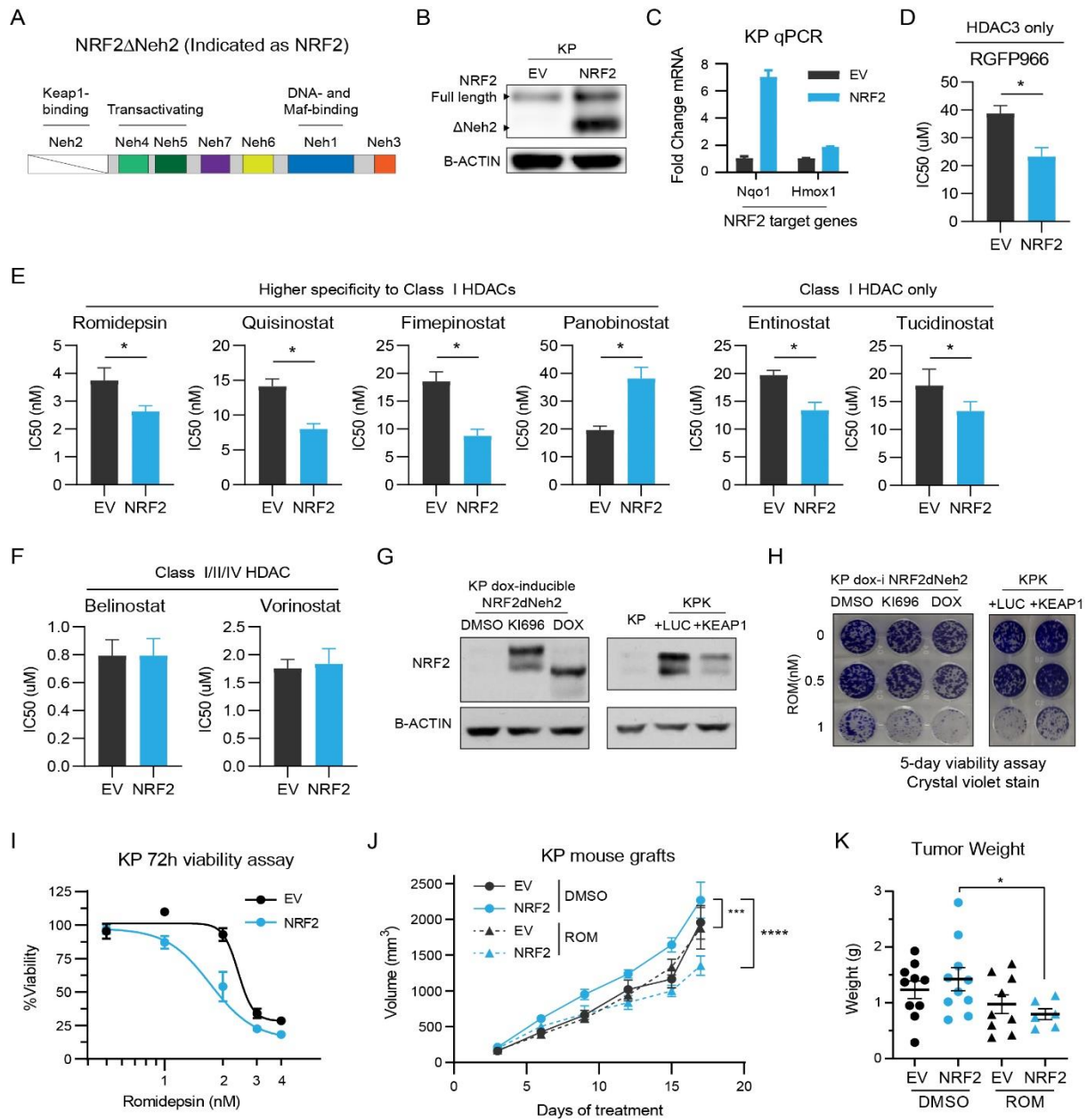
Figure 2.2. NRF2 activation confers HDAC inhibitor sensitivity. A. Schematic indicating domains of the NRF2ΔNeh2 over-active mutant isoforms of NRF2 protein. **B.** NRF2 protein levels upon of overexpression of NRF2ΔNeh2 in KP cells (NRF2). **C.** Expression of NRF2 target genes upon overexpression of NRF2ΔNeh2 in KP cells. **D-F.** Comparison of KP EV and NRF2 cells IC50s to various HDAC inhibitors derived from 3-day viability assays (error bars are confidence intervals). Specificity of HDAC inhibitors is indicated. **G.** NRF2 protein levels of KP cells carrying dox-inducible NRF2ΔNeh2 upon treatment with DMSO, KI696 or doxycycline (DOX) and of KPK cells overexpressing luciferase(LUC) or KEAP1. **H.** Viability assay of KP and KPK cells treated with the indicated concentrations for 5 days. **I.** Viability assay of KP cells treated with the indicated concentrations of Romidepsin for 72h. **J.** Growth of subcutaneous KP tumors in C57/BL6 mice treated with Romidepsin or vehicle, and tumor weight at the end of treatment (**K**).

(**Figures 2.2G-H**). Consistently, transient NRF2 overexpression was associated with lower IC50 to class I specific and not pan-HDAC inhibitors (**Figure 2.S2E**).

NRF2-active cells were significantly more sensitive to Romidepsin *in vitro,* relative to their KP controls (**Figure 2.2I**). Additionally, Romidepsin significantly suppressed the *in vivo* growth of KP tumors overexpressing NRF2ΔNeh2, but not control tumors (**Figures 2.2J-K**). siRNA mediated silencing of Hdac3 in conjunction with Romidepsin treatment indicated that the NRF2-specific effect of Romidepsin is mediated primarily through Hdac3 inhibition (**Figures 2.S2E-G**).

HDAC inhibitors are associated with DNA damage and programmed cell death[21–23]. To assess apoptosis and DNA damage levels, we looked at phosphorylation of H2A.X (γH2AX) and cleaved caspase 3 upon Romidepsin treatment at a concentration where NRF2-activated cells showed increased sensitivity (**Figure 2.S2C**). Results indicate modest increase in DNA damage and apoptosis, which were similar between EV and NRF2 cells, suggesting that the observed differences in Romidepsin sensitivity are not due to increased DNA damage and/or apoptosis (**Figure 2.S2D**).

2.5.3 Romidepsin alters gene expression by genomic redistribution of histone acetylation and BRD4.

Class I HDACs are major regulators of histone acetylation. To investigate how HDAC inhibition affects histone acetylation to reprogram gene expression, we performed CUT&Tag[24] upon Romidepsin treatment to profile genomic distribution of histone acetylation marks H3K27ac and H4ac (poly-acetylation on H4K5, H4K8, H4K12, H4K16), as well as BRD4, a histone acetylation reader protein that activates gene transcription, in replicates (**Figure 2.S3A**). We also

performed RNA-sequencing and integrated the epigenomic datasets to correlate changes in histone acetylation landscape to differential gene expression.

HDAC inhibition with Romidepsin induced broad gene expression changes including decreased expression of 1,692 genes (**Figure 2.3A**), which were highly concordant between control and NRF2-active cells (**Figure 2.S3B**). CUT&Tag of HDAC2 indicated similar genomic distribution between EV and NRF2 cells (**Figures 2.S3C-D**), which suggests that class I HDAC activity is not affected by NRF2 activation and is in agreement with the observed similarity in transcriptional response to Romidepsin.

As expected, Romidepsin induced global increase in histone acetylation levels, while BRD4 levels were largely unchanged (**Figure 2.S3E**). We first assessed how genome-wide histone acetylation and BRD4 distributions were affected by HDAC inhibition. We annotated genomic features of H4ac and BRD4 peaks and found that Romidepsin induced a redistribution of peaks from promoters to distal intergenic regions (**Figure 2.3B**). Consistently, H4ac signal and BRD4 binding at promoter-associated peaks were reduced following Romidepsin treatment (**Figure 2.3C**). Furthermore, we measured H4ac reads at peaks vs. random genomic regions and observed that upon Romidepsin treatment H4ac was reduced at peaks and increased in random regions (**Figure 2.3D**). Indeed, Romidepsin treatment led to a >2-fold decrease in the ratio of H4ac peak signal over genome average (**Figure 2.3D**). Finally, we found that the initial levels of H4ac and BRD4 enrichment correlated with the degree of loss in H4ac and BRD4 binding following Romidepsin treatment (**Figures 2.3E, 2.S3F**). Together, these results suggest a model where HDAC inhibition alters the ratio between the abundance of H4ac at promoter-associated

41
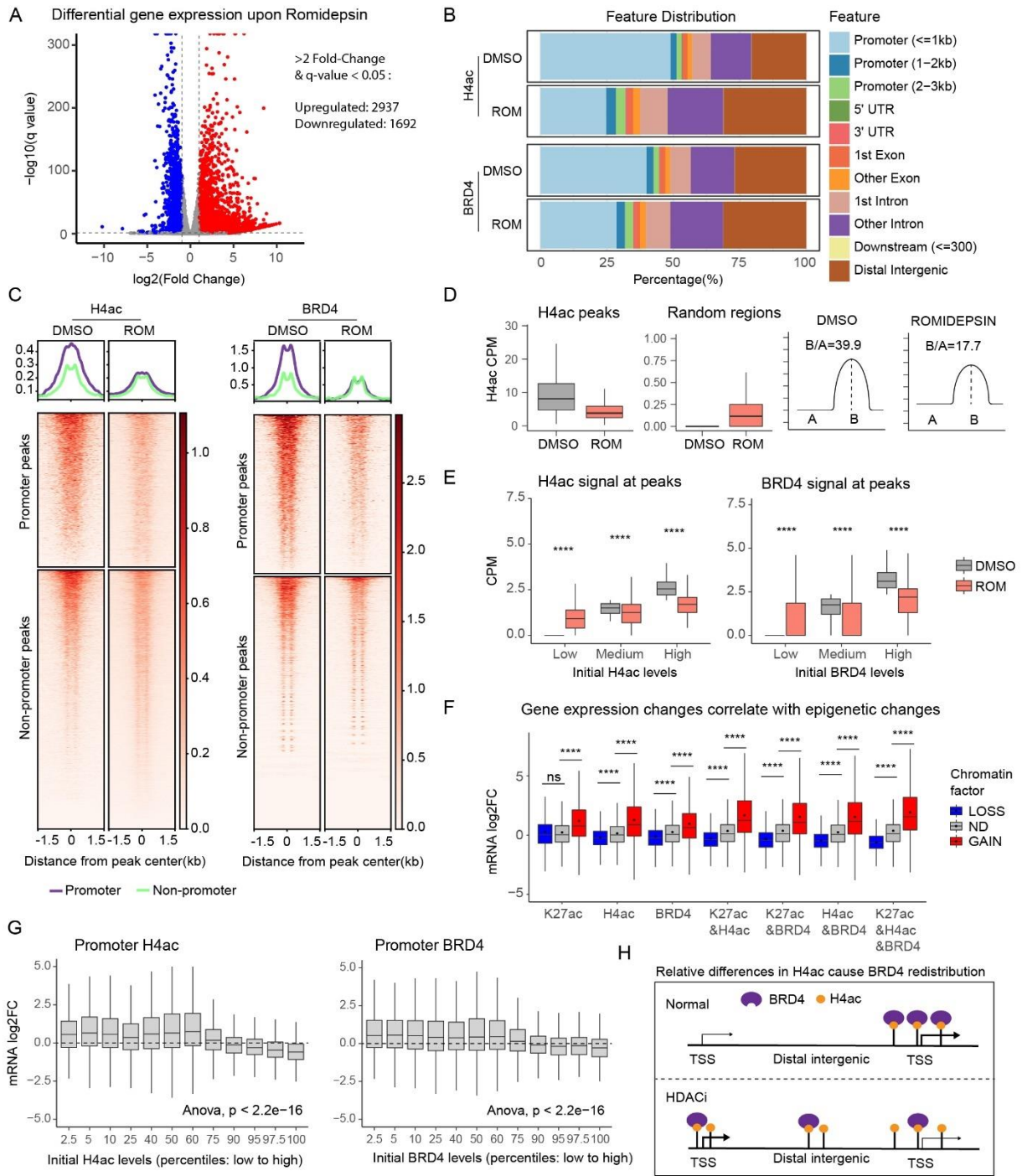
Figure 2.3. Romidepsin alters gene expression by genomic redistribution of histone acetylation and BRD4. A. Volcano plot of differential gene expression upon Romidepsin treatment (5nM, 16h) of KP NRF2 cells. **B**. Distribution of called H4ac and BRD4 peaks (n=2) across genomic features. **C**. Heatmaps of histone acetylation signal at peaks that do or do not overlap with promoters (within 2.5 from a TSS). **D**. Box plots of read counts per million (CPM) at called peaks or random regions and illustrations indicating the ratio of signal at peaks compared to background (random regions). **E.** Box plots of read CPM at consensus peaks with low, medium or high levels at DMSO treatment (cutoff: peaks were ranked by CPM and split into thirds; one out of two replicates shown). **F**. Fold-change expression (ROM/DMSO; DEseq2 analysis of RNA-seq) of genes that gain, lose, or have no difference (ND) in promoter histone acetylation and/or BRD4 binding (cutoff: 1.5-fold change). **G**. Fold-change expression (as in **F**) of genes with variable initial levels of H4ac and BRD4 binding (promoters were ranked by CPM and split into percentiles; average of two replicates shown). **H**. Illustration of how HDAC inhibition can cause gene expression changes by displacing and diffusion of BRD4 binding due to global gain of H4ac.

peaks and at distal intergenic regions, which in turn dilutes BRD4 binding at H4ac-high promoters (**Figure 2.3H**).

Importantly, these relative changes in histone acetylation, particularly H4ac, and BRD4 binding at gene promoters correlated strongly with changes in gene expression (**Figure 2.3G**). Consistently, genes with high levels of H4ac and BRD4 binding at promoters also showed the largest degree of decrease in expression following HDAC inhibition (**Figure 2.3G**). We also measured absolute (with spike-in normalization) changes in H3K27ac, H4ac and BRD4 (**Figures 2.S3G-H**). When adjusting histone acetylation signal based on total abundance, there was increased histone acetylation associated with both upregulated and downregulated genes (**Figure 2.S3G**), indicating poor correlation with gene expression changes. Therefore, the relative changes in H4ac appear to be a major driver of BRD4 re-targeting and transcriptomic changes. Overall, these results suggest that Romidepsin induces gene expression changes, primarily as a result of broad redistribution of H4ac and BRD4 binding. In particular, we find diffusion of H4 acetylation away from promoters and highly acetylated peaks. Previous report suggests that BRD4 distribution is affected similarly to relative H4ac changes, including displacement from gene promoters[25]. Indeed, we found that genome-wide changes in BRD4 binding correlated well with H4ac changes and to a less degree H3K27ac (**Figure 2.S3I**). This suggests a model where HDAC inhibition induces redistribution of BRD4 driven by changes in relative H4ac levels and alters gene expression (**Figure 2.3H**).

2.5.4 Romidepsin regulates expression of genes that represent known and novel metabolic vulnerabilities of NRF2-active cells.

Since Romidepsin induced similar transcriptomic changes in control and NRF2 active cells (**Figure 2.S3B**) but showed preferential toxicity towards NRF2 active cells, we reasoned that the differentially expressed genes could affect pathways that are more essential for NRF2-active cell viability. To explore this hypothesis, we first examined if known vulnerabilities of KEAP1 loss and NRF2 activation are transcriptionally regulated by Romidepsin. It has been well documented that NRF2 activation is associated with a specific dependency on glutamine uptake and catabolism[10,11,26]. In addition, NRF2 activation has been shown to promote serine and glycine biosynthesis and dependency[27,28]. Therefore, we examined expression of genes involved in glutamine uptake[29]/metabolism and serine/glycine biosynthesis pathway. We found that Romidepsin induced downregulation of these genes *in vitro* (**Figures 2.4A**, **2.S4A**). Moreover, Romidepsin treatment *in vivo* led to a reduction in protein levels of ATF4, a master transcriptional regulator of amino acid metabolism (**Figures 2.S4B-C**). In contrast, we did not find consistent gene expression changes in glycolysis, TCA cycle and NRF2 target genes (**Figure 2.4A**).

We next analyzed the CERES genome-wide CRISPR screen dataset of human cell lines from the DepMap database[16,17]. We identified genes that represent specific dependencies for *KEAP1*-mutant NSCLC cell lines and intersected them with the genes downregulated by Romidepsin (**Figure 2.4B**). Gene ontology revealed enrichment in MYC targets (**Figure 2.4C**), including *Myc* itself and its target genes involved in purine and pyrimidine synthesis (**Figure 2.S4D**). Using a competitive cell proliferation assay, we confirmed that genetic knock-out of *Myc* and several *de novo* nucleotide synthesis genes was more detrimental to the survival of KP

44
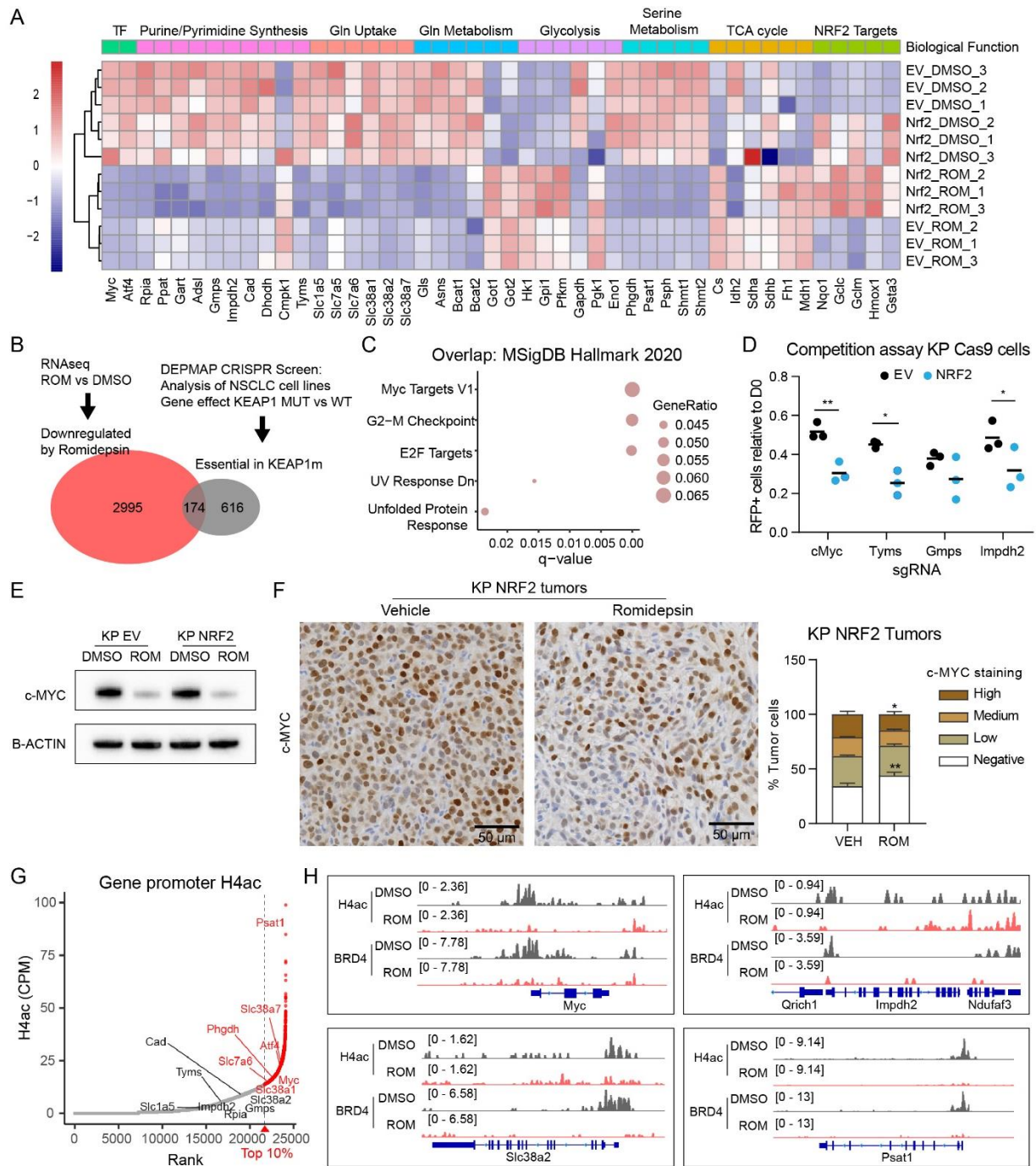
Figure 2.4. Romidepsin regulates expression of genes that represent known and novel metabolic vulnerabilities of NRF2-active cells. A. Heatmap showing expression of metabolic genes (RNA-seq; normalized by DEseq2 and scaled for each gene). **B**. Venn diagram showing overlap between genes downregulated by Romidepsin (cutoff: 1.5-fold change and FDR<0.05) in KP NRF2 cells and genes that are more essential in KEAP-mutant NSCLC cell lines from the CERES DepMap dataset (cutoff: 0.05 gene effect difference), and MsigDB Hallmark ontology of the overlapping genes (**C**). **D**. Competition assay showing fraction of RFP+ KP Cas9 cells after 14 population doublings, indicating percentage of cells that carry sgRNA against the indicated genes (n=3). **E**. Western blot showing levels of c-MYC and H4ac upon Romidepsin treatment of KP cells (5nM for 24h). **F**. Immunohistochemistry (IHC) staining of c-MYC and quantitation in KP NRF2 tumors after 17 days of treatment with DMSO or Romidepsin (related to figure 2G-H). **G**. Rank plot of gene promoter H4ac (relevant metabolic genes are noted). **H**. Bedgraphs of H4ac and BRD4 binding at indicated gene loci.

cells with NRF2 activation (**Figures 2.4D, S4E**). Furthermore, Romidepsin reduced MYC protein levels *in vitro* and *in vivo* (**Figures 2.4A, 2.4E-F, 2.S4F**).

Taken together, our results suggest that Romidepsin induces downregulation of several metabolic genes that are more essential for the survival of cells with NRF2 activation. CRISPR/Cas9-mediated knock-out of Hdac3 in KP cells led to downregulation of most of these metabolic genes (**Figure 2.S4G-H**). Importantly, several of these genes have high levels of promoter H4ac (**Figure 2.4H**). In agreement with our global analyses (**Figure 2.3E**), we found loss of H4ac and BRD4 binding at the promoters of these genes upon Romidepsin treatment (**Figures 2.4G, 2.S4I**). Overall, these findings suggest that the epigenetic reprogramming induced by Romidepsin leads to downregulation of genes involved in known and novel NRF2-specific metabolic vulnerabilities.

2.5.5 Romidepsin disrupts metabolic processes that are essential for NRF2-active cells.

To examine how Romidepsin-induced changes in metabolic gene expression affect metabolic flux, we performed targeted metabolite tracing analysis. KP cells with or without NRF2 activation were treated with DMSO, Romidepsin or the glutaminase inhibitor CB-839 for 24 hours, and then cultured in ^{13}C-glucose for 1 and 24 hours, or ^{13}C-glutamine for 8 hours before harvesting (**Figures 2.5A-B, 2.S5A-B**). Glutamine tracing indicated that in Romidepsin-treated but not CB-839-treated cells, the proportion of ^{13}C-labeled glutamine was reduced, indicating reduced glutamine uptake (**Figure 2.5C**). Consistent with this finding, media glutamine consumption was reduced upon Romidepsin treatment (**Figure 2.S5C**). Romidepsin treatment also reduced ^{13}C incorporation into further steps of glutamine metabolism (**Figure 2.5D**; M+5 glutamate, M+3 αKG). Interestingly, in NRF2-active cells, Romidepsin and CB-839
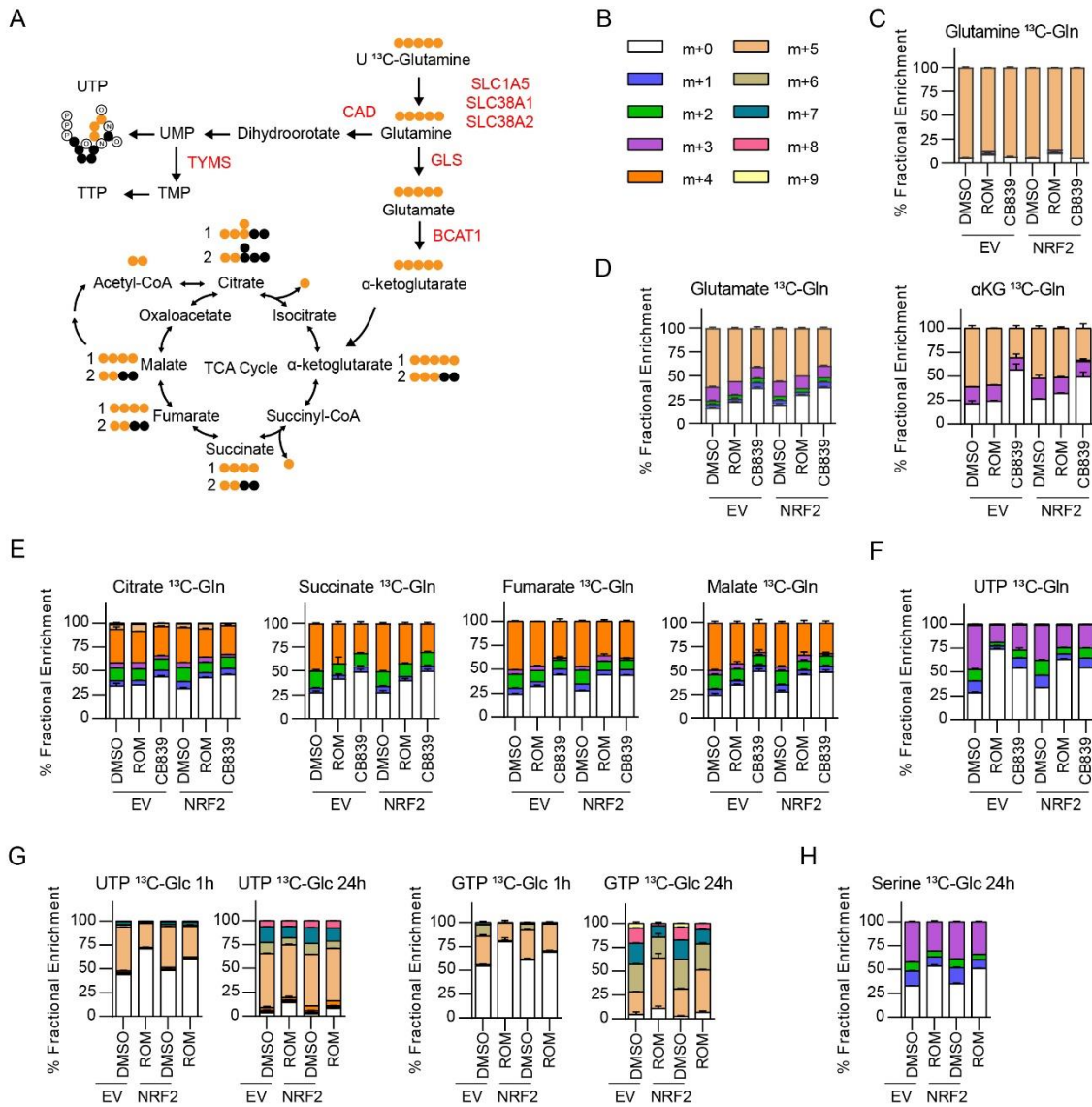
Figure 2.5. Romidepsin disrupts metabolic processes that are vulnerable in NRF2-active cells. A. Schematic indicating glucose and glutamine metabolic processes, labeled glutamine carbon contribution and genes that are downregulated upon Romidepsin treatment. **B.** Color indications of isotopologues. **C-F.** Bar graphs showing isotopologue percentages for the indicated metabolites after U-13C glutamine tracing for 8h. **G-H.** Bar graphs showing isotopologue percentages for the indicated metabolites after U-13C glucose tracing for the indicated time.

had a comparable effect on reducing glutamine-derived ^{13}C incorporation into TCA cycle metabolites (**Figure 2.5E;** M+4 citrate, M+4 succinate, M+4 fumarate, M+4 malate). In addition, we found strongly reduced incorporation of glutamine in pyrimidine nucleotides (**Figure 2.5F;** M+1, +2 and +3 UTP), which suggests a disruption of *de novo* nucleotide synthesis. While glycolysis has been reported to be suppressed by HDAC inhibition in other tumor models[30,31], we didn't find this to be the case in our experimental system (**Figures 2.S5D-E**), in agreement with our gene expression data (**Figure 2.4A**). However, we did find reduced incorporation of glucose-derived ^{13}C in purine and pyrimidine nucleotides (**Figure 2.5G**; 1h M+5 UTP, 24h M+6 and +7 UTP, 1h M+5 and +6 GTP, 24h M+7, +8 and +9 GTP), again consistent with the gene expression results, and indicates reduced rate of *de novo* nucleotide synthesis. Moreover, we found reduced incorporation of glucose-derived ^{13}C into serine, which suggests a possible defect in serine biosynthesis (**Figure 2.5H**; M+1, +2 and +3).

Overall, these metabolomic results suggest that Romidepsin disrupts key metabolic processes (serine/glutamine metabolism and *de novo* nucleotide synthesis) that support viability in NRF2-active cells. Specifically, Romidepsin disrupts glutamine flux into the TCA cycle in a similar manner to glutaminase inhibition, which underlies the NRF2-specific sensitivity to glutaminase inhibitor[11].

2.5.6 Glutamine metabolism suppression underlies the NRF2-specific effect of Romidepsin on cell growth.

Our findings suggest that glutamine uptake and utilization is a major aspect of the NRF2-specific effect of Romidepsin in cell viability. To further investigate this, we overexpressed SLC1A5, an amino acid transporter with higher affinity for glutamine, in KP EV and NRF2 cells (**Figure 2.6A**). SLC1A5 overexpression did not affect expression of other metabolic genes or NRF2 pathway activation (**Figures 2.6A-B**). Moreover, SLC1A5 overexpression in KP NRF2 cells

restored Romidepsin sensitivity to EV levels and had no significant effect in EV cells (**Figures 2.6C, 2.S6A**). Similarly, Romidepsin treatment of subcutaneous tumors had a significant effect on KP NRF2 tumor growth, but no significant effect in NRF2 tumors overexpressing SLC1A5 and EV tumors with and without SLC1A5 overexpression (**Figures 2.5D-E**). These results suggest that suppression of glutamine utilization mediates the NRF2-specific effect of Romidepsin on cell viability.

In agreement with this notion, Romidepsin treatment *in vivo* showed similar efficacy to CB-839 (**Figures 2.6F-G, S6B-C**). Interestingly, the combination of Romidepsin and CB-839 resulted in improved tumor response than either treatment alone (**Figures 2.6F-G, S6B-C**), without a significant effect on mouse weight (**Figure 2.S6D**). When we performed the chromatin-focused CRISPR/Cas9 screen in the context of CB-839 treatment we found that Hdac3 remained more essential in KPK cells compared to KP (**Figure 2.6I**). Next, we generated CB-839 resistant cell lines by treating NRF2 overexpressing cells with increasing doses of CB-839 up to 500nM for 2 weeks (**Figures 2.6J, 2.S6E**). Gene expression profiling by RNA-seq indicated few gene expression changes between control (DMSO-treated) and CB-839 resistant KP NRF2 cells, suggesting that resistance is mediated through other mechanisms, such as metabolic rewiring (**Figure 2.6K**). In addition, none of the metabolic genes that are downregulated by Romidepsin were differentially expressed. Control and CB-839 resistant cells showed similar response to Romidepsin treatment in vitro (**Figures 2.6L, 2.S6F**). Overall, these results suggest that the mechanisms of glutamine metabolism and growth inhibition by
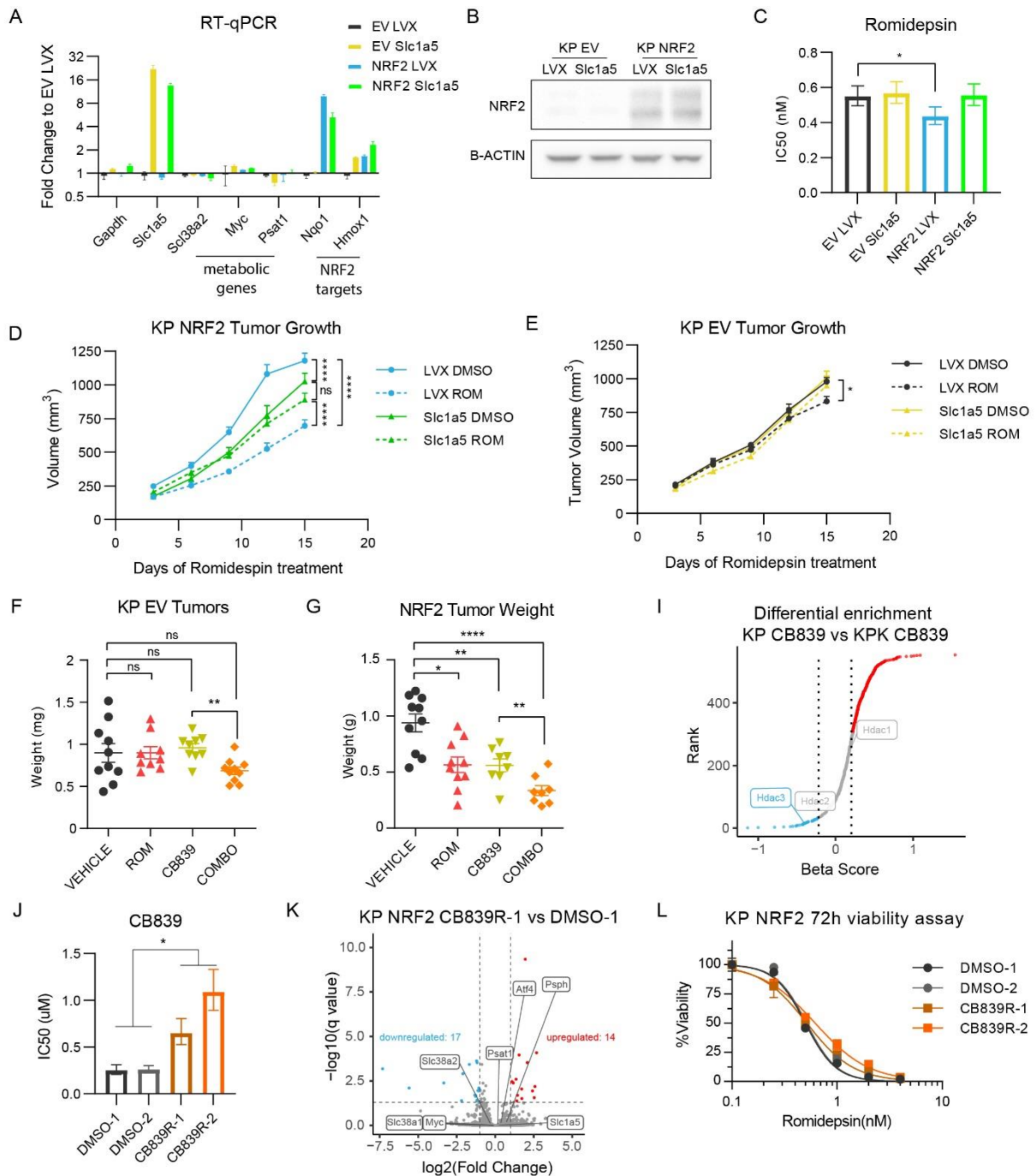
Figure 2.6. Glutamine metabolism suppression underlies the NRF2-specific effect of Romidepsin on cell growth.
A. Expression of indicated genes in KP EV and NRF2 cells carrying empty vector (LVX) or Slc1a5 overexpression. **B**. Western blot indicating protein levels of NRF2 after Slc1a5 overexpression. **C**. Romidepsin IC50 of KP cells transduced with empty vector (LVX) or overexpressing Slc1a5 (SLC1A5); error bars represent 95% confidence interval. **D-E**. Growth of subcutaneous KP EV and NRF2 tumors carrying empty vector (LVX) or Slc1a5 overexpression in C57/BL6 mice treated with Romidepsin (Statistical significance determined by two-way Anova). **F-G**. Weights of KP EV and NRF2 tumors treated as indicated for 2 weeks (Significance determined by Mann-Whitney U-test). **I**. CRISPR/Cas9 focused screen scatter plot of genes ranked by beta-score of KPK - KP cells treated with CB839 for 14 population doublings (as in Figure 1A). **J**. CB839 IC50 of KP NRF2 control (DMSO-1 and -2) and CB839-resistant cell lines (error bars represent 95% confidence interval). **K**. Differential gene expression analysis of KP NRF2 CB839-resistant cells to control (cuttoff: 2-fold change). **L**. Viability assay of KP NRF2 control (DMSO) and CB839-resistant cell lines to Romidepsin treatment.

50

Romidepsin and CB-839 are distinct, which supports the rationale for HDAC glutaminase inhibition combinations in NRF2-active cancer.

2.5.7 NRF2-activation confers sensitivity to HDAC inhibition in human cells and patient-derived xenografts (PDX).

To if the association between NRF2 activation and HDAC inhibitor sensitivity is conserved in human cells, we used the *KEAP1*-mutant LUAD cell line A549 and targeted *NFE2L2* using the CRISPR/Cas9 system, which led to a partial reduction in NRF2 protein levels and NRF2 target gene expression (**Figures 2.7A-B**), without affecting proliferation *in vitro*. Consistent with our findings in the murine cell lines, Romidepsin suppressed expression of *MYC*, *ATF4* and several genes involved in *de novo* nucleotide synthesis, glutamine transport and serine synthesis (**Figures 2.7C-D**). In addition, siRNA-mediated silencing of *HDAC3* in A549 cells led to downregulation of several genes involved in glutamine uptake, and de novo nucleotide and serine synthesis (**Figure 2.S7A**). NRF2 WT A549 cells were more sensitive to Romidepsin than NRF2 KO cells *in vitro* (**Figure 2.7E**) and *in vivo* (**Figures 2.7F, 2.S7B**). Additionally, induction of NRF2 activation in the *KEAP1* wild-type cell line NCI-H2009 cell line by overexpression of KEAP1[R470C], a dominant negative mutant form of KEAP1[32], led to increased sensitivity to Romidepsin (**Figures 2.S7C-D**). In patient-derived xenografts of *KEAP1* wild-type (WT) or mutant tumors, that were generated as previously described[10], Romidepsin treatment caused earlier and stronger suppression of growth in NRF2-active tumors (**Figures 2.7G-H, 2.S7E**), as well as reduction in c-MYC levels (**Figure 2.S7F**). Finally, A549 xenograft tumors were sensitive to the combination of Romidepsin and CB-839 (**Figures 2.7I-J**). These results show that the phenotype and mechanism of HDAC inhibition we described in murine LUAD can be
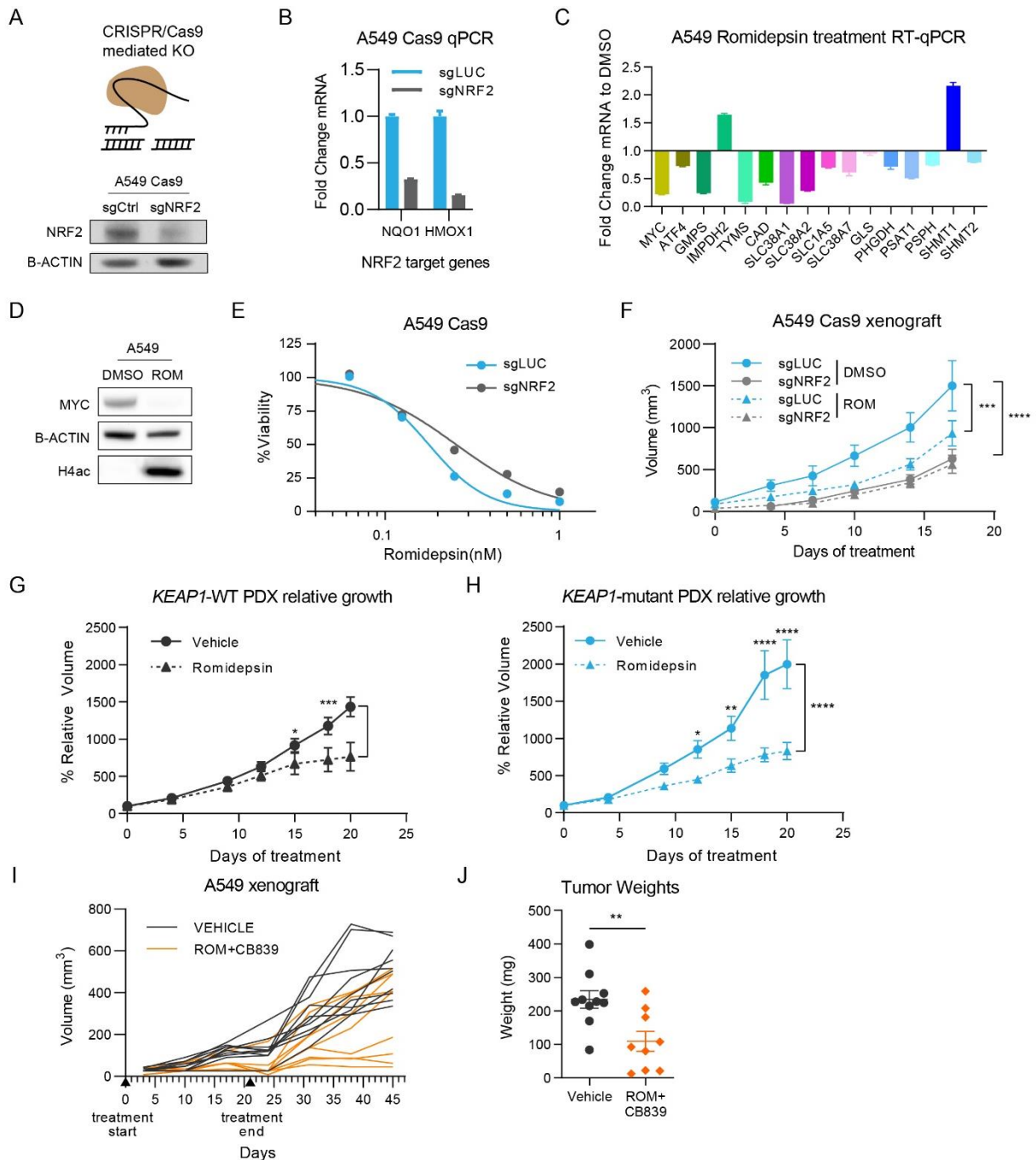
Figure 2.7. NRF2-activation confers sensitivity to HDAC inhibition in human cells and patient-derived xenografts (PDX).
A. Schematic of CRISPR-mediated KO of NRF2, and NRF2 protein levels upon of NRF2 KO in a population of A549 cells (sgNRF2). **B**. Expression of NRF2 target genes upon NRF2 KO in A549 cells. **C**. Fold-Change expression of indicated genes upon Romidepsin treatment of A549 cells determined by RT-qPCR. **D**. Western blot showing levels of MYC and H4ac upon Romidepsin treatment of A549 cells 0.5nM for 24h. **E**. Viability assay of A549 cells treated with the indicated concentrations of Romidepsin for 72h. **F**. Growth of subcutaneous A549 tumors in nude mice treated with Romidepsin or vehicle. **G-H**. Relative growth curves of PDX tumors that are wild-type or mutant for *KEAP1* treated with vehicle or Romidepsin. **I**. Longterm growth of A549 subcutaneous tumors treated with Romidepsin/CB839 combination or vehicle and (**J**) tumor weights at endpoint.

extrapolated to human settings and provide pre-clinical evidence of Romidepsin as a potential therapeutic for LUAD with NRF2-activation.

2.6 Discussion

In this study, we used a focused CRISPR/Cas9 genetic screen to identify chromatin vulnerabilities driven by NRF2 activation in LUAD. We identified a preferential dependency on Class I HDAC genes, which translated to increased sensitivity to the Class I HDAC inhibitor Romidepsin. Following HDAC inhibition, global hyperacetylation of the genome displaces transcription co-activators such as BRD4 from genes with high levels of histone acetylation, such as those involved in cell metabolism. As a result, we observed reduced rate of glutamine uptake/catabolism as well as *de novo* nucleotide synthesis which imposed selective metabolic stress on NRF2-active cancer cells, causing anti-tumor effects that can be observed *in vitro* and *in vivo* using human NSCLC cell lines and patient-derived xenografts.

These preclinical findings have several mechanistic and translational implications. First, targeting of KEAP1/NRF2 alterations in cancer remains a key clinical priority. NRF2 hyperactivation promotes aggressive tumor growth and resistance to chemotherapy, radiation and immunotherapy, leading to poor patient prognosis. A number of therapeutic strategies have been explored, including small molecules targeting NRF2 itself or its interaction with KEAP1[32,33], tumor immune-modulating agents[34,35], and inhibiting metabolic pathways as synthetic lethal events[10,11,27,36]. In particular, inhibitors of glycolysis and glutaminolysis have shown promising effects in preclinical models[10,36,37], as NRF2 activation causes significant changes to central carbon and amino acid metabolism. Nevertheless, the glutaminase inhibitor CB-839 as monotherapy has shown limited success in treating *KEAP1* mutant NSCLC in clinical trials. Our study suggests that repurposing the FDA-approved HDAC inhibitor Romidepsin could represent

another synthetic lethal approach to target NRF2-active tumors. Our *in vivo* study suggests that Romidepsin has similar efficacy as CB-839 and the combination of both inhibitors offers additional therapeutic effects. Moreover, our in vitro experiments suggest that Romidepsin remains an effective treatment of CB-839 resistant cells. These results provide strong preclinical rationale for evaluating Romidepsin, alone or combined with CB-839, for treating NSCLC or other tumor types harboring dysregulated KEAP1/NRF2 pathway. In addition to glutamine metabolism, our epigenome and transcriptome analysis also identified *de novo* nucleotide synthesis as a novel metabolic vulnerability of NRF2-active cancer cells, which was confirmed by metabolomic and functional studies. Future efforts are required to evaluate the efficacy of inhibiting nucleotide synthesis, such as inhibitors of dihydroorotate dehydrogenase (DHODH), in treating NRF2 hyperactive tumors.

Mechanistically, our multi-omics analysis revealed that the impact of Romidepsin on histone acetylation, particularly H4ac, is more complex than previously reported. Specifically, the genome-wide modest gain in diffuse H4ac signal drives a relative loss of H4ac at strong promoter peaks. This redistribution in H4ac was associated with concomitant changes in BRD4 binding and gene expression. These findings are in agreement with a recent report[24] and suggest that the initial chromatin state can be predictive of the epigenetic and transcriptional effects of HDAC inhibition. Transcriptomic and metabolomic analysis indicated that HDAC inhibition suppressed metabolic gene expression and activity in LUAD cells. Specifically, we found disruption of pathways that support viability and growth during NRF2 activation, including purine and pyrimidine synthesis, glutamine uptake and hydrolysis, serine synthesis, and the TCA cycle. The paradigm of metabolic gene expression modulation by epigenetic perturbation has been described in several other contexts, including *KMT2D*-deficient lung cancer[38], H3K27-

mutant glioma[39] and childhood posterior fossa group A ependymomas[40]. In addition, dependency on transcriptional regulation of serine and nucleotide synthesis has been described in AML[41]. Future studies are warranted to investigate how chromatin abnormality can be hijacked by cancer cells to transcriptionally reprogram metabolism and if combined targeting of chromatin and metabolism represents an effective therapeutic strategy in additional settings.

Cancer-associated chromatin abnormality is emerging as a major target for therapeutic intervention, and specific and potent inhibitors of many chromatin-modifying enzymes have been developed[42]. Nevertheless, only a handful of chromatin-targeted drugs have been approved to treat mainly hematologic malignancies, including HDAC inhibitors (Romidepsin and Vorinostat) which are used for treatment of refractory T-cell lymphoma[43,44], as well as DNA methyltransferase inhibitors which are used as first-line treatment of myeloid malignancies[45]. In part, this gap reflects our limited understanding of the mechanisms of action and the lack of robust biomarkers for epigenetic therapies[46]. Previous studies assessed the efficacy of HDAC inhibitors mainly through phenotypic observations, gene expression analysis and analogue-based drug discovery[47]. As a result, their precise mechanism of cell killing is not well understood. Our findings indicate that Romidepsin transcriptionally reprograms amino acid metabolism and *de novo* nucleotide synthesis which renders selective toxicity to NRF2-active cancer cells. This is consistent with previous reports that HDAC inhibitors synergize with inhibitors of electron transport chain and fatty acid oxidation in glioblastoma[29]. Moreover, disruption of metabolic pathways by HDAC inhibitors has been reported by several other groups[48–50]. Taken together, these results suggest that metabolic alterations such as NRF2 hyperactivation could serve as effective biomarkers to predict the efficacy of HDAC inhibitors for treating solid tumors. We believe that similar concepts and strategies may be applicable to the identification of new

biomarkers and broaden the number of cancer patients who could benefit from other epigenetic drugs.

In summary, our findings provide the evidence and mechanistic basis for Class I HDACs as potent and specific chromatin vulnerabilities of tumors with NRF2 activation. Moreover, they advocate retrospective or prospective studies on the NRF2 pathway as biomarkers to predict solid tumors' response to HDAC inhibitors. We propose that the development of effective epigenetic therapies requires rational design of pre-clinical studies and patient stratification that consider the interplay between the genetic, chromatin and metabolic state of the cancer cell.

2.7 Methods

2.7.1 Cell culture.

KP and KPK cell lines were established as described previously[10]. For experiments outlined in **Figures 2.2.1 and 2.S1**, two independent KP and two independent KPK cell lines were used. For all other experiments, KP and KPK cells refer to one of the two KP and KPK cell lines respectively and n refers to the number of experimental replicates. All cells were maintained in either DMEM or RPMI-1640 (Sigma-Aldrich) supplemented with 10% FBS (Sigma-Aldrich) and 1x Penicillin-Streptomycin (Sigma-Aldrich). Cells were incubated at 37 degrees in 5% CO_2 atmosphere. All cell lines were routinely tested for mycoplasma contamination. For antibiotic-based selection, puromycin (Sigma-Aldrich) was used at 5ug/ml, hygromycin (Sigma-Aldrich) at 500ug/ml and blasticidin (Sigma-Aldrich) at 5ug/ml. For fluorophore-based selection, cells were sorted by the Flow Cytometry Shared Resource at Columbia University using a BD Influx Cell Sorter.

2.7.2 Plasmid construction and Lentivirus production

Lentivirus were generated by transfecting 293T cells with the indicated expression plasmid and the psPAX2 (Addgene) and pVSVG (Addgene) packaging vectors at a ratio of 4:2:3, respectively. Viral supernatants were collected 48 and 72 hrs after transfection, filtered and used for transduction of cells in 1:1 ratio with medium. NRF2ΔNeh2, Keap1 (mouse and human), and KEAP1^R470C overexpression constructs were generated by the Papagiannakopoulos lab. For CRISPR/Cas9 gene knock-out, we used the lentiCas9-blast plasmid (Addgene) and the pUSEPR vector for sgRNA (U6-sgRNA-EFS-Puro-P2A-TurboRFP in pLL3-based lentiviral backbone). For sgRNA design the CRISPick platform (BROAD institute) was used. For Slc1a5 overexpression, cDNA was obtained from Addgene (Plasmid #71458) and cloned into pLVX-IRES-mCherry (Takara Bio).

2.7.3 sgRNA library

The gRNA library targeting murine chromatin regulators was constructed as previously described[51]. Briefly, it consisted of sgRNA sequences (six per gene) targeting 612 mouse chromatin regulators that were designed using BROAD sgRNA Designer[52] and 36 non-targeting control sgRNAs[15].This library was synthesized by Agilent Technologies and cloned into the pUSEPR lentiviral vector to ensure a library representation of >10,000X using a modified version of a previously described protocol[52]. Then, it was selectively amplified using barcoded forward and reverse primers that append cloning adapters at the 5 - and 3 -ends of the sgRNA insert, purified using the QIAquick PCR Purification Kit (Qiagen), and ligated into BsmBI-digested and dephosphorylated pUSEPR vector using high-concentration T4 DNA ligase (NEB). Ligated pUSEPR plasmid DNA was electroporated into Endura electrocompetent cells

(Lucigen), recovered for one hour at 37⁰C, plated across four 15cm LB-Carbenicillin plates (Teknova), and incubated at 37⁰C for 16 hours. The total number of bacterial colonies was quantified to ensure a library representation of >10,000X. Bacterial colonies were scraped and briefly expanded for 4 hours at 37⁰C in 500mL of LB-Carbenicillin. Plasmid DNA was isolated using the Plasmid Plus Maxi Kit (Qiagen).

2.7.4 Focused CRISPR/Cas9 Screen.

Derivatives of KP and KPK cells were generated by stable lentiviral transduction of Cas9 with blasticidin resistance (Addgene#52962). Cells were maintained with blasticidin selection throughout the experiment. Transduction of Cas9-expressing KP/KPK cells was performed at an MOI of approximately 0.2 by incubating cell suspension in lentiviral supernatant and centrifugation at 1500 rpm for 1.5 hours at room temperature before being returned to a humidified incubator. An initial population was infected to represent a 2500x representation of the epigenetic library; 36 hours post-transduction cells were resuspended and replated in 10 ug/mL puromycin and selected for another 48 hours. After complete puromycin selection cells were trypsinized, pooled, a cell sample representing time-0hr (t_0) of the screen was reserved and stored at -20⁰C. The remaining cells from each line were then passaged into Vehicle (**Figures 2.2.1A-D**) or CB839 250nM (**Figure 2.6I**) conditions. Each condition was performed in technical triplicate for the entire screen and maintained in 15 cm tissue culture dishes (Corning) with at least 2500x library representation maintained throughout all culture and library preparation steps. Population doublings for each cell line and condition were recorded and a sample was collected when a particular condition had reached 14 cumulative population doublings and stored at -20⁰C.

Genomic DNA from collected cell pellets were prepared with purelink mini kit (ThermoFisher) according to the manufacturer's suggested protocol. Amplification of 5ug gDNA equivalent was done as described previously[51,53] and sequenced using an Illumina Nextseq 500 high output with 40% PhiX spike-in.

Computational analysis was done using MAGeCK[54]. Briefly, the sequencing data were de-barcoded and the 20 bp sgRNA sequence was mapped to the reference sgRNA library without allowing for any mismatches. The read counts were calculated for each individual sgRNA and normalized, and differential analysis was done between KP and KPK samples. Quality control, gene hit identification and graphs were generated using MAGeCKFlute[55].

2.7.5 Cell growth competition assay.

Cells were transduced with Cas9, selected with blasticidin for 1 week, and then transduced with the sgRNA constructs containing RFP overexpression (at least 2 per gene). At 3 days (t_0) and then after 14 population doublings (t_1), cells were analyzed by flow cytometry. Flow cytometry data was acquired on 16 laser BDFortessa. All data were analyzed using the FlowJo^{TM} (V10) software. The percentage of RFP positive cells was determined by gating using uninfected Cas9 cells for each cell line.

2.7.6 Protein Extraction and Western blot analysis

Whole cell lysates were prepared in SDS Lysis Buffer (ThermoFisher) and resolved on 3-8% or 4-12% gradient SDS-PAGE gels (ThermoFisher) transferred to nitrocellulose membrane, blocked in 5% non-fat milk in PBS plus 0.5% Tween-20, probed with primary antibodies and detected with horseradish peroxidase-conjugated α-rabbit or α-mouse secondary antibodies (Cell

Signaling). The blots were imaged using a ChemiDoc MP Imaging system (Bio-Rad) or exposed to X-Ray films (Research Products International).

2.7.7 Viability assays and drug treatments.

For 72h viability assays, 1500 KP cells, 3000 A549 or 5000 H2009 cells were plated in 96-well plates in RPMI-1640 medium, the next day cells were treated, and cell viability was determined 72h post treatment using CCK8 assay (Dojindo). AUC and IC50s were determined using the Graphpad Prism v6 and v9 software. For 5-day assays, 1500 KP or KPK cells were plated in 12-well plates in RPMI-1640 medium, the next day cells were treated , and cell viability was determined post treatment by Crystal Violet stain (Sigma). For induction of NRF2 activation in KP carrying dox-inducible NRF2ΔNeh2, cells were treated with 1μM KI-696 (Papagiannakopoulos lab) or 1µg/ml Doxycycline (Sigma-Aldrich) for 7 days before experiments.

The concentration of *in vitro* Romidepsin treatments throughout the study varies due to use of two stocks with different potency (second batch of drug was 5 to 10-fold more potent), as well as to account for differences in cell number and plate well size. For specific experiments the concentrations used were: CUT&Tag and RNA-seq: 5nM for 17h, ^{13}C-glucose tracing experiment: 5nM, ^{13}C-glutamine tracing experiment: 1nM as indicated in **Figure 2.S5A**.

2.7.8 Allograft and Xenograft studies.

For KP and A549 *in vivo* studies, 6-8 weeks old male C57BL/6 mice (Cat# 000664) and *Foxn1^{nu}* mice (Cat# 007850) were purchased from The Jackson Laboratory. All mice were housed under specific-pathogen-free (SPF) conditions and followed the guidelines of Columbia University

animal facility. All mice experiments were carried out with the protocol approved by the Institutional Animal Care and Use Committee (IACUC) at Columbia University. C57BL/6 mice or *Foxn1^{nu}* mice were subcutaneously injected with KP (5×10^5 per injection) and A549 (**Figures 2.7F&S7B** 5×10^6 per injection; **Figures 2.7I-J** 2×10^6 per injection) cells respectively into the flanks (2 injections/mouse). Mice were treated after tumor establishment, approximately 5 days post injection. Subsequent intraperitoneal (IP) treatments and tumor measurements were performed 2-3 times a week on the days indicated in each figure. Romidepsin (1mg/kg IP; Medchem Express) was dissolved in 10% DMSO in Corn oil (Sigma Aldrich). CB-839 (200mg/kg Orally; twice a day; CALITHERA) was formulated in 25% (w/v) hydroxypropyl-β-cyclodextrin in 10 mmol/L citrate (pH 2.0), at 20 mg/mL for a final dosing volume of 10 mL/kg. For the Patient-derived xenograft (PDX) experiment, the study was approved by the NYU Langone Medical Center Institutional Animal Care and Use Committee. Animals were housed according to IACUC guidelines in ventilated cages in a specific pathogen-free (SPF) animal facility. PDX tumors were stored in cryo-tubes in 10% dimethyl sulphoxide (DMSO) containing Dulbecco's Modified Eagle Medium (DMEM) media containing 10% FBS and 20 ug/ml Gentamicin. After stabilized and expanding in NOD-scid IL2R gamma null (NSG) mice, tumors were trimmed with the size of 3 mm x 3 mm x 3 mm and subcutaneously transplanted near both flanks into NSG male and female littermates approximately 6-8 weeks in age. Engraftment was checked every 5 days after transplantation. After the tumor establishment phase, animals were randomized and assigned to a treatment group. Tumor volume was measured by caliper and volume was calculated (Length x Width^2 x 0.5). Animals either received Romidepsin 1 mg/kg or vehicle Corn Oil twice weekly administered through intraperitoneal injection. The treatment volume was settled as 100 µl per mouse. Tumor growth was tracked for a minimum of 8 tumors

per experimental group. Tumors with volume less than 20mm^3 at the time of the first measurement were excluded from the final analysis.

Statistical analyses were done using Prism (v9), specifically 2-way ANOVA was used for comparison of tumor growth between each condition and Fisher's Least Significant Difference for multiple comparisons. For comparisons of tumor volumes and weights, the test was chosen by performing D'Agostino-Pearson and Shapiro-Wilk normality test: if both conditions passed both tests, Student's t-test was used, otherwise we performed Mann-Whitney U-test.

2.7.9 CUT&Tag

CUT&Tag was performed as described previously[23], with an additional step of light fixation to better preserve histone acetylation/TF binding. In brief, 1×10^5 cells were lightly fixed with 0.1% paraformaldehyde 5', neutralized by Glycine 125mM, and washed once with 1 ml of wash buffer (20 mM HEPES pH 7.5, 150 mM NaCl, 0.5 mM Spermidine (Sigma-Aldrich), 1× Protease inhibitor cocktail (Roche)). Concanavalin A-coated magnetic beads (Bangs Laboratories) were washed twice with binding buffer (20 mM HEPES pH 7.5, 10 mM KCl, 1 mM MnCl2, 1 mM CaCl2). 10 µl/sample of beads were added to cells in 400ul of wash buffer and incubated at room temperature for 15 min. Beads-bound cells were resuspended in 100 µl of antibody buffer (20 mM HEPES pH 7.5, 150 mM NaCl, 0.5 mM Spermidine, 0.06% Digitonin (Sigma-Aldrich), 2 mM EDTA, 0.1% BSA, 1× Protease inhibitor cocktail and incubated with indicated antibodies or normal rabbit IgG (Cell Signaling) at 4 degrees overnight on nutator. After being washed once with Dig-wash buffer (20 mM HEPES pH 7.5, 150 mM NaCl, 0.5 mM Spermidine, 0.05% Digitonin, 1× Protease inhibitor cocktail), beads-bound cells were incubated with 1 µl Guinea pig anti-rabbit secondary antibody (Antibodies Online ABIN101961) and 2 µl Hyperactive pA-

Tn5 Transposase adapter complex in 100 µl Dig-300 buffer (20 mM HEPES•NaOH, pH 7.5, 0.5 mM Spermidine, 1× Protease inhibitor cocktail, 300 mM NaCl, 0.01% Digitonin) at room temperature for 1 h. Cells were washed three times with Dig-300 buffer to remove unbound antibody and Tn5 and then resuspended in 300 µl of tagmentation buffer (10 mM MgCl2 in Dig-300 buffer) and incubated at 37 °C for 1 h. 10 µl of 0.5 M EDTA, 3 µl of 10% SDS and 5 µl of 10 mg/ml Proteinase K were added to each sample and incubated at 50 °C for 1 h to terminate tagmentation. DNA was purified using chloroform isoamyl alcohol (Sigma Aldrich) and eluted with 25 µl ddH2O. For library amplification, 21 µl of DNA was mixed with 2µL i5 unique index primer (10 µM), 2 µL i7 unique index primer (10 µM) and 25 µL NEBNext High-Fidelity 2X PCR Master Mix (NEB) and subjected to the following PCR program: 72°C, 5 min; 98°C, 30 sec; 13 cycles of 98°C, 10 sec and 63°C, 10 sec; 72°C, 1 min and hold at 10°C. To purify the PCR products, 1.1× volumes of pre-warmed Ampure XP beads (Beckman Coulter) were added and incubated at room temperature for 10 min. Libraries were washed twice with 80% ethanol and eluted in 20 µl of 10 mM Tris-HCl, pH 8. Libraries were sequenced on an NextSeq 550 platform (Illumina, 75 cycles High Output Kit v2.0) and 75-bp paired-end reads were generated. To determine global level differences in histone acetylation signal we used spike-in controls. For H3K27ac, 2ul of SNAP-ChIP K-AcylStat panel nucleosomes (EpiCypher) was added as spike-in control at the primary antibody incubation step. For H4ac, 5000 S2 Drosophila cells were added at the cell-bead binding step.

2.7.10 CUT&Tag data analysis

CUT&Tag reads of KP cell samples were mapped to the mouse genome assembly mm10 using Bowtie2 (v2.3.5.1, parameters: --local --very-sensitive-local --no-unal --no-mixed --no-

discordant --phred33 -I 10 -X 700). Potential PCR duplicates were removed by the function

"MarkDuplicates" (parameter: REMOVE_DUPLICATES=true) of Picard (v2.24.2). Genomic

enrichments of CUT&Tag signals were generated using deeptools (v3.3.2, parameters

bamCoverage --normalizeUsing CPM --binSize 25 --smoothLength 100) and visualized using

IGV. Peaks were called using MACS2 (parameters: --f BAMPE -g mm --broad). Consensuses of

H3K27ac, H4ac and BRD4 peaks across conditions were generated by the 'cat' function (Linux)

and 'sort' and 'merge' functions of bedtools (v2.27.1). The read counts of H3K27ac, H4ac and

BRD4 CUT&Tag data in genomic elements were measured by featureCounts (v2.0.0).

Differential analysis was performed using DEseq2(v1.32.0). Peak annotation was done using

ChIPseeker[56](v1.28.3). Heatmaps were generated using deeptools (v3.3.2) functions

computeMatrix and plotHeatmap. For visualization we used the R package ggplot2 (v3.3.2). For

genome-wide signal difference correlations we used deeptools (v3.3.2) functions

multiBigwigSummary and plotCorrelation. Promoters were defined as 2.5kb regions centered

around the TSS. For the signal diffusion analysis, random regions were generated using the

bedtools(v2.27.1) 'shuffle' function and the called peaks consensus as input. For the assignment

of genes into quantiles (Figures 2.3E and 3G), genes were ranked by their promoter CPM and

split into percentiles (3E: 0-33, 33-66 and 66-100, 3G as labeled). For all analyses, all replicates

were considered. For peak annotation we use the consensus of two replicates (**Figure 2.3B**). For

normalized signal heatmaps a representative pair of replicates is shown (**Figures 2.3C, 2.S3G**).

For figures indicating CPM we calculate the average of two replicates (**Figures 2.3D, 2.3E,**

2.3G, 2.S3F, 2.4G). For differential read count analysis we performed DEseq2 analysis with two

replicates (**Figure 2.3F**).

To determine global level differences in histone acetylation we compared the ratio of spike-in reads to total number of reads. For K27ac, the number of reads for each barcode was counted to determine the scaling factor. For H4ac, reads were mapped to the Drosophila genome (Dmel_A4_1.0) and the mapping percentage was used to determine the scaling factor. For BRD4, reads were mapped to the human genome (GRCh38) and the mapping percentage was used to determine the scaling factor.

2.7.11 RNA isolation, quantitative reverse transcription PCR (RT-qPCR) and RNA-sequencing

Total RNA was extracted in TRIzol (Invitrogen) and precipitated in ethanol (DECON Labs). For qRT-PCR, cDNA was then synthesized with cDNA Synthesis Kit (Takara) according to the manufacturer's protocols. The relative expression of targeted genes was measured by qRT-PCR with indicated primers and SYBR Green Master Mix (ThermoFisher) using the ABI 7500 Real-Time PCR Detection System (Applied Biosystems). For RNA-sequencing, RNA samples were submitted to Columbia University Genome Center for library preparation, sequencing and bioinformatic analysis up to generation of a reads count table of each gene. The differential gene expression was calculated by the R package DESeq2 (v1.28.0), and visualization was done using ggplot2 (v3.3.2) R package.

2.7.12 DepMap dataset analysis

The datasets that were used were the CERES 21Q3 Public+Score and the Prism repurposing secondary screen 19Q4. Data was downloaded for subsets that included NSCLC cell lines with or without KEAP1 mutations. For statistical analysis, the test was chosen by performing

D'Agostino-Pearson and Shapiro-Wilk normality test: if both conditions passed both tests, Student's t-test was used, otherwise we performed Mann-Whitney U-test. For CERES, comparison of the mutant and wild-type cell line subsets was done by calculating the gene-effect difference between the two.

2.7.13 Metabolic tracing

For glucose tracing analysis, $2x10^5$ KP cells (n=3) were plated in 6-well plates overnight in RPMI medium (Sigma). After 24 hours, the media was replaced with fresh RPMI medium containing DMSO or 5nM Romidepsin. At 48 hours the media was replaced with fresh glucose-free RPMI medium (Sigma) containing 10% dialyzed fetal bovine serum (Gibco), 2.0 g/L $^{13}C_6$-glucose (Sigma) and DMSO or 5nM Romidepsin. Cells were harvested at 49 and 72 hours and processed as described below.

For glutamine tracing, $2x10^5$ KP cells (n=3) were plated in 6-well plates overnight in RPMI medium (Sigma). After 24 hours, the media was replaced with fresh RPMI medium containing DMSO, 1nM Romidepsin or 150nM CB-839. At 48 hours the media was replaced with fresh glutamine-free RPMI medium (Sigma) containing 10% dialyzed fetal bovine serum (Gibco), 2.0 g/L $^{13}C_6$-glutamine (Cambridge Isotope Laboratories) and DMSO, 1nM Romidepsin or 150nM CB-839. Cells were harvested at 56 hours and processed as described below.

2.7.14 Metabolite harvesting and liquid chromatography-mass spectrometry analysis

Cells were washed with cold PBS, lysed in 80% Ultra LC-MS acetonitrile (Thermo Scientific) supplemented with 20 µM deuterated 2-hydroxyglutarate (D-2-hydroxyglutaric-2,3,3,4,4-d5 acid (d5-2HG), Cambridge Isotope Laboratories) as an internal standard on ice for 15 minutes, and

centrifuged for 10 minutes at 20,000 x g at 4 °C. 200 µL of supernatants were subjected to mass

spectrometry analysis. Liquid chromatography was performed using an Agilent 1290 Infinity LC

system (Agilent, Santa Clara, US) coupled to a Q-TOF 6545 mass spectrometer (Agilent, Santa

Clara, US). A hydrophilic interaction chromatography method with a ZIC-pHILIC column (150

x 2.1 mm, 5 µm; EMD Millipore) was used for compound separation at 35 °C with a flow rate of

0.3 mL/min. Mobile phase A consisted of 25 mM ammonium carbonate in water and mobile

phase B was acetonitrile. The gradient elution was 0—1.5 min, 80% B; 1.5—7 min, 80% B →

50% B, 7—8.5 min, 50% B; 8.5—8.7 min, 50% B → 80% B, 8.7-13 min, 80% B. The overall

runtime was 13 minutes, and the injection volume was 5 µL. The Agilent Q-TOF was operated

in negative mode and the relevant parameters were as listed: ion spray voltage, 3500 V; nozzle

voltage, 1000 V; fragmentor voltage, 125 V; drying gas flow, 11 L/min; capillary temperature,

325 °C; drying gas temperature, 350 °C; and nebulizer pressure, 40 psi. A full scan range was set

at 50 to 1600 (m/z). The reference masses were 119.0363 and 980.0164. The acquisition rate was

2 spectra/s. Targeted analysis, isotopologues extraction (for the metabolic tracing study), and

natural isotope abundance correction were performed by the Agilent Profinder B.10.00 Software

(Agilent Technologies).

2.7.15 Histology

Tumors were fixed in 10% Formalin (Fisher Chemical) for 48 hours and then stored in 70%

ethanol at 4°C. Paraffin embedding and sectioning was done at the Histology Service of the

Molecular Pathology Shared Resource at Columbia University Medical center.

Immunohistochemistry experiments were done at Experimental Pathology Research Laboratory

at New York University Langone Health. Quantitation of signal was done using QuPath software

(v0.3.2) and statistical analysis using Prism (v9) and Fisher's Least Significant Difference for multiple comparisons; at least 4 tumors per condition were assessed.

2.7.16 Glutamine and glutamine consumption

$2x10^5$ KP cells (n=3) were plated in 6-well plates overnight in RPMI medium (Sigma). After 24 hours, the media was replaced with fresh RPMI medium containing DMSO, 1nM Romidepsin or 150nM CB-839. At 48 hours the media was replaced with fresh glutamine-free RPMI medium (Sigma) containing DMSO, 1nM Romidepsin or 150nM CB-839. Media were harvested at 56 hours, centrifuged to remove dead cells and frozen at -80ºC. Cells were harvested and counted. Measurement of metabolites was done using a YSI 7000 enzymatic analyzer at the Cell Metabolism core that is part of the Donald B. and Catherine C. Marron Cancer Metabolism Center at the Memorial Sloan Kettering Cancer Center. Consumption was calculated by comparison to media from wells without any cells.

2.8 Author Contributions

D.K., T.P. and C.L. conceived the study. D.K. executed the experiments with the help of W.W (CRISPR/Cas9 focused genetic screen), A.L. (metabolomics), M.H. (PDX), X.C., X.X., M.Y and V.M. F.J.S.-R. and Y.M.S.F. provided reagents and guidance for the CRISPR/Cas9 genetic screen. T.P. and J.Y. provided reagents, expertise, and feedback. C.L. supervised the study. D.K. and C.L. wrote the manuscript, with contributions and input from all authors.

2.9 Acknowledgements

2.10 Declaration of interests

Authors declare no competing interests.

2.11 References

1. Lu, C. & Thompson, C. B. Metabolic regulation of epigenetics. *Cell Metab* **16**, 9–17 (2012).
2. Carrer, A. *et al.* Acetyl-CoA Metabolism Supports Multistep Pancreatic Tumorigenesis. *Cancer Discov* **9**, 416–435 (2019).

3. Figueroa, M. E. *et al.* Leukemic IDH1 and IDH2 mutations result in a hypermethylation phenotype, disrupt TET2 function, and impair hematopoietic differentiation. *Cancer Cell* **18**, 553–567 (2010).

4. Lu, C. *et al.* IDH mutation impairs histone demethylation and results in a block to cell differentiation. *Nature* **483**, 474–478 (2012).

5. Menegon, S., Columbano, A. & Giordano, S. The Dual Roles of NRF2 in Cancer. *Trends in Molecular Medicine* **22**, 578–593 (2016).

6. Mitsuishi, Y. *et al.* Nrf2 Redirects Glucose and Glutamine into Anabolic Pathways in Metabolic Reprogramming. *Cancer Cell* **22**, 66–79 (2012).

7. Itoh, K. *et al.* An Nrf2/small Maf heterodimer mediates the induction of phase II detoxifying enzyme genes through antioxidant response elements. *Biochem. Biophys. Res. Commun.* **236**, 313–322 (1997).

8. Hammerman, P. S., Hayes, D. N. & Grandis, J. R. Therapeutic insights from genomic studies of head and neck squamous cell carcinomas. *Cancer Discov* **5**, 239–244 (2015).

9. Ichimura, Y. *et al.* Phosphorylation of p62 Activates the Keap1-Nrf2 Pathway during Selective Autophagy. *Molecular Cell* **51**, 618–631 (2013).

10. Romero, R. *et al.* Keap1 loss promotes Kras-driven lung cancer and results in dependence on glutaminolysis. *Nature medicine* **23**, 1362–1368 (2017).

11. Sayin, V. I. *et al.* Activation of the NRF2 antioxidant program generates an imbalance in central carbon metabolism in cancer. *eLife* **6**, e28083 (2017).

12. Song, S. *et al.* Loss of SWI/SNF Chromatin Remodeling Alters NRF2 Signaling in Non-Small Cell Lung Carcinoma. *Mol Cancer Res* **18**, 1777–1788 (2020).

13. Karlsson, A. *et al.* Genome-wide DNA Methylation Analysis of Lung Carcinoma Reveals One Neuroendocrine and Four Adenocarcinoma Epitypes Associated with Patient Outcome. *Clin Cancer Res* **20**, 6127–6140 (2014).

14. Sánchez-Rivera, F. J. *et al.* Rapid modelling of cooperating genetic events in cancer through somatic genome editing. *Nature* **516**, 428 (2014).

15. Soto-Feliciano, Y. M. *et al.* A molecular switch between mammalian MLL complexes dictates response to Menin-MLL inhibition. *Cancer Discovery* CD-22-0416 (2022) doi:10.1158/2159-8290.CD-22-0416.

16. Pacini, C. *et al.* Integrated cross-study datasets of genetic dependencies in cancer. *Nat Commun* **12**, 1661 (2021).

17. Meyers, R. M. *et al.* Computational correction of copy number effect improves specificity of CRISPR-Cas9 essentiality screens in cancer cells. *Nat Genet* **49**, 1779–1784 (2017).

18. Itoh, K. *et al.* Keap1 represses nuclear activation of antioxidant responsive elements by Nrf2 through binding to the amino-terminal Neh2 domain. *Genes Dev.* **13**, 76–86 (1999).

19. Furumai, R. *et al.* FK228 (Depsipeptide) as a Natural Prodrug That Inhibits Class I Histone Deacetylases. *Cancer Res* **62**, 4916–4921 (2002).

20. Gaymes, T. J. *et al.* Histone Deacetylase Inhibitors (HDI) Cause DNA Damage in Leukemia Cells: A Mechanism for Leukemia-Specific HDI-Dependent Apoptosis? *Mol Cancer Res* **4**, 563–573 (2006).

21. Stankov, M. V. *et al.* Histone deacetylase inhibitors induce apoptosis in myeloid leukemia by suppressing autophagy. *Leukemia* **28**, 577–588 (2014).

22. Karagiannis, D. & Rampias, T. HDAC Inhibitors: Dissecting Mechanisms of Action to Counter Tumor Heterogeneity. *Cancers* **13**, 3575 (2021).

23. Kaya-Okur, H. S. *et al.* CUT&Tag for efficient epigenomic profiling of small samples and single cells. *Nature Communications* **10**, 1930 (2019).
24. Slaughter, M. J. *et al.* HDAC inhibition results in widespread alteration of the histone acetylation landscape and BRD4 targeting to gene bodies. *Cell Reports* **34**, 108638 (2021).
25. Galan-Cobo, A. *et al.* LKB1 and KEAP1/NRF2 Pathways Cooperatively Promote Metabolic Reprogramming with Enhanced Glutamine Dependence in KRAS-Mutant Lung Adenocarcinoma. *Cancer Res* **79**, 3251–3267 (2019).
26. DeNicola, G. M. *et al.* NRF2 regulates serine biosynthesis in non–small cell lung cancer. *Nat Genet* **47**, 1475–1481 (2015).
27. LeBoeuf, S. E. *et al.* Activation of Oxidative Stress Response in Cancer Generates a Druggable Dependency on Exogenous Non-essential Amino Acids. *Cell Metab.* **31**, 339-350.e4 (2020).
28. Bhutia, Y. D. & Ganapathy, V. Glutamine transporters in mammalian cells and their functions in physiology and cancer. *Biochimica et Biophysica Acta (BBA) - Molecular Cell Research* **1863**, 2531–2539 (2016).
29. Nguyen, T. T. T. *et al.* HDAC inhibitors elicit metabolic reprogramming by targeting super-enhancers in glioblastoma models. *J Clin Invest* **130**, 3699–3716 (2020).
30. Wardell, S. E. *et al.* Glucose Metabolism as a Target of Histone Deacetylase Inhibitors. *Mol Endocrinol* **23**, 388–401 (2009).
31. Hast, B. E. *et al.* Cancer-Derived Mutations in KEAP1 Impair NRF2 Degradation but not Ubiquitination. *Cancer Research* **74**, 808–817 (2014).
32. Davies, T. G. *et al.* Monoacidic Inhibitors of the Kelch-like ECH-Associated Protein 1: Nuclear Factor Erythroid 2-Related Factor 2 (KEAP1:NRF2) Protein–Protein Interaction with High Cell Potency Identified by Fragment-Based Discovery. *J. Med. Chem.* **59**, 3991–4006 (2016).
33. Hammad, A., Namani, A., Elshaer, M., Wang, X. J. & Tang, X. "NRF2 addiction" in lung cancer cells and its impact on cancer therapy. *Cancer Letters* **467**, 40–49 (2019).
34. Zavitsanou, A.-M. *et al.* KEAP1 mutation in lung adenocarcinoma promotes immune evasion and immunotherapy resistance. 2021.09.24.461709 Preprint at https://doi.org/10.1101/2021.09.24.461709 (2021).
35. Singh, A. *et al.* NRF2 Activation Promotes Aggressive Lung Cancer and Associates with Poor Clinical Outcomes. *Clin Cancer Res* **27**, 877–888 (2021).
36. Ding, H. *et al.* Activation of the NRF2 antioxidant program sensitizes tumors to G6PD inhibition. *Science Advances* **7**, eabk1023 (2021).
37. Fu, J. *et al.* Hyperactivity of the transcription factor Nrf2 causes metabolic reprogramming in mouse esophagus. *Journal of Biological Chemistry* **294**, 327–340 (2019).
38. Alam, H. *et al.* KMT2D Deficiency Impairs Super-Enhancers to Confer a Glycolytic Vulnerability in Lung Cancer. *Cancer Cell* **37**, 599-617.e7 (2020).
39. Chung, C. *et al.* Integrated Metabolic and Epigenomic Reprograming by H3K27M Mutations in Diffuse Intrinsic Pontine Gliomas. *Cancer Cell* **38**, 334-349.e9 (2020).
40. Panwalkar, P. *et al.* Targeting integrated epigenetic and metabolic pathways in lethal childhood PFA ependymomas. *Sci Transl Med* **13**, eabc0497 (2021).
41. Marcantonio, D. D. *et al.* ATF3 coordinates serine and nucleotide metabolism to drive cell cycle progression in acute myeloid leukemia. *Molecular Cell* **81**, 2752-2764.e6 (2021).
42. Bates, S. E. Epigenetic Therapies for Cancer. *New England Journal of Medicine* **383**, 650–663 (2020).

43. Iyer, S. P. & Foss, F. F. Romidepsin for the Treatment of Peripheral T-Cell Lymphoma. *The Oncologist* **20**, 1084–1091 (2015).

44. Mann, B. S., Johnson, J. R., Cohen, M. H., Justice, R. & Pazdur, R. FDA Approval Summary: Vorinostat for Treatment of Advanced Primary Cutaneous T-Cell Lymphoma. *The Oncologist* **12**, 1247–1252 (2007).

45. Diesch, J. *et al.* A clinical-molecular update on azanucleoside-based therapy for the treatment of hematologic cancers. *Clinical Epigenetics* **8**, 71 (2016).

46. Pfister, S. X. & Ashworth, A. Marked for death: targeting epigenetic changes in cancer. *Nat Rev Drug Discov* **16**, 241–263 (2017).

47. Ganesan, A., Arimondo, P. B., Rots, M. G., Jeronimo, C. & Berdasco, M. The timeline of epigenetic drug discovery: from reality to dreams. *Clinical Epigenetics* **11**, 174 (2019).

48. Alcarraz-Vizán, G., Boren, J., Lee, W.-N. P. & Cascante, M. Histone deacetylase inhibition results in a common metabolic profile associated with HT29 differentiation. *Metabolomics* **6**, 229–237 (2010).

49. Srivatsan, S. R. *et al.* Massively multiplex chemical transcriptomics at single-cell resolution. *Science* **367**, 45–51 (2020).

50. Yang, J. *et al.* Inhibiting histone deacetylases suppresses glucose metabolism and hepatocellular carcinoma growth by restoring FBP1 expression. *Sci Rep* **7**, (2017).

51. Soto-Feliciano, Y. M. *et al.* A molecular switch between mammalian MLL complexes dictates response to Menin-MLL inhibition. *bioRxiv* 2021.10.22.465184 (2022) doi:10.1101/2021.10.22.465184.

52. Doench, J. G. *et al.* Optimized sgRNA design to maximize activity and minimize off-target effects of CRISPR-Cas9. *Nat Biotechnol* **34**, 184–191 (2016).

53. Strezoska, Ž. *et al.* Optimized PCR Conditions and Increased shRNA Fold Representation Improve Reproducibility of Pooled shRNA Screens. *PLOS ONE* **7**, e42341 (2012).

54. Li, W. *et al.* MAGeCK enables robust identification of essential genes from genome-scale CRISPR/Cas9 knockout screens. *Genome Biology* **15**, 554 (2014).

55. Wang, B. *et al.* Integrative analysis of pooled CRISPR genetic screens using MAGeCKFlute. *Nat Protoc* **14**, 756–780 (2019).

56. Wang, Q. *et al.* Exploring Epigenomic Datasets by ChIPseeker. *Current Protocols* **2**, e585 (2022).

2.12 Supplementary Figures

A

B
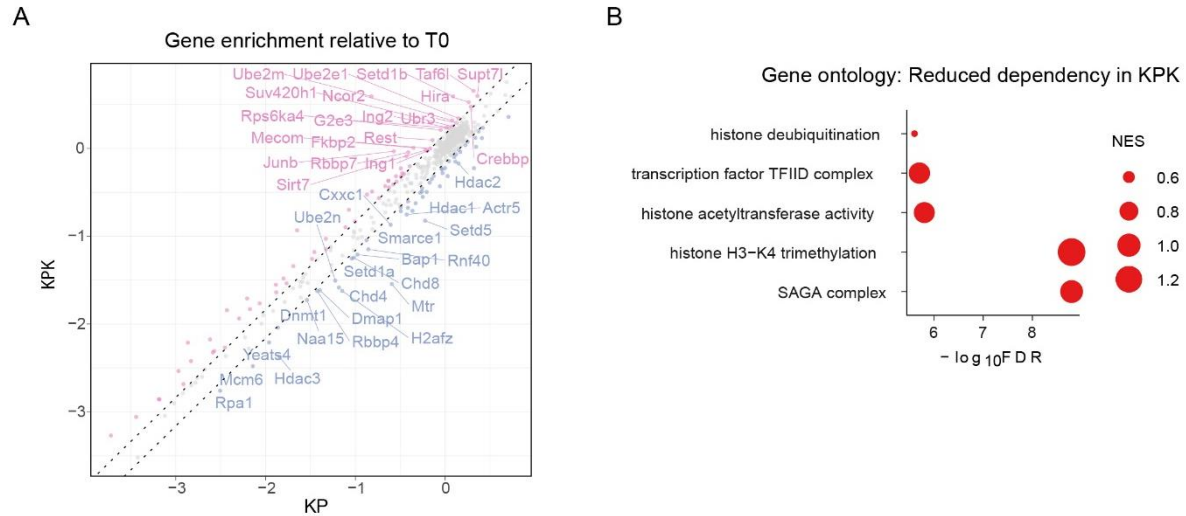
Figure 2.S1. A. Scatter plot of gene enrichment compared to T0 for each condition and indicated are the top 20 differentially enriched genes. B. Ontology analysis of genes that are more essential in KP cells.
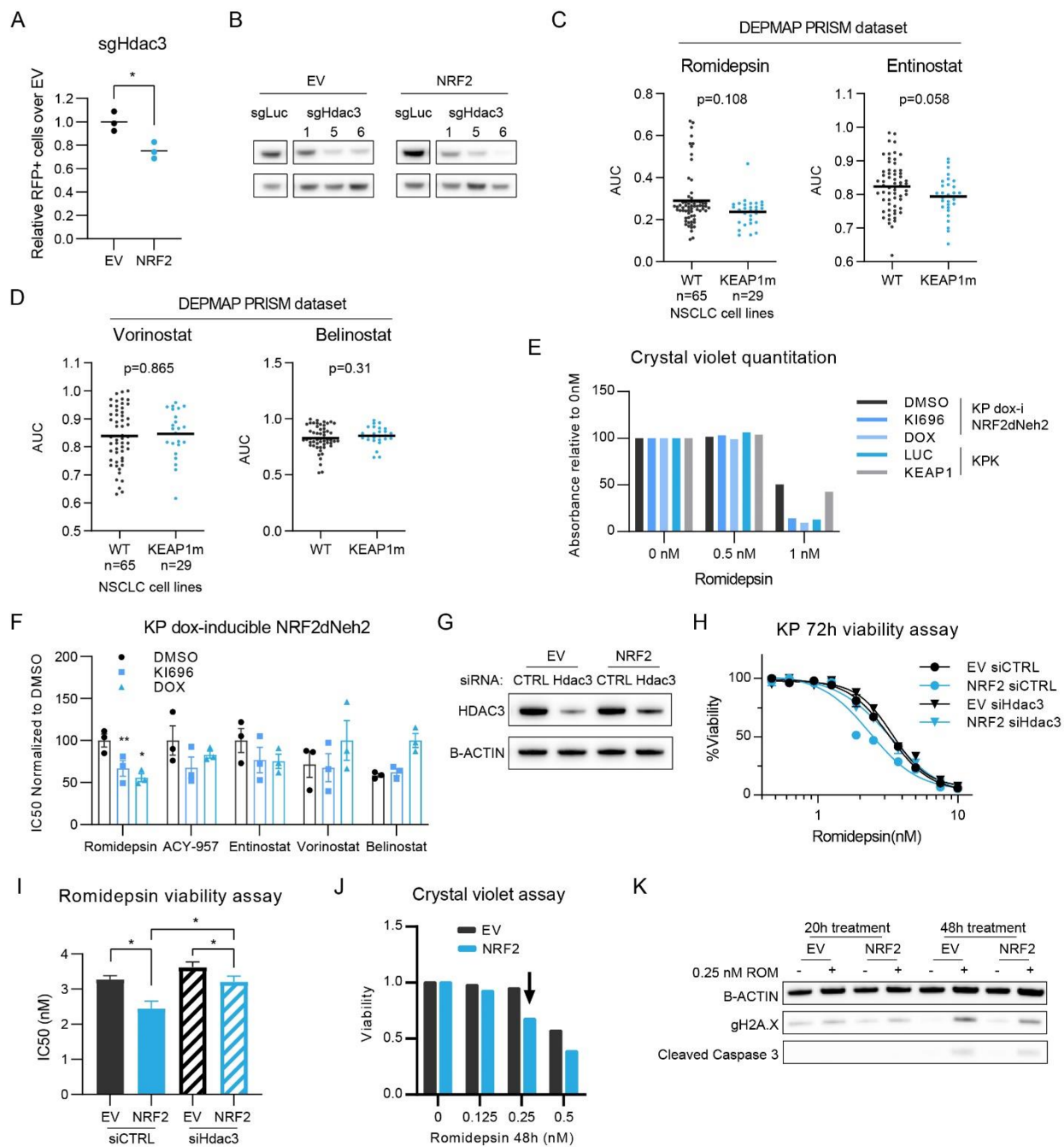
Figure 2.S2. A. Competition assay of KP EV and NRF2ΔNeh2 overexpressing cells expressing Cas9 and a sgRNA against Hdac3 (n=3, statistical significance determined by students t-test). **B**. Western blot of HDAC3 upon selection of KP EV and NRF2ΔNeh2 expressingCas9 and sgRNA against Luciferase or Hdac3. **C-D**. HDAC inhibitor AUC (area under curve) comparison of KEAP1 WT and mutant NSCLC cell lines from the DepMap Prism repurposing secondary screen 19Q4. **E**. Quantitation of crystal violet assay (related to figure 2G) **F**. Bar graph indicating IC50s to various HDAC inhibitors, derived from 3-day viability experiments (n=3) in KP cells carrying dox-inducible NRF2ΔNeh2 pre-treated with DMSO, KI696 or DOX for 1 week (Statistical significance determined by paired t-test). **G**. Western blot indicating protein levels of HDAC3 upon treatment with siRNA that are either non-targeting (CTRL) or against Hdac3 for 3 days. **H**. Romidepsin concentration gradient curve and IC50 bar graph (**I**; error bars indicate 95% confidence i nterval) of KP cells treated with control or Hdac3-targeting siRNA for 3 days. **J-K**. Protein levels of phosphorylated H2A.X and cleaved caspase 3 upon treatment with Romidepsin at a concentration were the difference in cell viability between control and NRF2 activated cells is more pronounced.

75
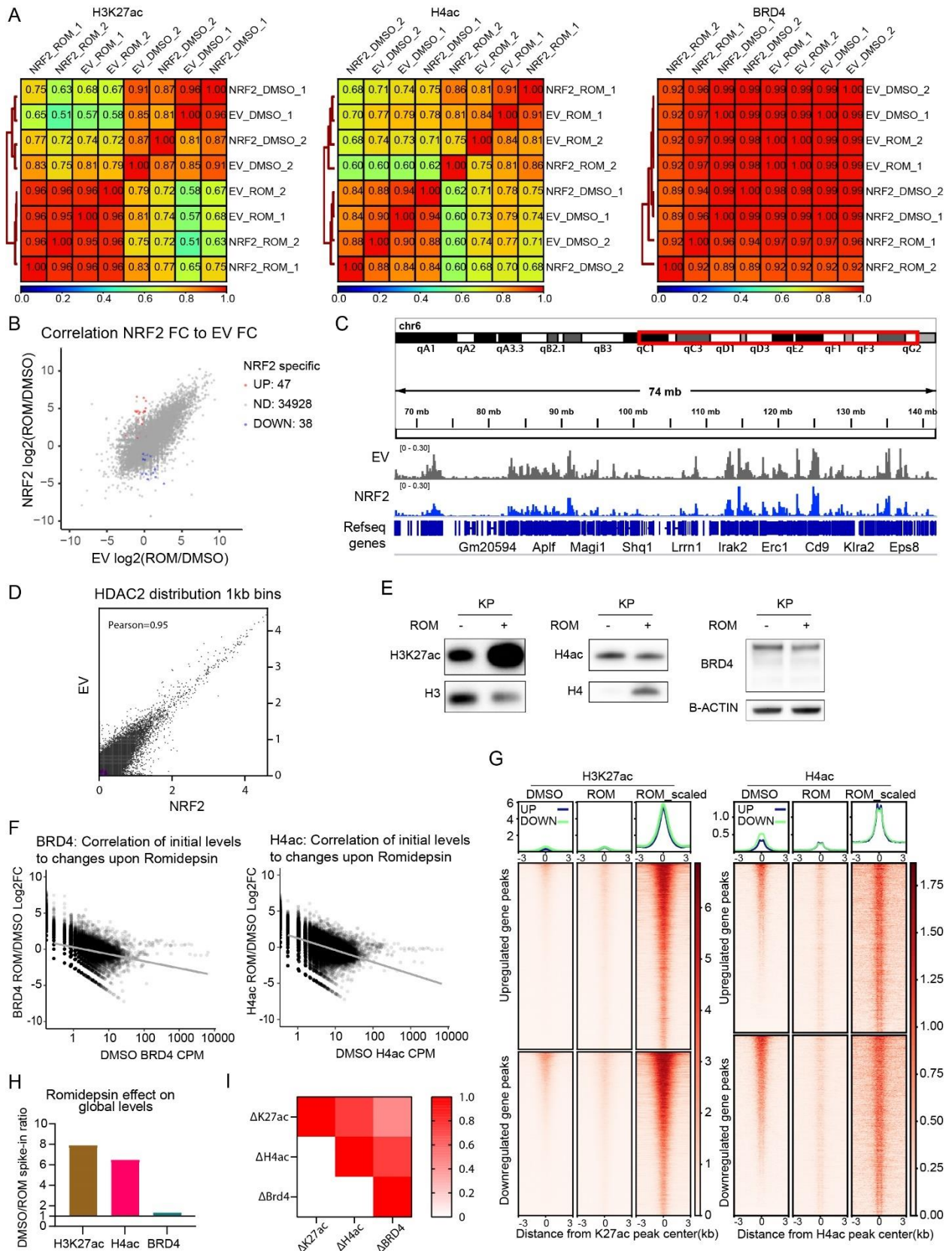
Figure 2.S3. A. Pearson correlation heatmaps of all conditions and replicates. **B**, Correlation plot of Fold change differences between KP EV and NRF2 cells upon Romidepsin treatement; indicated are transcripts that are significantly up- or down-regulated only in NRF2 cells (cutoffs: NRF2: 2-fold change and FDR<0.05, EV: 1.5-fold change). **C.** Genome browser view of HDAC2 distribution at chromosome 6 in EV and NRF2 cells. **D**. Correlation plot of normalized HDAC2 signal across the genome (1kb bin resolution). **E.** Western blot analysis of indicated proteins upon treatment of KP NRF2 cells with Romidepsin (5nM, 24h). **F.** Correlation plots of fold-change histone acetylation and BRD4 binding to levels of acetylation/binding at DMSO treatment at consensus peaks (normalized by DEseq2; n=2). **G.** Heatmaps of histone acetylation signal at peaks associated with differentially expressed genes in KP cells treated with DMSO or Romidepsin (scaled by RPKM or spike-in control). H. Relative levels of H3K27 and H4 acetylation and BRD4 binding after Romidepsin treatment (5nM, 24h), determined by the spike-in ratio of Romidepsin to DMSO in CUT&Tag. **I**. Pearson correlation of genome-wide signal difference (ROM-DMSO) split into 10kb bins between histone acetylation marks and BRD4 (mean of two replicates).

A

Gene expression (RNA-seq)

B

KP NRF2 DMSO TUMOR   KP NRF2 ROM TUMOR

C

KP NRF2 Tumors   KP EV Tumors

ATF4 staining
High
Medium
Low

D

KEAP1 mutant vs wild−type NSCLC cell lines

E

F

KP EV Tumors

MYC staining
High
Medium
Low
Negative

G

KP Cas9

H

KP Cas9 sgHdac3

I
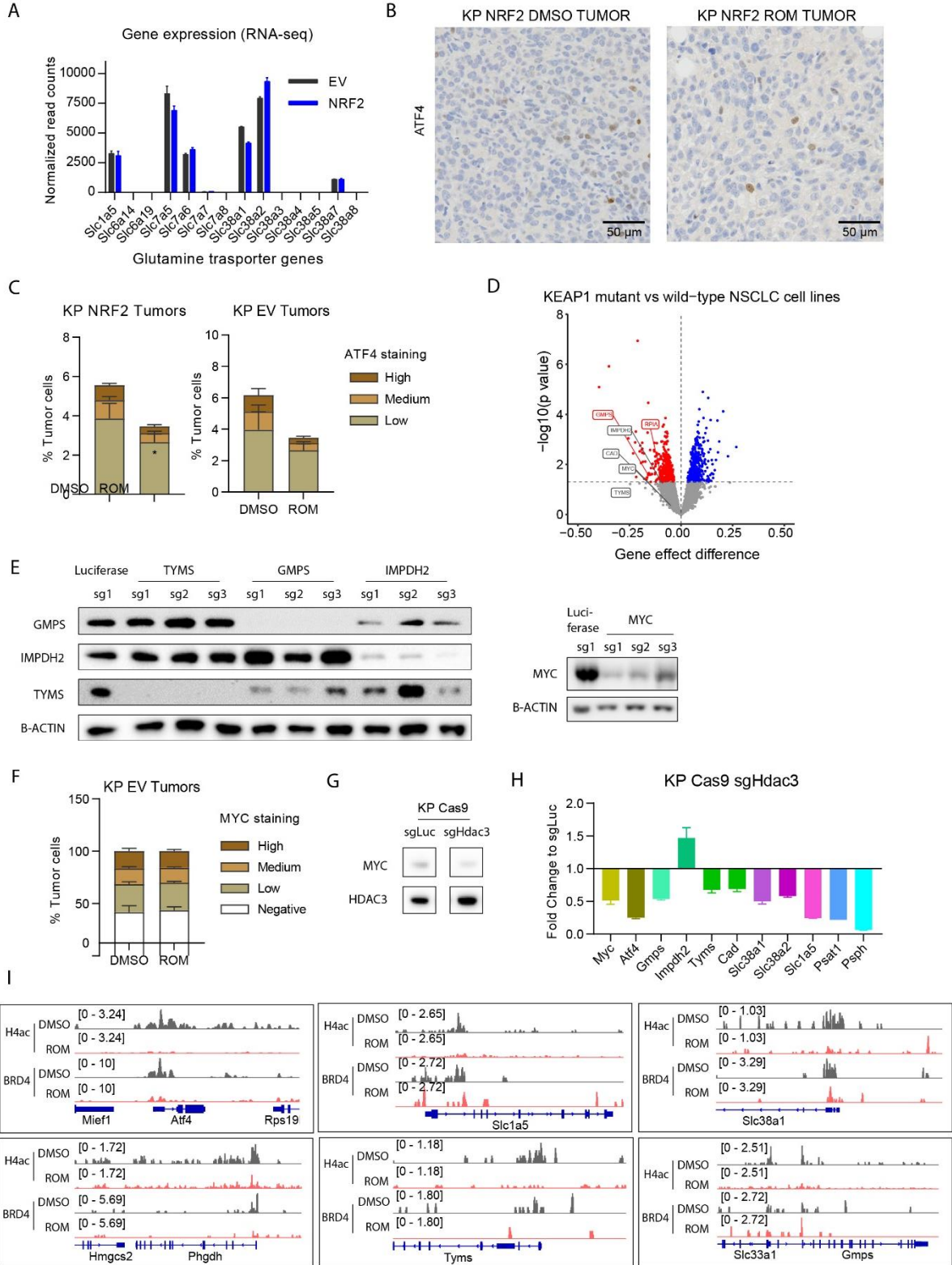
Figure 2.S4. A. Normalized RNA-seq read counts (by DESeq2) of amino-acid transporters involved in glutamine uptake. **B**. IHC staining of ATF4 and quantitation (**C**) in KP tumors after 17 days of treatment with DMSO or Romidepsin (related to figure 2.2J-K. **D**. Volcano plot showing gene effect difference between KEAP1 wild-type and mutant NSCLC cell line from the CERES DepMap dataset. **E**. Western blots indicating levels of indicated proteins upon CRISPR/Cas9 KO in KP cells - associated with competition assay in 4F. **F**. Quantitation of IHC staining of c-MYC in KP EV tumors (related to figure 2G-H). **G**. Western blot indicating HDAC3 levels upon CRISPR/Cas9-mediated knock-out in KP cells (samples were run on the same gel) **H**. RT-qPCR indicating expression of metabolic genes in Hdac3 KO KP cells. **I**. Bedgraphs of H4ac and BRD4 binding at indicated gene loci.
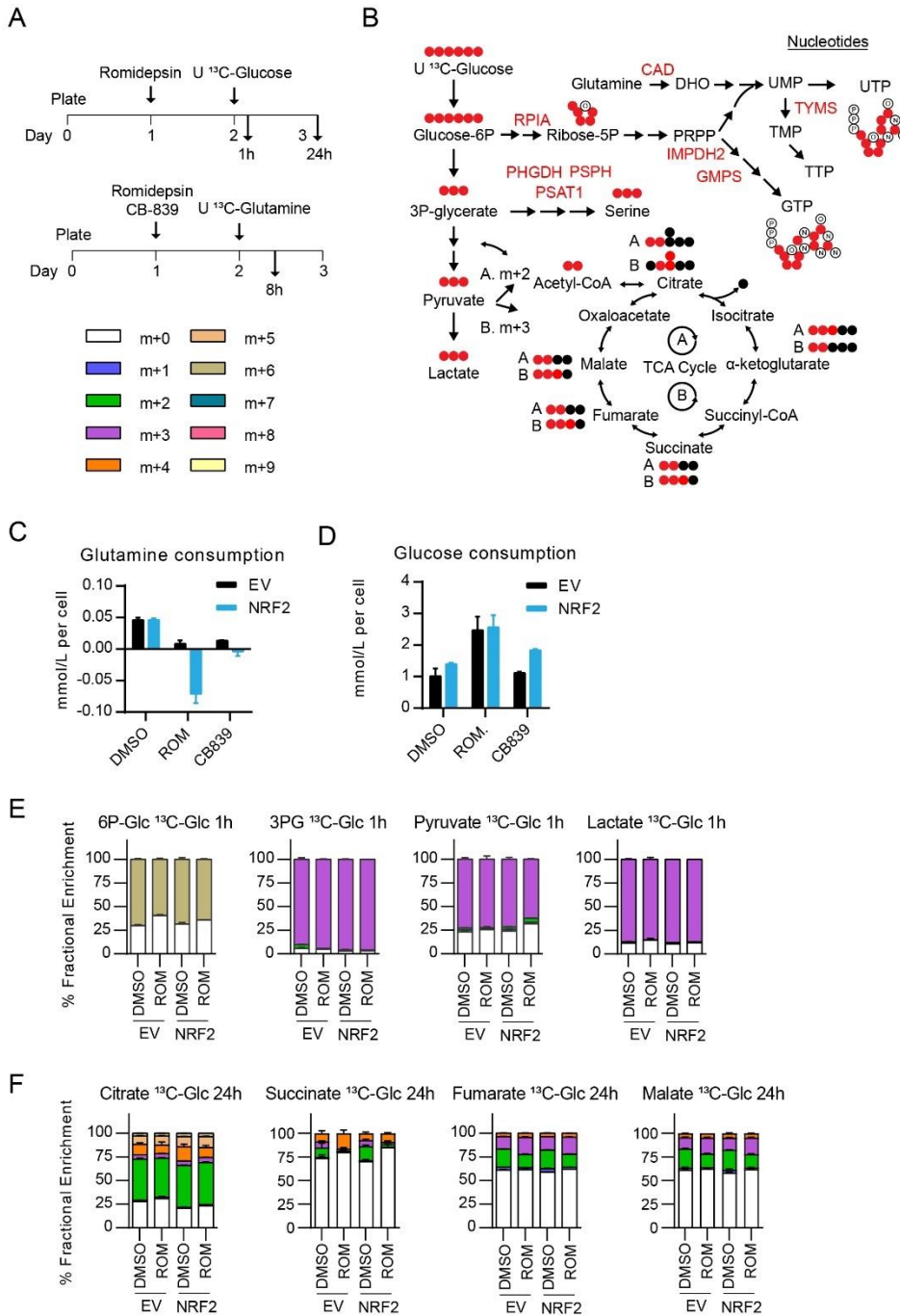
Figure 2.S5. A. Schematics of glucose and glutamine U-^{13}C isotope tracing LC-MS experiments. **B**. Schematic indicating glucose and glutamine metabolic processes, labeled glucose carbon contribution and genes that are downregulated upon Romidepsin treatment. **C**. Glutamine consumption of KP cells after treatment with the indicated drugs for 8h. **D**. Bar graphs showing isotope percentages for GTP after U-^{13}C glutamine tracing for 8h and color indications of isotopologues. **D**. Glucose consumption of KP cells after treatment with the indicated drugs for 8h. **E-F**. Bar graphs showing isotope percentages for the indicated metabolites after U-^{13}C glucose tracing for the indicated time.
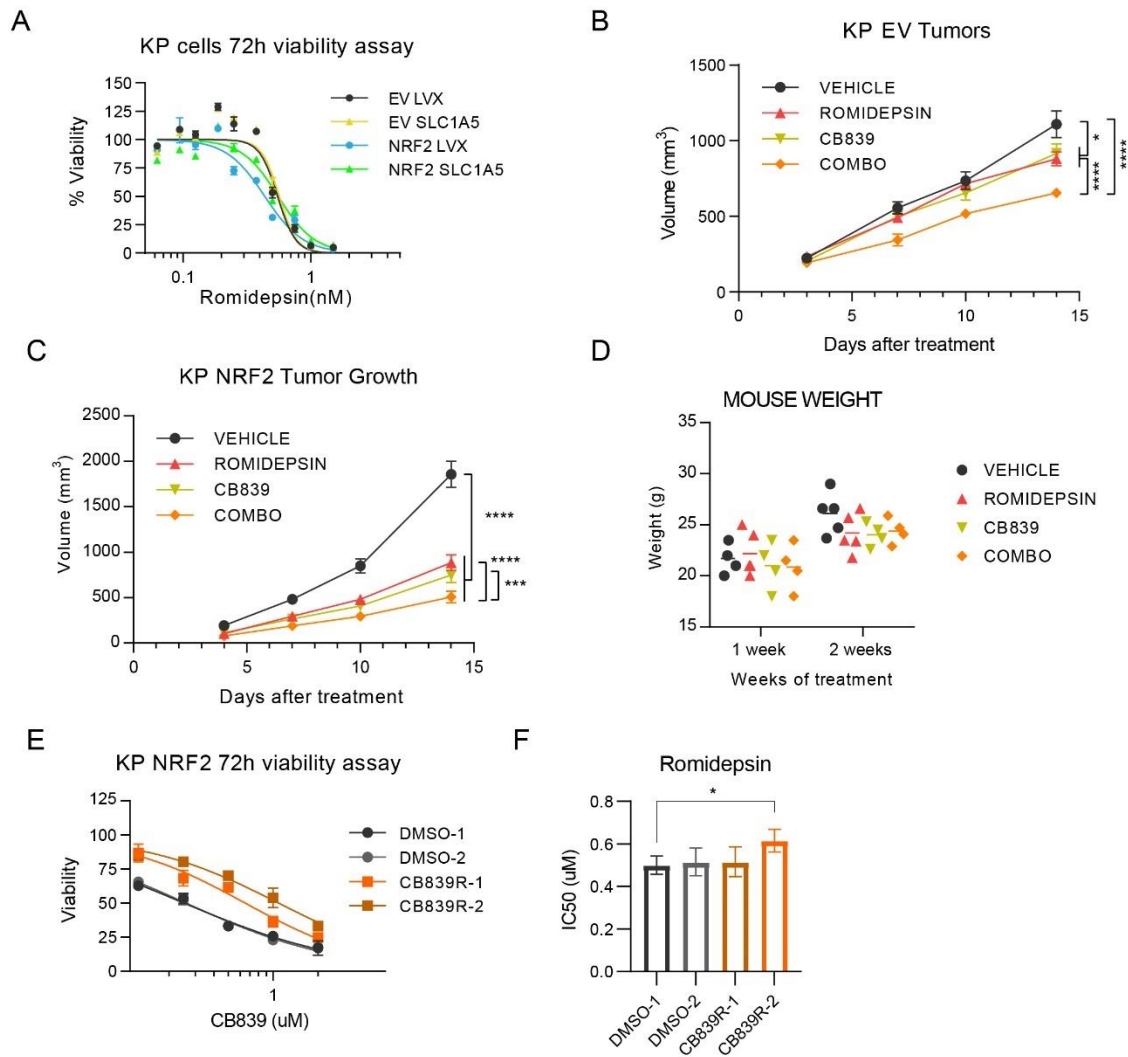
Figure 2.S6. A. Romidepsin treatment viability assay of KP EV and NRF2 carrying empty vector (LVX) or Slc1a5 overexpression. **B-C**. Growth of subcutaneous KP EV and NRF2 tumors in C57/BL6 mice treated as indicated. (Statistical significance determined by two-way Anova). **D**. Weight of mice that were treated as indicated (related to figure S6C). **E**. CB-839 treatment viability assay of KP NRF2 control (DMSO) or CB839-resistant cell lines and Romidepsin IC50 (**F**).
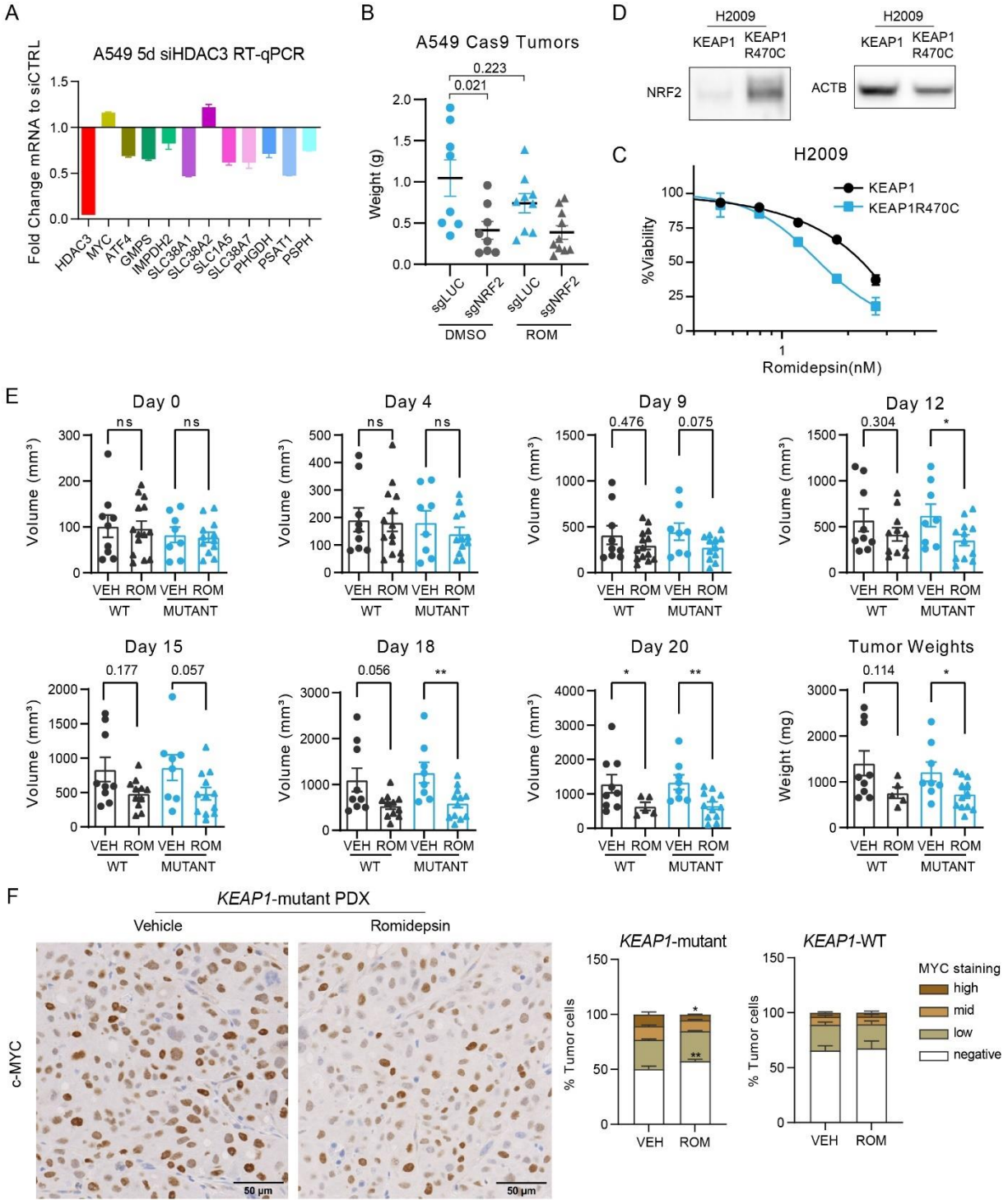
Figure 2.S7. A. Gene expression in A549 cells treated with siRNA against HDAC3 for 5 days, relative to treatment with non-targeting siRNA (siCTRL). **B**. NRF2 protein levels upon overexpression of wild-type or R470C mutant KEAP1 in NCI-H2009 cells. **C**. Viability assay of H2009 cells treated with the indicated concentrations of Romidepsin for 72h. **D**. Weight of subcutaneous A549 tumors in nude mice treated with Romidepsin or vehicle (related to figure 7D). **E**. Tumor volumes of PDX tumors at the indicated days of treatment and tumor weights at the experiment endpoint (related to 7G-H). **F**. IHC staining of c-MYC and quantitation in PDX tumors after 17 days of treatment with Vehicle (VEH) or Romidepsin (related to figure 7G-H).

Chapter 3: Epigenetic regulation of p63 controls basal to neuroendocrine cell fate transition during esophagus development and malignancy.

3.1 Preface and Respective Contributions

This chapter consists of a manuscript that is under preparation in collaboration with the Jianwen Que laboratory. I include this manuscript in my dissertation since I contributed significantly by designing, performing, and analyzing several key experiments that uncovered how the p63 locus and squamous identity in NEC is epigenetically regulated. Specifically, all experiments described in **Figures 3.1** and **3.2,** as well as the immunofluorescence staining of human NEC samples (**Figure 3.3A**) were performed by Yongchun Zhang of the Que laboratory. All experiments involving 3D culture and immunofluorescence stainings of TYUC-1 cells were performed by Helu Liu of the Que laboratory (**Figures 3.4** and **3.6**). All RNA-seq and CUT&Tag experiments in TYUC-1 cells, as well as the epigenetic drug screen and the siRNA experiment were performed by me (**Figures 3.3-3.6**). The manuscript was written by Yongchun Zhang, Helu Liu, me, Chao Lu, and Jianwen Que, with feedback from all listed authors.

3.2 Summary

Cell fate determination and maintenance play critical roles in establishing and preserving tissue identity and function during organ development. Aberrant cell fate transitions can lead to cancer cells acquiring lineage plasticity, resulting in tumor heterogeneity and resistance to treatment. Trp63 (p63) is a transcription factor important for the formation of the stratified squamous epithelium in the esophagus. Here, we report an unexpected role of p63 in protecting esophageal basal progenitor cells from committing to a neuroendocrine fate. Deletion of p63 in developing murine esophagus and in human embryonic stem cells results in extensive differentiation towards neuroendocrine lineage. We found that p63 is transcriptionally silenced by EZH2-mediated histone H3K27 trimethylation (H3K27me3) in rare but aggressive esophageal neuroendocrine tumors. Overexpression or epigenetic reactivation of p63 through EZH2 inhibition promotes trans-differentiation to squamous identity and suppresses the growth of esophageal neuroendocrine tumor cells. Together these studies uncover the epigenetic regulation of p63 as an important determinant in coordinating the transition between neuroendocrine and squamous cell states during esophageal development and tumor progression.

3.3 Introduction

Cell fate determination is critical for organ development and maintenance. Aberrant differentiation can lead to the ectopic emergence of cells that are incompatible with organ function. For example, the aberrant presence of acid-secreting cells in the esophagus contributes to pathological lesions known as inlet patch.[1] Additionally, abnormal cell type conversions are found in premalignant lesions such as Barrett's metaplasia where the stratified squamous epithelium is replaced by simple columnar cells in the distal portion of the esophagus.[2-4]

Chemotherapy and targeted therapy treatments have also been shown to cause switch in cancer histology, including androgen deprivation-induced prostate adenocarcinoma conversion into squamous cell carcinoma.[5,6] Moreover, neuroendocrine cell transdifferentiation was identified as a potential cause of drug resistance in several types of cancer, including prostate adenocarcinoma and rectal adenocarcinoma.[7,8] Interestingly, chemoradiotherapy can also cause esophageal cancer to switch from squamous cell carcinoma (SCC) to neuroendocrine carcinoma.[9] Despite an increasing appreciation of the prevalence and significance of such tumor lineage plasticity, the underlying molecular mechanisms remain largely unknown.

The adult esophagus is lined with a stratified squamous epithelium, which starts with simple columnar cells in the early foregut.[10,11] Genetic studies have shown that the Bone Morphogenetic Protein (BMP) pathway plays a critical role in this transformation, involving the specification of basal progenitor cells into squamous epithelium.[12] Downstream of BMP signaling, there exists the transcription factor Trp63 (p63), which is specifically enriched in basal progenitor cells.[13] Deletion of *p63* blocks the formation of stratified squamous epithelium in the esophagus and skin.[14] In skin keratinocytes, p63 has been shown to modulate the epigenetic and chromatin landscape through chromatin regulators.[15-17] Although abundant ciliated cells and mucous producing cells have been reported in the esophagus of *p63* null mutants,[12,18] how p63 is involved in cell fate determination in the esophagus progenitor cells remains incompletely understood.

Neuroendocrine cells are a minor population of epithelial cells residing in the stomach, intestine, and lung but absent in the esophagus.[19-21] Neuroendocrine cells sense a variety of stimuli and produce neuropeptides to modulate chemoreception, mechanotransduction and immune cell responses.[19,21,22] On rare occasions, neuroendocrine cells transform into neuroendocrine

carcinoma, which is a very rare type of cancer seen in the gastrointestinal tract and pulmonary tract. Intriguingly, although neuroendocrine cells are absent, esophageal neuroendocrine carcinomas (eNEC) can also occur and account for ~1% of esophageal cancer.[23] eNEC is highly aggressive and composed of cancer cells characterized by high expression levels of neuroendocrine cell markers such as SYP and CHGA, similar to small-cell lung cancer (SCLC).[24,25] It is noteworthy that eNECs are negative for the expression of p63[26], yet genome sequencing reveals no mutation in the gene encoding p63,[27] suggesting an epigenetic mechanism underlying p63 silencing during tumor progression.

Histone posttranslational modifications such as methylation and acetylation can modulate the structure of chromatin and impact gene transcription. The trimethylation of lysine 27 on histone H3 (H3K27me3) is catalyzed by the methyltransferase EZH2, a core subunit of Polycomb Repressive Complex 2 (PRC2).[28] H3K27me3 generally represses transcription of genes that are essential for lineage specification.[29] Hence, EZH2 is important for tissue development, homeostasis and tumorigenesis.[28] Histone acetylation, in contrast, generally activates gene transcription.[30] Histone acetylation is regulated by both histone acetyltransferase (e.g., p300/CBP) and histone deacetylases (HDACs).[31] Additionally, the Bromodomain and Extraterminal (BET) protein family including BRD2, BRD3, BRD4, and BRDT, can recognize and bind to acetylated lysine residues of histones to recruit RNA polymerase II to promote gene transcription.[32] Accordingly, histone acetylation marks such as H3K27 acetylation (H3K27ac) demarcate active *cis*-regulatory elements critical for tissue development.[33]

Here, we report that epigenetic regulation of p63 is critical for esophageal development and tumor lineage plasticity. p63 acts as a conserved guardian against neuroendocrine cell fate, and *p63* deletion leads to abundant neuroendocrine cell differentiation in the developing esophagus.

Conversely, overexpression of p63 confers squamous cell differentiation in eNEC. We further showed that the expression of p63 is epigenetically suppressed by H3K27me3 and activated by H3K27ac in eNEC. Treatment with the EZH2 inhibitor reduces H3K27me3, leading to the reactivation of p63 and squamous cell genes in eNEC organoids.

3.4 Results

3.4.1 p63 represses neuroendocrine cell differentiation in the developing mouse esophagus

We and others have shown that deletion of *p63* causes the emergence of mucociliated cells in the esophagus.[3,12,18] To comprehensively study the cell types present in the *p63*-null developing esophagus, we compared the gene expression of the esophageal epithelium between *p63 KO* mutants and the littermate controls at E12.5 (**Figure 3.S1A**). Differential expression analysis revealed that 954 and 703 genes were significantly upregulated and downregulated in *p63 KO* mutants, respectively (**Figure 3.1A**). Gene ontology analysis and gene set enrichment analysis (GSEA) revealed a significant impact on cell fate pathways and related biological processes (**Figures 3.1B-1D and 3.S1B**). Specifically, we observed downregulation of genes associated with basal and squamous cell identity and extracellular matrix organization (**Figures 3.1B**-**C**). By contrast, we found that genes upregulated in mutants were enriched for genes regulating neuroendocrine cell identity and neurotransmitter processes (**Figures 3.1B**-**D**). Consistently, the basal cell signature genes *Krt5* and *Krt15*, and adhesion molecules including *Itga3, Itga6, Itgb4* and *Lamb3* were reduced in the mutant esophageal epithelium (**Figure 3.1E**).

A Differential expression KO vs WT

Up: 954
Down: 703

Trp63, Insm1, Krt15, Itgb4, Syp, Chga, Krt5

B Up: Descartes Cell Types and Tissues 2021

ENS neurons in Intestine
Neuroendocrine cells in Lung
Islet endocrine cells in Pancreas
Visceral neurons in Lung
Chromaffin cells in Intestine

GeneRatio
0.25
0.30
0.35
0.40

Down: Descartes Cell Types and Tissues 2021

Vascular endothelial cells in Cerebrum
Vascular endothelial cells in Cerebellum
Squamous epithelial cells in Stomach
Ureteric bud cells in Kidney
Thymic epithelial cells in Thymus

GeneRatio
0.15
0.20
0.25
0.30

C Enrichment plot: DESCARTES_MAIN_FETAL_NEUROENDOCRINE_CELLS

FDR q-value: 0.12

D Enrichment plot: BUSSLINGER_ESOPHAGEAL_PROLIFERATING_BASAL_CELLS

FDR q-value: 0.17

E WT, p63 KO

Basal cell keratins: Krt5, Krt14, Krt15
Adhesion molecules: Itga3, Itga6, Itgb4, Lamb3
Ciliated cell: Tuba1a, Tubb4a
Columnar cell keratins: Krt7, Krt8, Krt18

RNA levels in FPKM

Neuroendocrine cell: Ascl1, Insm1, Cgrp, Syp, Pyy, Chga, Chgb, Edn1, Eno2, Cck, Uchl1, Sst, Gfi1, Ncam1

F INSM1 DAPI — WT, p63 KO — E14.5 Eso

G CGRP INSM1 DAPI — WT, p63 KO — E18.5 Eso

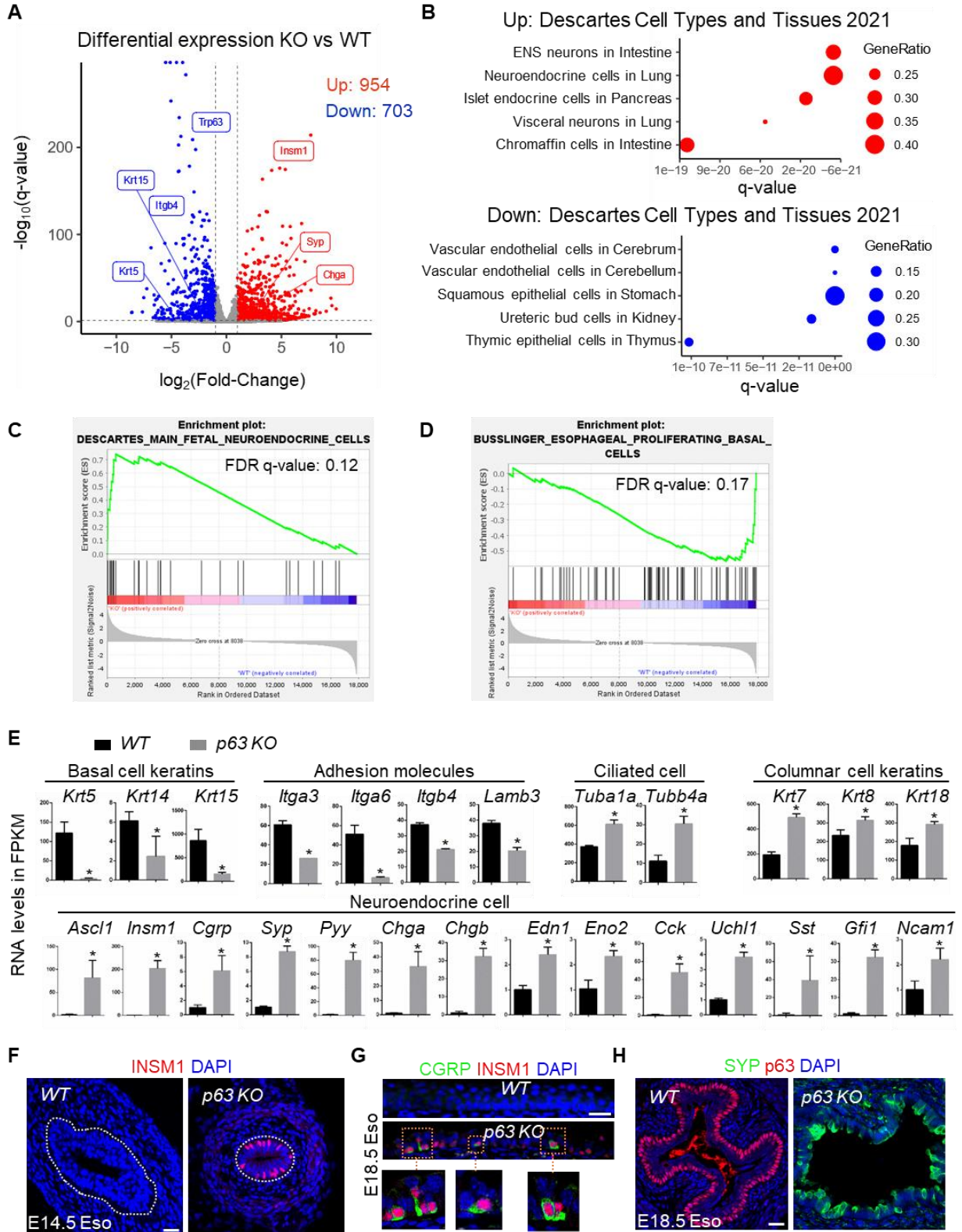**H** SYP p63 DAPI — WT, p63 KO — E18.5 Eso

87

Figure 3.1. Loss of p63 leads to neuroendocrine cell differentiation in the developing murine esophagus. (A) Volcano Plot of differentially expressed genes between *WT* and *p63 KO* esophageal epithelium. Noted are genes involved in basal and neuroendocrine cell identity. **(B)** Cell types and tissues gene ontology of genes upregulated (red) and downregulated (blue) in *p63 KO* esophageal epithelium. **(C-D)** Gene set enrichment analysis indicating upregulation of neuroendocrine cell signature and downregulation of esophageal basal cell signature. **(E)** p63 deletion reduces the transcriptional levels of basal cell keratins *Krt5, Krt14* and Krt15, adhesion molecules *Itga3, Itga5, Itgb4* and *Lamb3,* but increases the levels of ciliated cell genes *Tuba1a* and *Tubb4a*, columnar cell keratins *Krt7, Krt8* and *Krt18*. *p < 0.05. **(F)** Neuroendocrine progenitor marker INSM1 is ectopically expressed in the *p63 KO* esophageal epithelium at E14.5. **(G-H)** Neuroendocrine progenitor marker INSM1 and maturation marker CGRP and SYP are expressed in the *p63 KO* esophageal epithelium. Eso, esophagus. Scale bars: 20 µm.

As expected, the expression levels of the ciliated genes *Tuba1a* and *Tubb4a*, and columnar cell keratins *Krt7, Krt8* and *Krt18* were significantly increased upon *p63* deletion (**Figure 3.1E**). Surprisingly, we observed enrichment of neuroendocrine cell signature genes including *Ascl1*, *Insm1*, *Cgrp*, *Syp*, *Chga*, *Chgb*, *Edn1*, *Eno2*, *Cck*, *Uch1*, *Gfi1,* and *Ncam1* in mutants (**Figure 3.1E**). We further used immunofluorescence (IF) staining to confirm the ectopic presence of INSM1^{+} neuroendocrine progenitor cells in the esophagus of mutants but not the control littermates (**Figure 3.1F**). We also observed abundant mature neuroendocrine cells expressing CGRP and SYP in the mutant esophagus at E18.5 (**Figures 3.1G-1H and 3.S1C).** These data confirm that loss of p63 leads to the ectopic presence of neuroendocrine cells, suggesting that p63 is required to protect against aberrant neuroendocrine differentiation in the normal esophagus.

3.4.2 p63 plays a conserved role in repressing neuroendocrine cell fate in human iPSC-derived esophageal progenitor cells (EPCs)

To address whether p63 plays a similar role in inhibiting neuroendocrine cell formation in human esophageal progenitor cells (EPCs), we deleted *p63* in the H9 human embryonic stem cell (hESC) line. We then differentiated H9 into EPCs in a 2D system using the protocol we previously described.[34,35] Remarkably, we detected increased expression of the neuroendocrine genes *ASCL1, INSM1, SYP, CGRP, CHGA*, and *SST* at day 24 of differentiation (**Figure 3.2A**). Consistently, ASCL1$^+$ neuroendocrine cells were present in the *p63 KO* EPCs as shown by immunostaining (**Figure 3.2B**). Furthermore, we embedded the endodermal spheroids in the Matrigel and induced them into 3D esophageal organoids (**Figure 3.2C**). We collected the organoids after 7 weeks in culture and determined the expression of genes marking basal cells versus neuroendocrine cells. The expression of the basal cell markers p63, KRT5, and KRT13 was absent in the p63 *KO* organoids in comparison to their high levels of expression in the *WT* organoids (**Figures 3.2D-E**). More importantly, we observed the ectopic presence of INSM1$^+$SYP$^+$ neuroendocrine cells in organoids formed by *p63*-null hESC-derived EPCs. By contrast, INSM1$^+$SYP$^+$ cells were not detected in the organoids formed by control hESC-derived EPCs (**Figure 3.2F**). Taken together, these findings suggest a conserved role for p63 in repressing neuroendocrine cell differentiation during the development of the human esophagus.

A

ASCL1 INSM1 SYP CGRP CHGA SST

Fold change vs WT

B

p63 ASCL1 EPCAM DAPI

WT

p63 KO

C

WT & p63KO
H9 hESC → Endodermal induction → Endodermal spheroids → Spheroid embedding → 3D organoid [Matrigel] → Noggin SB431542 EGF → Anterior foregut and esophagus

D

p63 KRT5

WT

p63 KO

E

p63 KRT13 DAPI

WT

p63 KO

F

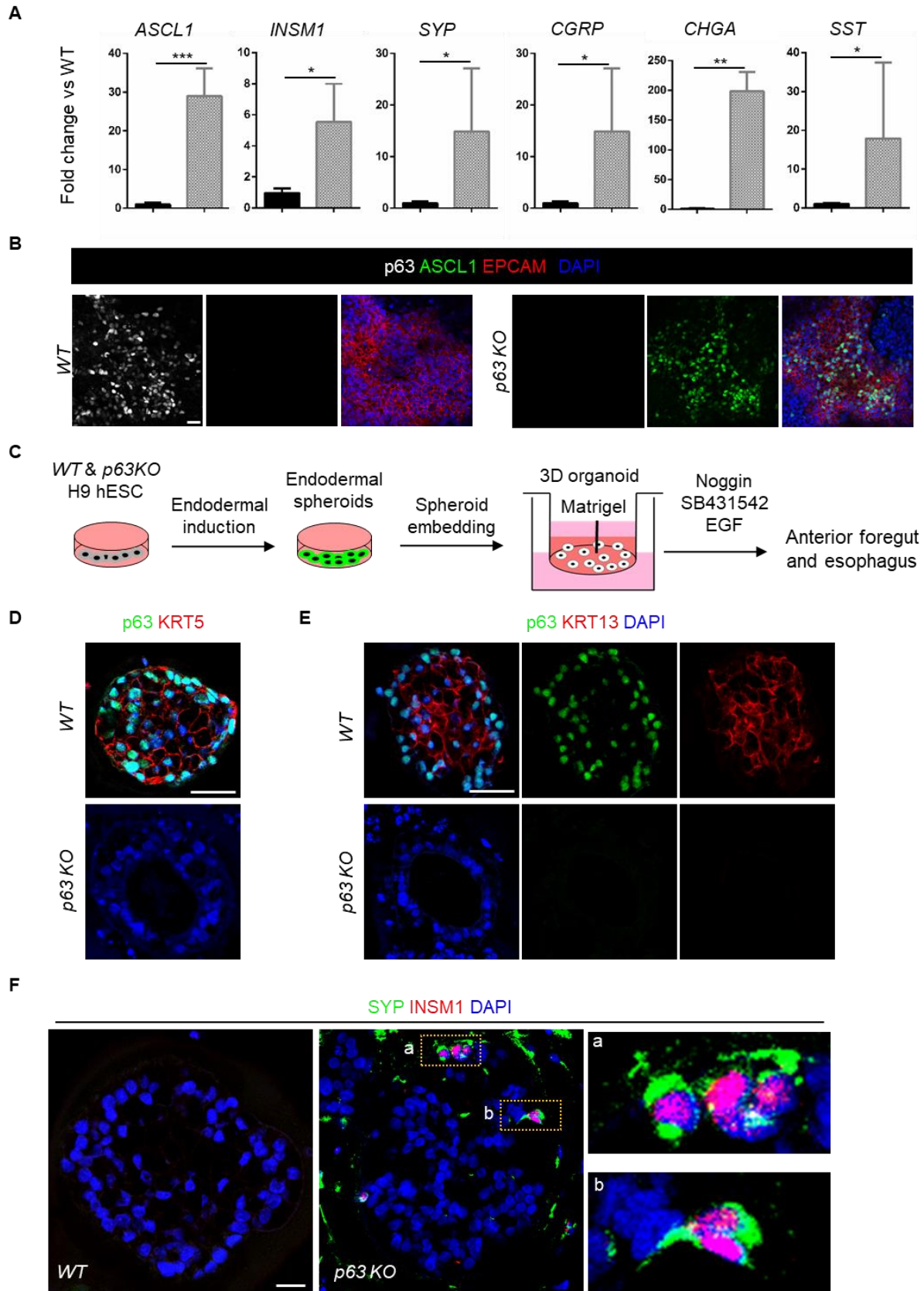SYP INSM1 DAPI

WT   p63 KO   a   b

Figure 3.2. p63 is required for promoting human esophageal squamous stratification and repressing neuroendocrine cell differentiation. (A-B) p63 loss of function (LOF) leads to ectopic neuroendocrine cell differentiation. Note the significant increase in the transcript levels of neuroendocrine markers *ASCL1*, *INSM1*, *SYP*, *CGRP*, *CHGA* and *SST* (A) and ectopic expression of ASCL1 by immunostaining (B). **(C)** Schematics to show differentiating H9 human embryonic stem cell (hESC) into esophageal organoids. Endodermal organoids derived from H9 hPSC cells were embedded in Matrigel and cultured in Noggin, SB431542 and EGF until day 53 to form esophageal organoids. **(D)** p63 LOF esophageal epithelial cells failed to express KRT5. **(E)** p63 knockout leads to failed esophageal stratification. Note the high expression of p63 in the periphery and high KRT13 expression in the center of the *WT* H9-derived esophageal organoids, compared to the loss of p63 expression in *p63 KO* organoids. **(F)** p63 LOF leads to ectopic expression neuroendocrine markers INSM1 and SYP (yellow boxes) in the developing *p63 KO* H9-derived organoids. *KO, knockout*. Scale bars: 20 µm.

3.4.3 ΔNp63 is the major isoform that controls basal cell identity genes in esophageal neuroendocrine tumor

p63 expression is lost in eNEC tumors.[24,26] Consistent with this finding, p63 protein was readily expressed in basal cells but undetectable in INSM1$^+$ neuroendocrine cancer cells in human eNEC specimens (**Figure 3.3A**). To investigate whether restoration of p63 activity impacts neuroendocrine cell identity, we used a dox-inducible system to overexpress p63 in the eNEC cell line TYUC-1 (**Figure 3.3B**). We chose to express two major p63 isoforms, TAp63α and ΔNp63α, to determine their effects on altering the cell fate of eNEC (**Figure 3.3B**). RNA-sequencing of TYUC-1 cells indicated that overexpression of ΔNp63α induced a higher expression of genes associated with the squamous identity than TAp63α (**Figure 3.3C**). We noticed that the induction by the ΔNp63α isoform was stronger compared to TAp63α in our RNA-seq experiment (**Figure 3.3C**). To exclude the possibility that the induction of squamous identity genes is due to differences in p63 isoform expression levels, we measured KRT5 expression at a concentration of doxycycline where TAp63α and ΔNp63α were induced at comparable levels, and confirmed that ΔNp63α was more potent in activating KRT5 expression
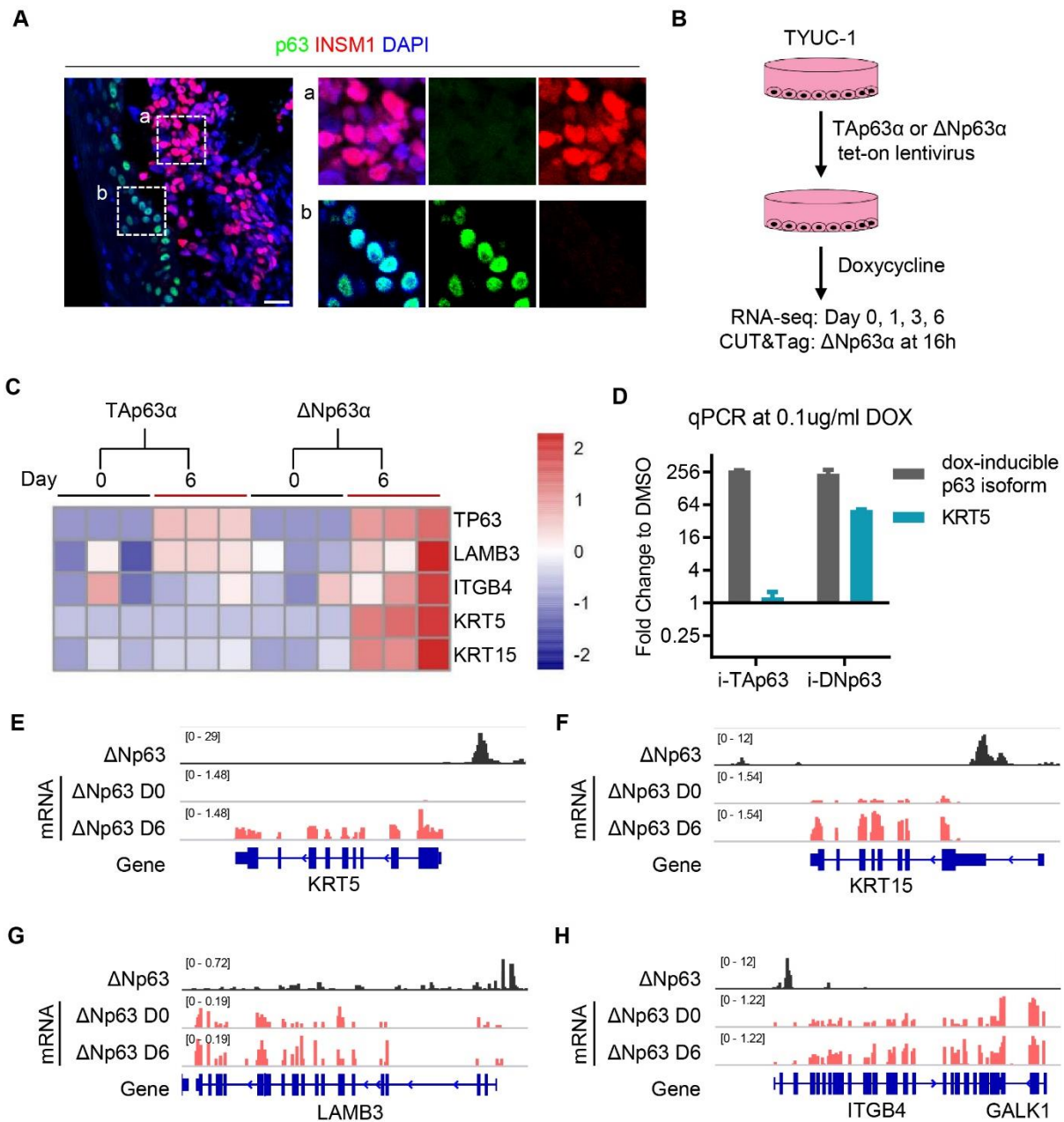
Figure 3.3. ΔNp63 is the major isoform that controls basal identity genes in esophageal neuroendocrine tumor cells. **(A)** p63 and INSM1 staining in human esophageal small cell carcinoma specimen indicating exclusion of the two markers. **(B)** Schematic illustration of ΔNp63α and TAp63α overexpression experiments in TYUC-1. **(C)** Heatmap of the transcript levels of squamous cell markers. Note that KRT5 and KRT15 were only induced by DNp63. **(D)** RT-qPCR of inducible p63 isoforms and KRT5 at a concentration of doxycycline where TAp63 is induced stronger than ΔNp63α. **(E-H)** Tracks of p63 CUT&Tag and RNA-seq upon induction of ΔNp63 expression. Note that Δp63 binds to *LAMB3*, *ITGB4*, *KRT5* and *KRT15*.

(**Figure 3.3D**). Notably, the dominant role of ΔNp63 over TAp63 in the regulation of keratin

gene expression has been reported previously in the context of keratinocyte differentiation.[36]

To determine if ΔNp63α re-expression directly activates squamous gene expression in eNEC

cells, we assessed ΔNp63α genomic distribution using Cleavage Under Targets and

Tagmentation (CUT&Tag) of ΔNp63α in TYUC-1 cells where ΔNp63α expression was induced

for 16 hours. Motif analysis of ΔNp63α peaks indicated expected enrichment for the p63 binding

motif (**Figure 3.S2A**). Peak annotation indicated that the majority of ΔNp63α peaks were found

within gene promoters and introns (**Figure 3.S2B**), consistent with the notion that ΔNp63α

regulates gene expression through binding at *cis*-regulatory elements.[37] Importantly, we found

ΔNp63α peaks close to the promoters of squamous identity genes including *KRT5*, *KRT15*,

ITGB4, and *LAMB3*, suggesting a direct regulation of their expression (**Figures 3.3E-3H and

3.S2A**). Overall, these results indicate that ΔNp63α but not TAp63α is the major isoform that,

upon re-expression, upregulates basal cell identity genes in eNEC cells through directly binding

at their promoters.

3.4.4 ΔNp63 overexpression enforced squamous cell differentiation of eNECs

We further characterized the transcriptomic changes upon ΔNp63α overexpression for 6 days

(**Figure 3.4A**). Differential gene expression analysis indicated that more genes were upregulated

than downregulated (207 vs. 41), suggesting a positive role for ΔNp63α in gene expression

(**Figure 3.4A**). Among the upregulated genes, there was an enrichment in the esophageal

squamous cell signature (**Figures 3.3.4B and 3.S3A**). Notably, we observed an increasing

predominance of squamous identity gene expression over time (**Figure 3.4C**). Among the genes

that were associated with at least one ΔNp63α peak, less than 2% were upregulated

A Differential expression ΔNp63α OE D6 vs D0

Down: 41   Up: 207

TP63
KRT5
KRT15

B Esophageal squamous cell signature

q-value=0.29

ΔNp63 day 6 vs day 0

C Squamous cell signature gene expression

Friedman test *p-value*<0.0001

Day of ΔNp63α induction

D

Genes with ΔNp63α peak
5877

Genes induced by ΔNp63α OE
90   117

E KRT5 p63 DAPI
Control   Dox-ΔNp63α

F KRT15 DAPI
Control   Dox-ΔNp63α

G KRT4 p63 DAPI
Control   Dox-ΔNp63α

H KRT13 p63 DAPI
Control   Dox-ΔNp63α

Figure 4. ΔNp63 reprograms esophageal neuroendocrine tumor cells into basal cells. (A) Volcano plot of differentially expressed genes upon induction of ΔNp63α expression by doxycycline for 6 days. **(B)** GSEA analysis showed that esophageal squamous cell gene signature is positively correlated with ΔNp63 overexpression over time. **(C)** Expression levels of genes of the 'Descartes Fetal Stomach Squamous Epithelial Cells' gene set at 0, 1, 3 and 6 days of doxycycline. **(E-F)** Immunofluorescence staining of p63, KRT5, KRT15, KRT4 and KRT13 in the TYUC-1 tumor organoids with doxycycline-induced overexpression of ΔNp63α (Dox-ΔNp63α) versus the organoids not treated by doxycycline (Control). Scale bars: 20 µm.
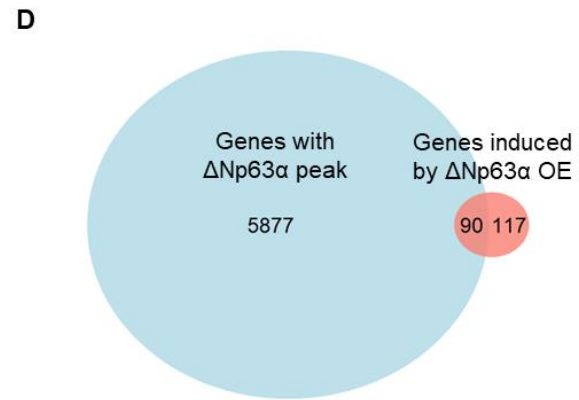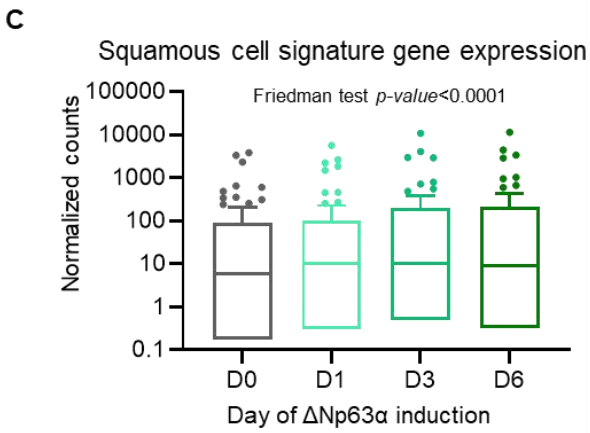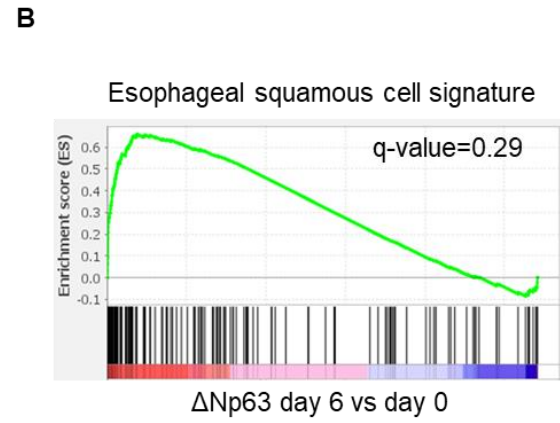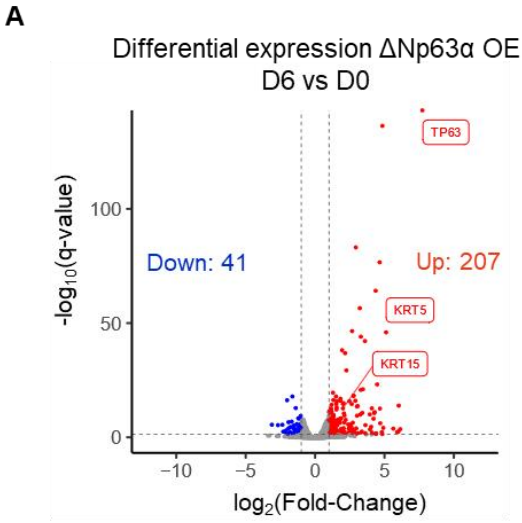
3.4.5 p63 expression is repressed by EZH2-mediated H3K27 methylation in eNECs

Mutational profiling of a large cohort indicated that *p63* is not mutated in eNECs[27]. We therefore asked whether p63 expression is silenced through epigenetic dysregulation. We first tested whether ΔNp63α expression can be modulated epigenetically by screening a panel of chromatin regulator inhibitors in eNEC TYUC-1 cells (**Figures 3.5A and 3.S4A**). Interestingly, we found that inhibiting EZH2, the histone methyltransferase that catalyzes H3K27me3 deposition, with EPZ-6438 induced the highest expression levels of ΔNp63α (**Figure 3.5A**), indicating that H3K27me3 repressed p63 expression. In addition, inhibiting histone deacetylases (HDACs) with either Vorinostat or Romidepsin also increased ΔNp63α expression (**Figure 3.5A**). Conversely, inhibiting histone acetyltransferase p300/CBP and BET proteins, "readers" of histone lysine acetylation, reduced ΔNp63α expression (**Figure 3.5A**). These results suggest that the post-translational modification state of H3K27 (acetylation vs. methylation) has a clear and direct effect on ΔNp63α expression. Consistently, the transcriptional activating effect of EZH2 inhibition (EPZ-6438) on ΔNp63α was abolished by co-treatments with either BET protein (JQ1) or CBP/p300 (A485) inhibitors (**Figure 3.5B**), suggesting that histone acetylation and BET protein binding are required for ΔNp63α expression following H3K27me3 depletion.

A ΔNp63α expression

Drug:	Target:
UNC0638	G9a
Seclidemstat	LSD1
EPZ6438	EZH2
Vorinostat	HDACs
A485	p300/CBP
Romidepsin	Class I HDACs
JQ1	BET proteins
5-Azacytidine	DNMTs
MG149	Tip60/MOF
PRT4165	PRC1 complex
EPZ5676	DOT1L

B ΔNp63α expression

C

D Differential expression EZH2 inhibition D6 vs D0
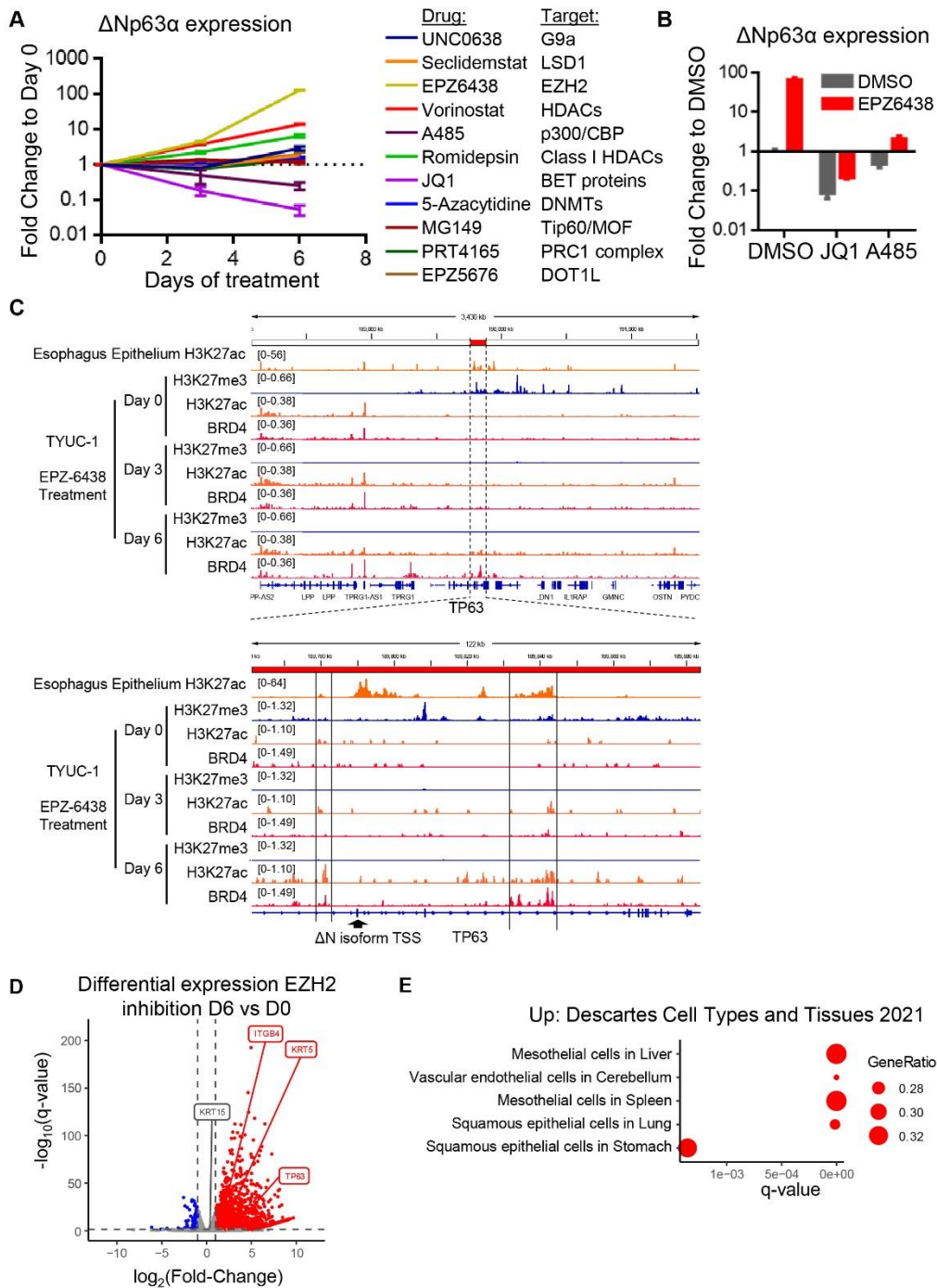
E Up: Descartes Cell Types and Tissues 2021

Figure 3.5. ΔNp63α expression is regulated by methylation and acetylation of H3 lysine 27. (A) The transcript levels of ΔNp63 in TYUC-1 esophageal neuroendocrine tumor cells treated with different epigenetic inhibitors. Note that the EZH2 inhibitor EPZ-6438 increased the expression of ΔNp63 to the highest levels compared to other inhibitors. **(B)** Transcript levels of ΔNp63 in TYUC-1 cells treated with EPZ-6438 or in combination with JQ1 or A485. **(C)** TP63 locus bedgraphs of esophagus epithelium H3K27ac ChIP-seq (ENCODE) and TYUC-1 cell H3K27me3, H3K27ac and BRD4 CUT&Tag upon treatment with EPZ-6438 for 3 and 6 days. Noted are putative enhancer elements near the ΔNp63 isoform TSS where H3K27 methylation is lost, and acetylation is restored. **(D)** Volcano plot of differentially expressed genes upon treatment of TYUC-1 cells treated with DMSO or 2μM EPZ-6438 for 6 days, and "Cell Types And Tissues" gene ontology of upregulated genes **(E)**. TSS: Transcription Start Site

To assess the chromatin landscape following EZH2 inhibition, we performed CUT&Tag of H3K27me3, H3K27ac and BRD4 upon EPZ-6438 treatment (**Figure 3.5C**). We found that in TYUC-1 cells, the *p63* locus was marked by H3K27me3, which, as expected, was lost upon EPZ-6438 treatment (**Figure 3.5C**). Interestingly, EPZ-6438-treated cells gained two peaks of H3K27ac and BRD4 binding at putative intronic enhancers close to the transcription start site (TSS) of ΔNp63 isoforms (**Figure 3.5C**). Notably, re-analysis of ChIP-seq data of esophageal epithelium from ENCODE indicated the presence of H3K27ac peaks at these sites, indicating that they represent physiologically relevant squamous-specific *cis*-regulatory elements associated with p63 expression (**Figure 3.5C**). RNA-seq study revealed that EZH2 inhibition induced the expression of *p63* and downstream squamous cell genes (**Figure 3.5D**), including the basal cell markers KRT5, KRT14, and SOX2 (**Figure 3.S4B**). Furthermore, upregulated genes following EZH2 inhibition were enriched for genes expressed in squamous epithelial cells in various organs (**Figure 3.5E**).

3.4.6 EZH2 inhibition promotes squamous cell commitment in neuroendocrine tumor by derepressing p63 expression.

We next examined whether EZH2 inhibition leads to phenotypic changes of eNEC cells. In 2D cultures of TYUC-1 cells, treatment with the EZH2 inhibitor EPZ-6438 increased the protein expression of p63 as assessed by IF staining analysis (**Figures 3.3.6A-B**). This was accompanied by increased apoptosis, as shown by the accumulation of cleaved caspase-3, as well as decreased cell proliferation (**Figure 3.S5A**). We also employed a 3D organoid culture to further explore the role of the EZH2-p63 axis in regulating eNEC cell fate (**Figure 3.S5C**). Treatment with the EZH2 inhibitor EPZ-6438 repressed both the efficiency and size of eNEC tumor organoid formation (**Figures 3.S5D and 3.S5E**). EZH2 inhibition also promoted the expression of *p63, KRT5,* and *SOX2* (**Figures 3.6C-E**). By contrast, the levels of H3K27me3 and expression of the neuroendocrine cell marker *SYP* were decreased in p63$^+$ cells (**Figures 3.6C and 3.6F**). Overall, p63 was ectopically expressed in 22.7% of organoids upon EZH2 inhibition (**Figure 3.6G**), and in these organoids, 73.6% of cells expressed p63 (**Figure 3.6H**). To rule out potential off-target effects of drug treatment, we used another EZH2 inhibitor, GSK126, and observed consistent reduced organoid formation (1.71 ± 0.06 % vs. 0.84 ± 0.15 %) (**Figure 3.S5F**). Organoids treated with GSK126 also exhibited increased expression of p63 and KRT5 (**Figures 3.S5G and S5H**). Furthermore, we used two independent shRNAs to knockdown EZH2 in TYUC-1 organoids (**Figures 3.S6A and 3.S6B**), and found that EZH2 knockdown consistently led to ectopic p63 and KRT5 expression (**Figure 3.S6C**).

To determine if the neuroendocrine-to-squamous transdifferentiation following EZH2 inhibition is mediated by p63, we used siRNA to knock down ΔNp63 and observed that knockdown of ΔNp63 significantly dampened the upregulation of squamous genes induced by EZH2 inhibition
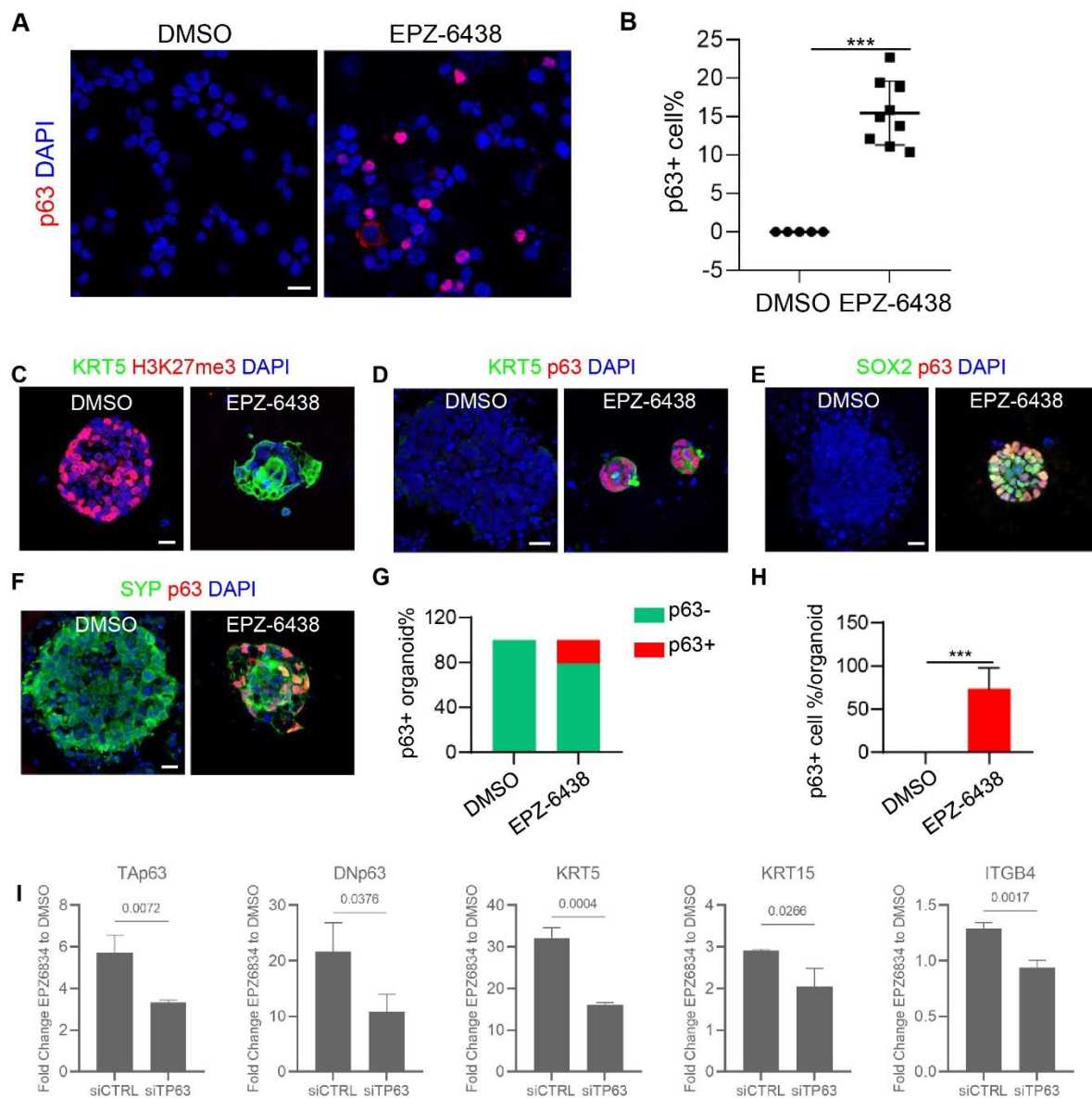
Figure 3.6. EZH2 inhibition in 3D neuroendocrine tumor organoid culture switches on the expression of basal cell markers through ΔNp63. (A-B) Immunofluorescence staining and quantification of p63 cells in EPZ-6438 treated TYUC-1 cells. p63 is expressed in the EPZ-6438 but is absent in DMSO treated group. **(C-F)** IF staining of H3k27me3, basal markers p63 and KRT5, SOX2 and neuroendocrine cell gene SYP in 3D TYUC-1 organoids. **(G-H)** Statistical analysis of p63 positive organoids (G) and p63 positive cells (H) in each organoid. ***p < 0.001. **(I)** Fold change in expression of p63 isoforms and squamous identity genes upon treatment with EPZ6834 and siRNA that either control or target p63α (Student's t-test p-value from 3 replicates is indicated). Scale bars are 20 μm.

(**Figure 3.6I**). *Ezh2* deletion causes the ectopic presence of p63$^+$ basal cells in the murine intrapulmonary airways.[38] We asked whether combined deletion of *p63* and *Ezh2* can reprogram these ectopic basal cells into neuroendocrine cells in *Shh-Cre;Ezh2$^{fx/fx}$;p63$^{fx/fx}$*, i.e. *Ezh2/p63 double knockout* (*DKO*) mice. Intriguingly, we observed an increased number of neuroendocrine cells in the intrapulmonary airways and trachea as compared to *Shh-Cre;Ezh2$^{fx/fx}$* mice (**Figures 3.S6D and 3.S6E**). Together, these results support that Ezh2 inhibits the expression of p63 in both developing lung and eNECs and that this epigenetic regulation of p63 critically governs the transition between squamous and neuroendocrine cell identities.

3.5 Discussion

Here, we showed that *p63* deletion promotes the differentiation of esophageal progenitor cells into neuroendocrine cells in mice. We used the hPSC differentiation system and hPSC-derived 3D organoids to reveal a conserved role of p63 in promoting basal cell differentiation while repressing neuroendocrine cell differentiation. Mechanistically, we showed that ΔNp63α overexpression reprograms neuroendocrine cells in eNEC into basal cells by binding directly to the promoter regions of squamous cell signature genes. Epigenetic inhibitor screening identified EZH2 as an important repressor of p63 by catalyzing H3K27me3 and reducing H3K27ac levels. Lastly, we used 3D tumor organoids to further demonstrate that repressing EZH2 turned on the expression of p63 to transdifferentiate the eNEC cells into basal cells. These results showed that epigenetic regulation of p63 by EZH2 is essential for the transition between basal and neuroendocrine cell fate in both the development and cancer context.

p63 is a master regulator of the esophageal basal cells. Ablation of *p63* leads to the failed conversion of esophageal progenitor cells into basal cells during mouse embryonic

development[12]. However, the cell fate of the esophageal progenitors following p63 deletion remained largely unclear. We harvested E12.5 esophageal epithelium from *p63 KO* mutants and *WT* controls and profiled gene expression by RNA sequencing. Consistently, basal cell genes such as *Krt5, Krt14*, and *Krt15* were reduced. Unexpectedly, we found that a group of neuroendocrine cell signature genes were highly upregulated. We confirmed the presence of neuroendocrine cells in the esophageal epithelium by IF staining of the maturation marker SYP. To determine whether p63 plays a conserved role in the developing human esophagus, we employed our recently developed hPSC differentiation approach.[35] We found that *p63 KO* also leads to increase expression levels of multiple neuroendocrine cell genes, such as neuroendocrine early progenitor transcription factors ASCL1 and INSM1, and maturation markers SYP, CGRP, and CHGA. We further utilized 3D hPSC-derived esophageal organoids to show that the esophageal epithelial cells lose basal cell identity, but a portion of the cells become neuroendocrine cells. These results together showed a conserved role of p63 in promoting basal cell differentiation while repressing neuroendocrine cell differentiation during both murine and human esophageal development.

eNEC is a rare type of esophageal cancer, but eNEC is an aggressive disease with poor diagnosis.[24] It has been reported that NECs can arise from ESCC, which is histologically characterized by high p63 expression basal cells when patients were treated with a combination of chemotherapy and radiotherapy.[9] Therefore, we set out to determine the role of p63 in regulating cell fates in eNECs. We overexpressed two distinctive isoforms of p63, i.e., TAp63 and ΔNp63α in the eNEC patient-derived cell line TYUC-1. The results showed that ΔNp63α highly upregulated basal cell signature genes as compared to TAp63. Further molecular studies revealed that ΔNp63α directly binds to the genomic regions of basal cell genes. We also used 3D

101

tumor organoids and immunostaining analysis to show that ΔNp63α overexpression is sufficient

to convert eNEC cells to basal cells. Hence, the role of p63 in promoting basal cell fates versus

neuroendocrine cells is also conserved in the context of cancer.

Epigenetic inhibitors have been used to study the function of epigenetic regulators in cancer

progression. We performed a small-scale screening with inhibitors of EZH2, HDACs, HAT,

DNMTs, and other epigenetic regulators to determine whether p63 can be turned on in the

context of eNECs. Interestingly, we found that EZH2 inhibition showed the highest upregulation

in p63 transcription levels. EZH2 is the methyltransferase catalytic subunit of PRC2 that

catalyzes H3K27me3. CUT&Tag studies show that EZH2 inhibition reduced H3K27me3 in the

p63 genomic region. There findings indicate that p63 transcription is repressed by EZH2-

mediated H3K37me3. HDAC inhibitors also increased p63 transcription. In contrast, inhibiting

HAT p300/CBP and BETs, readers of histone acetylation, reduced p63 expression, suggesting

that histone acetylation promotes p63 expression. Consistently, we observed upregulation in

acetylation levels and BRD4, a BET family protein, binding on the p63 genomic regions,

supporting that H3K27me3 and H3K27ac play antagonizing roles in regulating p63 transcription.

To further determine the impact of EZH2 on cell fate in eNEC cells. We treated the eNEC tumor

organoids with either inhibitors or shRNA. We found that EZH2 repression and knockdown both

switched on the ectopic expression of p63 and basal cell genes such as KRT4 and SOX2. We

therefore established that the epigenetic regulation of p63 plays an important role in determining

eNEC cell fates.

In summary, using mouse genetic models, we identified an important role of p63 in repressing

the differentiation of esophageal progenitor cells into neuroendocrine cells. hPSC esophageal

differentiation and 3D organoid culture further reveal the conserved function of p63 in

promoting basal cells against neuroendocrine cell fate during human esophageal development.

We further found that p63 is sufficient to transdifferentiate neuroendocrine cells to basal cell fate

in the eNEC. More importantly, we identified that EZH2-mediated H3K27me3 represses the

expression of p63 in eNEC. Inhibition of EZH2 switched on the expression of p63, which further

converted neuroendocrine cells into basal cells. Our findings therefore identify an important

regulatory mechanism for the EZH2-p63 axis in determining basal and neuroendocrine cell fates.

3.7 Experimental procedures

3.7.1 Mice

Shh-Cre[39] and *p63-CreERT2*[40] mice were maintained on a C57BL/6 and 129SvEv mixed

background. We crossed *p63-CreERT2* mice to generate *p63 KO* embryos (*p63-CreERT2*

homozygous). Mice were maintained in the animal facilities of Columbia University under a 12-

hour light/12-hour dark cycle. All animal experiments were conducted according to the

procedures approved by the Columbia University Institutional Animal Care and Use Committee.

3.7.2 Clinical samples

This study was approved by the ethics commissions of the participating hospitals with written

informed consent from the patients.

3.7.3 hPSC culture

p63 KO H9 cell lines were originally generated by Dr. Anthony Oro lab at Stanford University.[41]

H9 hPSC were maintained on mitotically arrested MEF feeder cells on medium: 80 ml of

DMEM/F1, 20 ml of Knockout Serum Replacement, 1 ml of GlutaMAX, 1 ml of MEM non-

essential amino acids solution, 0.7 µl of 2-mercaptoethanol, 0.2 ml of primocin and 20 ng/ml

FGF2. Cells were maintained in an incubator of 5% CO2 at 37°C. Human hPSC research was

conducted under the approval of the Columbia University Human Embryonic and Human

Embryonic Stem Research Committee.

3.7.4 hPSC differentiation into esophageal epithelial cells and organoids

For 2D esophageal differentiation, detailed protocols can be found in our previous studies.[34,35]

Serum free differentiation (SFD) medium was prepared as following: 150 ml of IMDM medium,

50 ml F12, 1.5 ml of 7.5% Bovine Albumin Fraction V Solution, 2 ml of GlutaMAX, 1 ml of

N2, 2 ml of B27, 2 ml of Penicillin/Streptomycin and 50 µg/ml L-Ascorbic acid and 0.04 µl/ml

1-Thioglycerol. hPSCs were differentiated into endodermal spheroids in SFD medium with 100

ng/ml Activin A, 0.5 ng/ml BMP2, 2.5 ng/ml FGF2 and 10 nM Y-27632 for 72 hours in 6-well

low-attachment plates. Endoderm spheroids were disassociated into single cells and replated in

fibronectin-coated 24-well plates and induced into foregut endoderm epithelial cells with 100

ng/ml Noggin and 10 mM SB431542 for 48 hours. To induce esophageal specification cells were

continued to be cultured in 100 ng/ml Noggin and 10 mM SB431542 plus 100 ng/ml EGF for 4

days and 100 ng/ml EGF for another 14 days. Esophageal epithelial cells were then subjected to

IF staining and qRT-PCR analysis. For esophageal organoid establishment, we embedded

endodermal spheroids in Matrigel and cultured the organoids with SFD medium supplemented

with 100 ng/ml Noggin, 10 mM SB431542 and 100 ng/ml EGF until day 53. Organoids were

then harvested for staining analysis.

3.7.5 TYUC1 cell culture and tumor organoid culture

TYUC-1 was originally established from a patient of eNEC.[42] TYUC1 was maintained in DMEM/F12 (Corning) plus 10% serum and 1% penicillin/streptomycin in suspension culture. For tumor organoids established, TYUC1 cells were digested with 0.05% Trypsin-EDTA at 37°C for 15 minutes and disassociated with P1000 pipettes into single cells. 20,000 cells in 100 µl of medium were then mixed with 100 µl of Matrigel (Corning) and added to the 24-well inserts. Matrigel-embedded cells were allowed to solidify in a cell culture incubator of 37°C for 30 minutes before medium was added. The organoid culture medium contains DMEM/F12 supplemented with 10% serum and 1% penicillin/streptomycin. Medium was refreshed every other day. To inhibit EZH2 activity, TYUC-1 cells or organoids were treated with either 2µM EPZ-6438 or 2µM GSK126 with DMSO as vehicle control. When organoids were established, EZH2 inhibitors were added to the medium and maintained until organoids were harvested.

3.7.6 EZH2 shRNA lentivirus generation

To knockdown EZH2 mRNA expression, two shRNAs targeting EZH2 (shEZH2-a: CCGGCCCAACATAGATGGACCAAATCTCGAGATTTGGTCCATCTATGTTGGGTTTTTG and shEZH2-b: CCGG CGGAAATCTTAAACCAAGAATCTCGAGATTCTTGGTTTAAGA TTTCCG TTTTTG) were designed and cloned into pLKO.1 vector (Addgene plasmid #10879) according to method by Moffat, *et al.*[43] The control sequence was CCTAAGGTTAAGTCGCCCTCGCTCGAGCGAGGGCGACTTAACCTTAGG. The constructed plasmids were amplified in *E. coli DH*5α and isolated using Qiagen QIAprep Spin Miniprep Kit (Qiagen) according to the manufacturer's instructions. Lentivirus was produced with with plasmids psPAX2 (Addgene plasmid #12260) and pMD2.G (Addgene plasmid

#12259) in 293T cells. TransIT (Mirus) was used to deliver the plasmids. Suspending TYUC-1 cells were infected with lentivirus. 1 μM polybrene was added to improve the infecting efficiency. Cells were collected 24 hours later and resuspended for organoid culture as mentioned above.

3.7.7 Overexpression of TAp63 and ΔNp63 in TYUC-1 cells

The codon sequence of TAp63 was amplified with high-fidelity Taq polymerase using primers TAp63-EX-F: gaataccggtgcgctgccaccATGAATTTTGAAACTTCACGGTGTGCC and TAp63-EX-R: cgggatccCTCCCCCTCCTCTTTGATGC, while the codon sequence of ΔNp63 with primes ΔNp63-EX-F: gaataccggtctagagctgccaccATGGGCTCCGGCTCCTTGTACCTGGAAAACAATGCC and TAp63-EX-R. PCR products were digested with AgeI and BamHI, and cloned into Tet-on plasmid TLCV2 (Addgene plasmid #87360) digested with same enzymes. Lentivirus was packaged with plasmids psPAX2 and pMD2.G in 293T cells. TYUC-1 cells were infected with lentivirus bearing TAp63 or ΔNp63, with original plasmid as control. Infected cells were maintained in culture medium supplemented with 1 μg/ml puromycin.

3.7.8 Immunostaining

Antigen retrieval on tissue slides were performed using antigen unmasking solution (Vector laboratories #H-3301-250). Cells were fixed with 4% paraformaldehyde in 1xPBS for 10 minutes. Tissues or cells were treated with blocking solution composed of 1xPBS with 3% donkey serum and 0.3% Triton X-100 for 30 minutes. Primary antibodies diluted in blocking solution were added to the top of tissue slides and cells and incubated at 4°C overnight. The next

day, tissues and cells were washed with 1xPBS for 3 times before fluorophore-tagged secondary antibodies were added and incubated at room temperature for 2 hours. Tissues and cells were washed with 1xPBS for 3 times. Tissue slides were mounted with DAPI contained mounting medium (Southern Biotech, #0100-20). Images were taken by Lecia DMi8 (Leica Microsystems) or LSM 700 laser scanning confocal microscope (Carl Zeiss). Representative images were generated by individual scanned images stitched with Leica Application Suite X software (Leica Microsystems) or Zen software (Carl Zeiss).

3.7.9 RNA sequencing

Esophageal epithelium was isolated from E12.5 *p63 KO* (*p63-CreERT2* homozygous) mouse esophagus and the littermates as control. The RNA was purified with PicoPure RNA Isolation Kit (Thermo Fisher Scientific). We determined RNA concentration with 2100 Bio-analyzer (Agilent Technologies). We then used Illumina TruSeq RNA prep kit (Illumina) to establish libraries and sequenced the libraries with Illumina HiSeq400. Samples were multiplexed in each lane, which yields targeted number of single-end/pair-end 100 bp reads for each sample, as a fraction of 180 million reads for the whole lane. RTA (Illumina) was used for base calling and bcl2fastq (version 1.8.4) for converting BCL to fastq format, coupled with adaptor trimming. We mapped the reads to a reference genome (Mouse: UCSC/mm9) using Tophat (version 2.1.0) with 4 mismatches (--read-mismatches = 4) and 10 maximum multiple hits (--max-multihits = 10). The expression levels of each gene were presented as Fragments Per Kilobase of transcript per Million (FPKM) in this study. For RNA-sequencing of TYUC-1 cells, total RNA was extracted in TRIzol (Invitrogen) and precipitated in ethanol (DECON Labs). For RNA-sequencing of doxycycline treated cells for induction of Tap63 and ΔNp63 expression, libraries were prepared

using NEBNext Ultra kit (New England Biolabs #E7490, #E7770, #E7335, #E7500) and sequenced using a Nextseq500/550 sequencer. Paired-end reads were obtained and mapped to the human genome assembly hg38 using HISAT2 (v2.1.0). The mapped reads count of each gene was measured by featureCounts (v1.6.1). For RNA-sequencing of EPZ6438 treated cells, RNA samples were submitted to Columbia University Genome Center for library preparation, sequencing and bioinformatic analysis up to generation of table of reads count of each gene. For both experiments, differential gene expression was calculated by the R package DESeq2 (v1.28.0) and gene set enrichment analysis (GSEA) was performed by using GSEA software (v4.1.0).[44] Visualization was done using the ggplot2 R package.

3.7.10 Quantitative Real-Time Polymerase Chain Reaction (qRT-PCR)

We used TRIzol to lyse cells or tissues and purify the RNA with RNeasy Mini Kit (QIAGEN). Reverse transcription was performed using the SuperScript III First-Strand SuperMix (Invitrogen). cDNA abundance was measured by real-time PCR using the iQ SYBR Green and StepOnePlus Real-Time PCR System (Applied Biosystems). The transcript levels of each gene were normalized to β-actin.

3.7.11 CUT&Tag

CUT&Tag was performed as described previously.[45] In brief, 2×10^5 cells were washed once with 1 ml of wash buffer (20 mM HEPES pH 7.5, 150 mM NaCl, 0.5 mM Spermidine (Sigma-Aldrich), 1x Protease inhibitor cocktail (Roche). Concanavalin A-coated magnetic beads (Bangs Laboratories) were washed twice with binding buffer (20 mM HEPES pH 7.5, 10 mM KCl, 1 mM MnCl2, 1 mM CaCl2). 10 μl/sample of beads were added to cells in 400 μl of wash buffer

and incubated at room temperature for 15 min. Beads-bound cells were resuspended in 100 μl of

antibody buffer (20 mM HEPES pH 7.5, 150 mM NaCl, 0.5 mM Spermidine, 0.06% Digitonin

(Sigma-Aldrich), 2 mM EDTA, 0.1% BSA, 1× Protease inhibitor cocktail and incubated with

H3K27me3 antibody (Cell Signaling Technology #9733), H3K27ac antibody (Active Motif

#39134), BRD4 antibody (Epicypher #13-2003) or normal rabbit IgG (Cell Signaling

Technology, #2729) at 4 °C overnight on nutator. After being washed once with Dig-wash buffer

(20 mM HEPES pH 7.5, 150 mM NaCl, 0.5 mM Spermidine, 0.05% Digitonin, 1x Protease

inhibitor cocktail), beads-bound cells were incubated with 1 μl Guinea pig anti-rabbit secondary

antibody (Antibodies Online ABIN101961) and 2 μl Hyperactive pA-Tn5 Transposase adapter

complex in 100 μl Dig-300 buffer (20 mM HEPES-NaOH, pH 7.5, 0.5 mM Spermidine, 1x

Protease inhibitor cocktail, 300 mM NaCl, 0.01% Digitonin) at room temperature for 1 h. Cells

were washed three times with Dig-300 buffer to remove unbound antibody and Tn5 and then

resuspended in 300 μl of tagmentation buffer (10 mM MgCl2 in Dig-300 buffer) and incubated at

37 °C for 1 h. 10 μl of 0.5 M EDTA, 3 μl of 10% SDS and 5 μl of 10 mg ml−1 Proteinase K were

added to each sample and incubated at 50 °C for 1 h to terminate tagmentation. DNA was

purified using chloroform isoamyl alcohol (Sigma Aldrich) and eluted with 25 μl ddH2O. For

library amplification, 21 μl of DNA was mixed with 2μL i5 unique index primer (10 μM), 2 μL

i7 unique index primer (10 μM) and 25 μL NEBNext® High-Fidelity 2X PCR Master Mix

(NEB) and subjected to the following PCR program: 72 °C, 5 min; 98 °C, 30 sec; 13 cycles of 98

°C, 10 sec and 63 °C, 10 sec; 72 °C, 1 min and hold at 10 °C. To purify the PCR products, 1.1x

volumes of pre-warmed Ampure XP beads (Beckman Coulter) were added and incubated at

room temperature for 10 min. Libraries were washed twice with 80% ethanol and eluted in 20 μl

of 10 mM Tris-HCl, pH 8. Libraries were sequenced on an NextSeq 550 platform (Illumina, 75

cycles High Output Kit v2.0) and 75-bp paired-end reads were generated. For H3K27me3 and

H3K27ac, 2 µl of SNAP-ChIP K-MetStat panel and K-AcylStat panel nucleosomes (EpiCypher)

respectively, were added as spike-in control at the primary antibody incubation step. For

H3K27ac and BRD4 CUT&Tag were initially lightly fixed with 0.1% paraformaldehyde for 5

minutes and neutralized by 125 mM Glycine to preserve target stability.

3.7.12 CUT&Tag data analysis

CUT&Tag reads of TYUC-1 cell samples were mapped to the mouse human assembly hg38

using Bowtie2 (v2.3.5.1, parameters: --local --very-sensitive-local --no-unal --no-mixed --no-

discordant --phred33 -I 10 -X 700). Potential PCR duplicates were removed by the function

"MarkDuplicates" (parameter: REMOVE_DUPLICATES=true) of Picard (v2.24.2). Genomic

enrichments of CUT&Tag signals were generated using deeptools (v3.3.2, parameters

bamCoverage --normalizeUsing CPM --binSize 25 --smoothLength 100 --scaleFactor 1). For

H3K27me3 and H3K27ac the number of reads for each barcode was counted to determine the

scaling factor. Tracks were visualized using IGV.

3.7.13 Chromatin chemical probe screen

For the chromatin chemical probe screening, 5×10^5 TYUC-1 cells were plated and treated with

EPZ6438 (2 µM), SAHA (1 µM), Romidepsin (1 nM), JQ1 (500 nM), Seclidemstat (500 nM),

EPZ5676 (10 µM), UNC0638 (1 µM), A485 (250 nM), MG149 (10 µM), PRT4165(10 µM) or

DMSO. Medium was refreshed every 2 days.

3.7.14 Quantification and statistical analysis

Data was presented as the mean ± SEM using GraphPad Software Prism. Statistical significance

was determined by Student's t test. At least 3 biological replicates were included. P values of

0.05 or less were considered to be statically significant.

3.8 Acknowledgements

3.9 References

1.   Jabbari, M., Goresky, C.A., Lough, J., Yaffe, C., Daly, D., and Cote, C. (1985). The inlet patch: heterotopic gastric mucosa in the upper esophagus. Gastroenterology *89*, 352-356. 10.1016/0016-5085(85)90336-1.
2.   Spechler, S.J., Zeroogian, J.M., Antonioli, D.A., Wang, H.H., and Goyal, R.K. (1994). Prevalence of metaplasia at the gastro-oesophageal junction. Lancet *344*, 1533-1536. 10.1016/s0140-6736(94)90349-2.
3.   Jiang, M., Li, H., Zhang, Y., Yang, Y., Lu, R., Liu, K., Lin, S., Lan, X., Wang, H., Wu, H., et al. (2017). Transitional basal cells at the squamous-columnar junction generate Barrett's oesophagus. Nature *550*, 529-533. 10.1038/nature24269.
4.   Quante, M., Bhagat, G., Abrams, J.A., Marache, F., Good, P., Lee, M.D., Lee, Y., Friedman, R., Asfaha, S., Dubeykovskaya, Z., et al. (2012). Bile acid and inflammation activate gastric cardia stem cells in a mouse model of Barrett-like metaplasia. Cancer Cell *21*, 36-51. 10.1016/j.ccr.2011.12.004.
5.   Braslis, K.G., Davi, R.C., Nelson, E., Civantos, F., and Soloway, M.S. (1995). Squamous cell carcinoma of the prostate: a transformation from adenocarcinoma after the use of a luteinizing hormone-releasing hormone agonist and flutamide. Urology *45*, 329-331. 10.1016/0090-4295(95)80028-x.
6.   Lee, J. (2019). Transformation of adenocarcinoma of prostate to squamous cell carcinoma following hormonal treatment: A case report and review of the literature. Radiol Case Rep *14*, 483-489. 10.1016/j.radcr.2019.01.015.
7.   Zou, M., Toivanen, R., Mitrofanova, A., Floch, N., Hayati, S., Sun, Y., Le Magnen, C., Chester, D., Mostaghel, E.A., Califano, A., et al. (2017). Transdifferentiation as a Mechanism of Treatment Resistance in a Mouse Model of Castration-Resistant Prostate Cancer. Cancer Discov *7*, 736-749. 10.1158/2159-8290.CD-16-1174.

8.   Shia, J., Tickoo, S.K., Guillem, J.G., Qin, J., Nissan, A., Hoos, A., Stojadinovic, A., Ruo, L., Wong, W.D., Paty, P.B., et al. (2002). Increased endocrine cells in treated rectal adenocarcinomas: a possible reflection of endocrine differentiation in tumor cells induced by chemotherapy and radiotherapy. Am J Surg Pathol 26, 863-872. 10.1097/00000478-200207000-00004.

9.   Morita, M., Saeki, H., Nakaji, Y.U., Zaitsu, Y., Hirahashi, M., Ohguri, T., Oki, E., Toh, Y., Oda, Y., and Maehara, Y. (2016). Conversion to Neuroendocrine Carcinoma from Squamous Cell Carcinoma of the Esophagus After Definitive Chemoradiotherapy. Anticancer Res 36, 4045-4049.

10.   Zhang, Y., Bailey, D., Yang, P., Kim, E., and Que, J. (2021). The development and stem cells of the esophagus. Development 148. 10.1242/dev.193839.

11.   Zhang, Y., Jiang, M., Kim, E., Lin, S., Liu, K., Lan, X., and Que, J. (2017). Development and stem cells of the esophagus. Semin Cell Dev Biol 66, 25-35. 10.1016/j.semcdb.2016.12.008.

12.   Daniely, Y., Liao, G., Dixon, D., Linnoila, R.I., Lori, A., Randell, S.H., Oren, M., and Jetten, A.M. (2004). Critical role of p63 in the development of a normal esophageal and tracheobronchial epithelium. Am J Physiol Cell Physiol 287, C171-181. 10.1152/ajpcell.00226.2003.

13.   Rodriguez, P., Da Silva, S., Oxburgh, L., Wang, F., Hogan, B.L., and Que, J. (2010). BMP signaling in the development of the mouse esophagus and forestomach. Development 137, 4171-4176. 10.1242/dev.056077.

14.   Yang, A., Schweitzer, R., Sun, D., Kaghad, M., Walker, N., Bronson, R.T., Tabin, C., Sharpe, A., Caput, D., Crum, C., and McKeon, F. (1999). p63 is essential for regenerative proliferation in limb, craniofacial and epithelial development. Nature 398, 714-718. 10.1038/19539.

15.   Mardaryev, A.N., Liu, B., Rapisarda, V., Poterlowicz, K., Malashchuk, I., Rudolf, J., Sharov, A.A., Jahoda, C.A., Fessing, M.Y., Benitah, S.A., et al. (2016). Cbx4 maintains the epithelial lineage identity and cell proliferation in the developing stratified epithelium. J Cell Biol 212, 77-89. 10.1083/jcb.201506065.

16.   Soares, E., and Zhou, H. (2018). Master regulatory role of p63 in epidermal development and disease. Cell Mol Life Sci 75, 1179-1190. 10.1007/s00018-017-2701-z.

17.   Rinaldi, L., Datta, D., Serrat, J., Morey, L., Solanas, G., Avgustinova, A., Blanco, E., Pons, J.I., Matallanas, D., Von Kriegsheim, A., et al. (2016). Dnmt3a and Dnmt3b Associate with Enhancers to Regulate Human Epidermal Stem Cell Homeostasis. Cell Stem Cell 19, 491-501. 10.1016/j.stem.2016.06.020.

18.   Wang, X., Ouyang, H., Yamamoto, Y., Kumar, P.A., Wei, T.S., Dagher, R., Vincent, M., Lu, X., Bellizzi, A.M., Ho, K.Y., et al. (2011). Residual embryonic cells as precursors of a Barrett's-like metaplasia. Cell 145, 1023-1035. 10.1016/j.cell.2011.05.026.

19.   Kuo, C.S., and Krasnow, M.A. (2015). Formation of a Neurosensory Organ by Epithelial Cell Slithering. Cell 163, 394-405. 10.1016/j.cell.2015.09.021.

20.   Sui, P., Wiesner, D.L., Xu, J., Zhang, Y., Lee, J., Van Dyken, S., Lashua, A., Yu, C., Klein, B.S., Locksley, R.M., et al. (2018). Pulmonary neuroendocrine cells amplify allergic asthma responses. Science 360. 10.1126/science.aan8546.

21.   Sinagoga, K.L., McCauley, H.A., Munera, J.O., Reynolds, N.A., Enriquez, J.R., Watson, C., Yang, H.C., Helmrath, M.A., and Wells, J.M. (2018). Deriving functional human enteroendocrine cells from pluripotent stem cells. Development 145. 10.1242/dev.165795.

22.   Branchfield, K., Nantie, L., Verheyden, J.M., Sui, P., Wienhold, M.D., and Sun, X. (2016). Pulmonary neuroendocrine cells function as airway sensors to control lung immune response. Science *351*, 707-710. 10.1126/science.aad7969.

23.   Law, S.Y., Fok, M., Lam, K.Y., Loke, S.L., Ma, L.T., and Wong, J. (1994). Small cell carcinoma of the esophagus. Cancer *73*, 2894-2899. 10.1002/1097-0142(19940615)73:12<2894::aid-cncr2820731204>3.0.co;2-m.

24.   Yun, J.P., Zhang, M.F., Hou, J.H., Tian, Q.H., Fu, J., Liang, X.M., Wu, Q.L., and Rong, T.H. (2007). Primary small cell carcinoma of the esophagus: clinicopathological and immunohistochemical features of 21 cases. BMC Cancer *7*, 38. 10.1186/1471-2407-7-38.

25.   van Meerbeeck, J.P., Fennell, D.A., and De Ruysscher, D.K. (2011). Small-cell lung cancer. Lancet *378*, 1741-1755. 10.1016/S0140-6736(11)60165-7.

26.   Egashira, A., Morita, M., Kumagai, R., Taguchi, K.I., Ueda, M., Yamaguchi, S., Yamamoto, M., Minami, K., Ikeda, Y., and Toh, Y. (2017). Neuroendocrine carcinoma of the esophagus: Clinicopathological and immunohistochemical features of 14 cases. PLoS One *12*, e0173501. 10.1371/journal.pone.0173501.

27.   Li, R., Yang, Z., Shao, F., Cheng, H., Wen, Y., Sun, S., Guo, W., Li, Z., Zhang, F., Xue, L., et al. (2021). Multi-omics profiling of primary small cell carcinoma of the esophagus reveals RB1 disruption and additional molecular subtypes. Nat Commun *12*, 3785. 10.1038/s41467-021-24043-6.

28.   Sparmann, A., and van Lohuizen, M. (2006). Polycomb silencers control cell fate, development and cancer. Nat Rev Cancer *6*, 846-856. 10.1038/nrc1991.

29.   Kass, S.U., Pruss, D., and Wolffe, A.P. (1997). How does DNA methylation repress transcription? Trends Genet *13*, 444-449. 10.1016/s0168-9525(97)01268-7.

30.   Wang, Z., Zang, C., Cui, K., Schones, D.E., Barski, A., Peng, W., and Zhao, K. (2009). Genome-wide mapping of HATs and HDACs reveals distinct functions in active and inactive genes. Cell *138*, 1019-1031. 10.1016/j.cell.2009.06.049.

31.   Struhl, K. (1998). Histone acetylation and transcriptional regulatory mechanisms. Genes Dev *12*, 599-606. 10.1101/gad.12.5.599.

32.   Shi, J., and Vakoc, C.R. (2014). The mechanisms behind the therapeutic activity of BET bromodomain inhibition. Mol Cell *54*, 728-736. 10.1016/j.molcel.2014.05.016.

33.   Creyghton, M.P., Cheng, A.W., Welstead, G.G., Kooistra, T., Carey, B.W., Steine, E.J., Hanna, J., Lodato, M.A., Frampton, G.M., Sharp, P.A., et al. (2010). Histone H3K27ac separates active from poised enhancers and predicts developmental state. Proc Natl Acad Sci U S A *107*, 21931-21936. 10.1073/pnas.1016071107.

34.   Bailey, D.D., Zhang, Y., van Soldt, B.J., Jiang, M., Suresh, S., Nakagawa, H., Rustgi, A.K., Aceves, S.S., Cardoso, W.V., and Que, J. (2019). Use of hPSC-derived 3D organoids and mouse genetics to define the roles of YAP in the development of the esophagus. Development *146*. 10.1242/dev.178855.

35.   Zhang, Y., Yang, Y., Jiang, M., Huang, S.X., Zhang, W., Al Alam, D., Danopoulos, S., Mori, M., Chen, Y.W., Balasubramanian, R., et al. (2018). 3D Modeling of Esophageal Development using Human PSC-Derived Basal Progenitors Reveals a Critical Role for Notch Signaling. Cell Stem Cell *23*, 516-529 e515. 10.1016/j.stem.2018.08.009.

36.   Truong, A.B., Kretz, M., Ridky, T.W., Kimmel, R., and Khavari, P.A. (2006). p63 regulates proliferation and differentiation of developmentally mature keratinocytes. Genes Dev *20*, 3185-3197. 10.1101/gad.1463206.

37.   Kouwenhoven, E.N., Oti, M., Niehues, H., van Heeringen, S.J., Schalkwijk, J., Stunnenberg, H.G., van Bokhoven, H., and Zhou, H. (2015). Transcription factor p63 bookmarks and regulates dynamic enhancers during epidermal differentiation. EMBO Rep *16*, 863-878. 10.15252/embr.201439941.

38.   Snitow, M.E., Li, S., Morley, M.P., Rathi, K., Lu, M.M., Kadzik, R.S., Stewart, K.M., and Morrisey, E.E. (2015). Ezh2 represses the basal cell lineage during lung endoderm development. Development *142*, 108-117. 10.1242/dev.116947.

39.   Harfe, B.D., Scherz, P.J., Nissim, S., Tian, H., McMahon, A.P., and Tabin, C.J. (2004). Evidence for an expansion-based temporal Shh gradient in specifying vertebrate digit identities. Cell *118*, 517-528. 10.1016/j.cell.2004.07.024.

40.   Lee, D.K., Liu, Y., Liao, L., Wang, F., and Xu, J. (2014). The prostate basal cell (BC) heterogeneity and the p63-positive BC differentiation spectrum in mice. Int J Biol Sci *10*, 1007-1017. 10.7150/ijbs.9997.

41.   Pattison, J.M., Melo, S.P., Piekos, S.N., Torkelson, J.L., Bashkirova, E., Mumbach, M.R., Rajasingh, C., Zhen, H.H., Li, L., Liaw, E., et al. (2018). Retinoic acid and BMP4 cooperate with p63 to alter chromatin dynamics during surface epithelial commitment. Nat Genet *50*, 1658-1665. 10.1038/s41588-018-0263-0.

42.   Okumura, T., Shimada, Y., Omura, T., Hirano, K., Nagata, T., and Tsukada, K. (2015). MicroRNA profiles to predict postoperative prognosis in patients with small cell carcinoma of the esophagus. Anticancer Res *35*, 719-727.

43.   Moffat, J., Grueneberg, D.A., Yang, X., Kim, S.Y., Kloepfer, A.M., Hinkle, G., Piqani, B., Eisenhaure, T.M., Luo, B., Grenier, J.K., et al. (2006). A lentiviral RNAi library for human and mouse genes applied to an arrayed viral high-content screen. Cell *124*, 1283-1298. 10.1016/j.cell.2006.01.040.

44.   Subramanian, A., Tamayo, P., Mootha, V.K., Mukherjee, S., Ebert, B.L., Gillette, M.A., Paulovich, A., Pomeroy, S.L., Golub, T.R., Lander, E.S., and Mesirov, J.P. (2005). Gene set enrichment analysis: a knowledge-based approach for interpreting genome-wide expression profiles. Proc Natl Acad Sci U S A *102*, 15545-15550. 10.1073/pnas.0506580102.

45.   Kaya-Okur, H.S., Wu, S.J., Codomo, C.A., Pledger, E.S., Bryson, T.D., Henikoff, J.G., Ahmad, K., and Henikoff, S. (2019). CUT&Tag for efficient epigenomic profiling of small samples and single cells. Nat Commun *10*, 1930. 10.1038/s41467-019-09982-5.
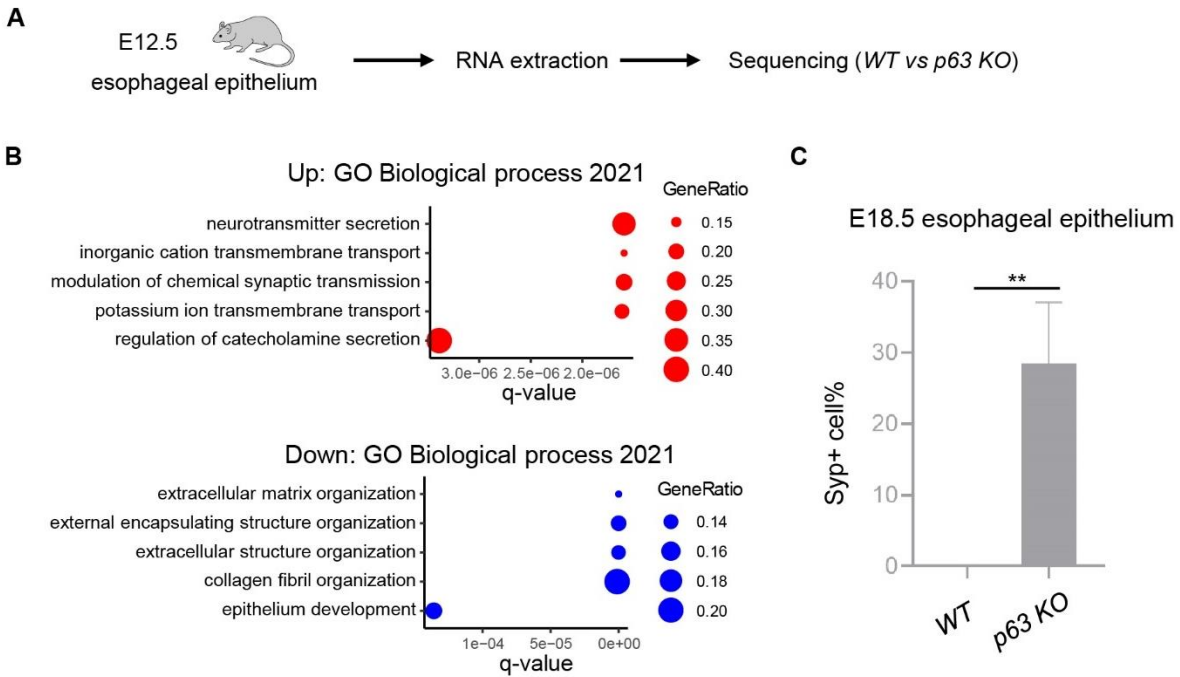
3.10 Supplementary Figures

A

E12.5
esophageal epithelium → RNA extraction → Sequencing (*WT vs p63 KO*)

B

Up: GO Biological process 2021

Down: GO Biological process 2021

C

E18.5 esophageal epithelium

Figure 3.S1. Related to Figure 1. (**A**) Schematics to show isolating esophageal epithelium from the WT and p63KO mice and extract RNA for sequencing. (**B**) Biological process gene ontology of genes upregulated(red) and downregulated (blue) in p63KO esophageal epithelium. (**C**) Quantitation of Syp- positive cells in E18.5 esophageal epithelium. **p < 0.01.

A

HOMER known motif analysis of ΔNp63α peaks

| Rank	Motif	Name	P-value	log P-pvalue	q-value (Benjamini)	# Target Sequences with Motif
1		p63(p53)/Keratinocyte-p63-ChIP-Seq(GSE17611)/Homer	1e-1886	-4.345e+03	0.0000	3435.0
2		p53(p53)/Saos-p53-ChIP-Seq(GSE15780)/Homer	1e-809	-1.865e+03	0.0000	1219.0
3		p53(p53)/Saos-p53-ChIP-Seq/Homer	1e-809	-1.865e+03	0.0000	1219.0
4		p73(p53)/Trachea-p73-ChIP-Seq(PRJNA310161)/Homer	1e-557	-1.283e+03	0.0000	764.0
5		Tcfcp2l1(CP2)/mES-Tcfcp2l1-ChIP-Seq(GSE11431)/Homer	1e-164	-3.799e+02	0.0000	627.0

B
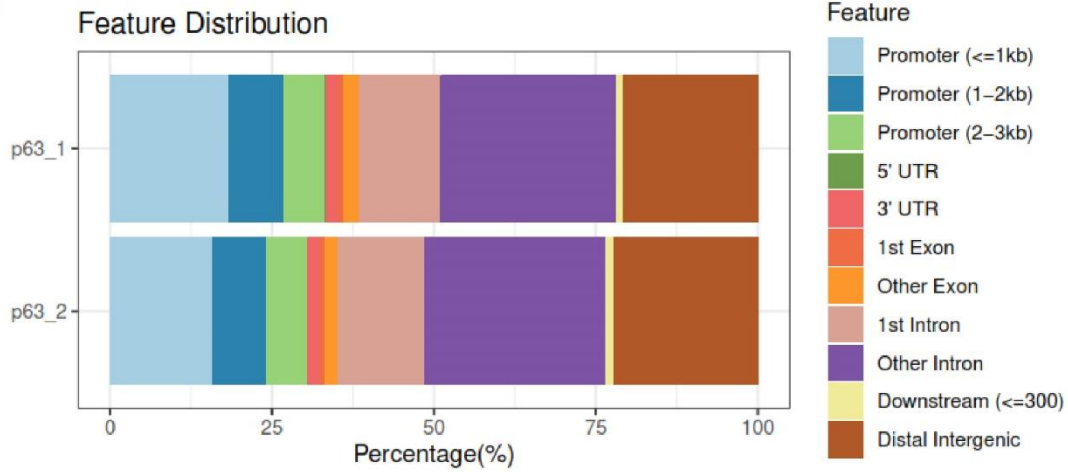
Figure 3.S2. Related to figure 3.3. (**A**) Homer known motif analysis of called peaks of p63α CUT&Tag upon induction of ΔNp63α and distribution across genomic features (**B**; two replicates shown).
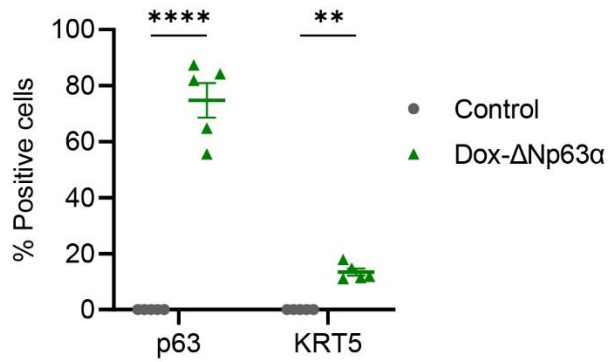
A
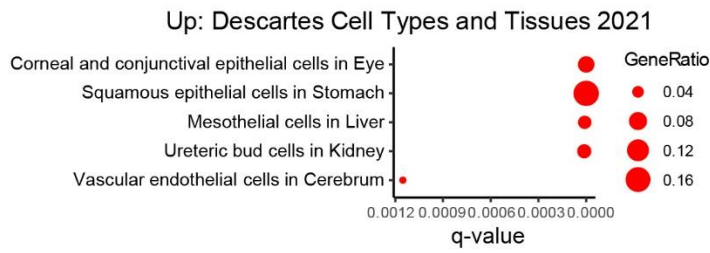
B

Figure 3.S3. Related to figure 3.4. (**A**) "Cell Types And Tissues" gene ontology of upregulated genes in TYUC-1 cells upon induction of ΔNp63α expression by doxycycline for 6 days. (**B**) Quantitation of p63 and KRT5 positive cells upon iinduction of ΔNp63α expression by doxycycline for 6 days – related to Figure 3.4E.
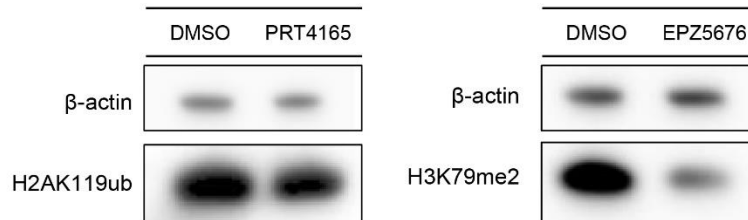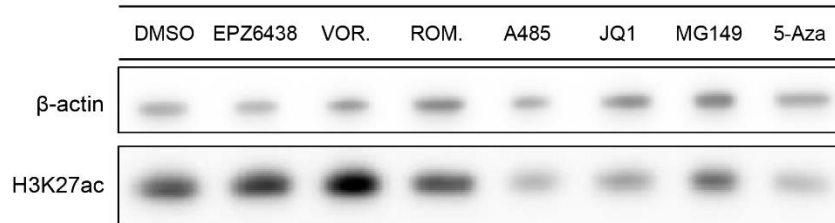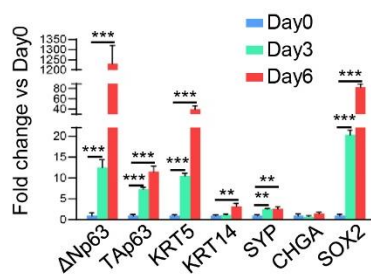
A

B

Figure 3.S4. Related to figure 3.5. (**A**) Western blots indicating levels of histone modifications upon treatment with inhibitors of chromatin regulators. (**B**) The transcript levels of basal cell markers ΔNp63, TAp63, KRT5, KRT4, SOX2 and neuroendocrine cell markers SYP and CHGA. **p < 0.01, ***p < 0.001.
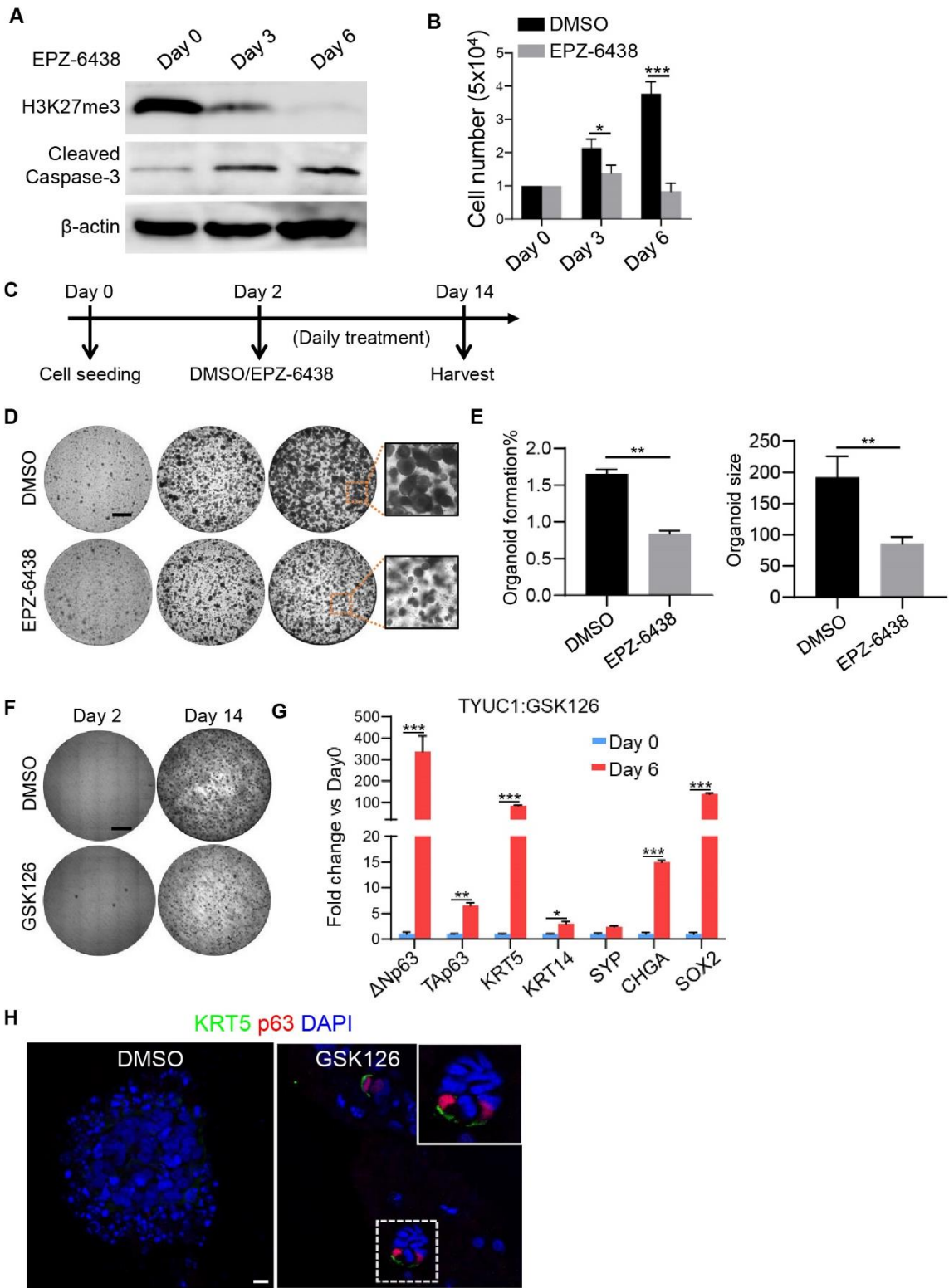
-low

119

Figure 3.S5. Related to figure 3.6. (A) Western blot indicating the protein levels of H3K27me3 and Cleaved Caspase-3 in TYUC-1 treated with EPZ-6438 for 3 or 6 days. The protein levels were determined by immunoblotting. **(B)** TYUC-1 cell numbers are significantly reduced with EPZ-6438 treatment for 3 or 6 days. $*p < 0.05$, $***p < 0.001$. **(C)** Schematics to show 3D culture of TYUC-1 cell in Matrigel. Organoids were treated with either DMSO or 2μM EPZ-6438 and sampled at day 14. **(D)** Bright images of TYUC-1 organoids treated with either DMSO or EPZ-6438. **(E)** Statistical analysis of TYUC-1 organoid formation efficiency and sizes. $**p < 0.01$ **(F)** Bright images of TYUC-1 organoids treated with DMSO or EZH2 inhibitor GSK126. **(G)** Transcript levels of genes in TYUC-1 cells treated with EZH2 inhibitor GSK126 for 6 days. $*p < 0.05$, $**p < 0.01$, $***p < 0.001$. **(H)** IF staining images TYUC-1 organoids treated with either DMSO or GSK126. Scale bars in (D) & (F) are 1 mm, and in (H), 20 μm.
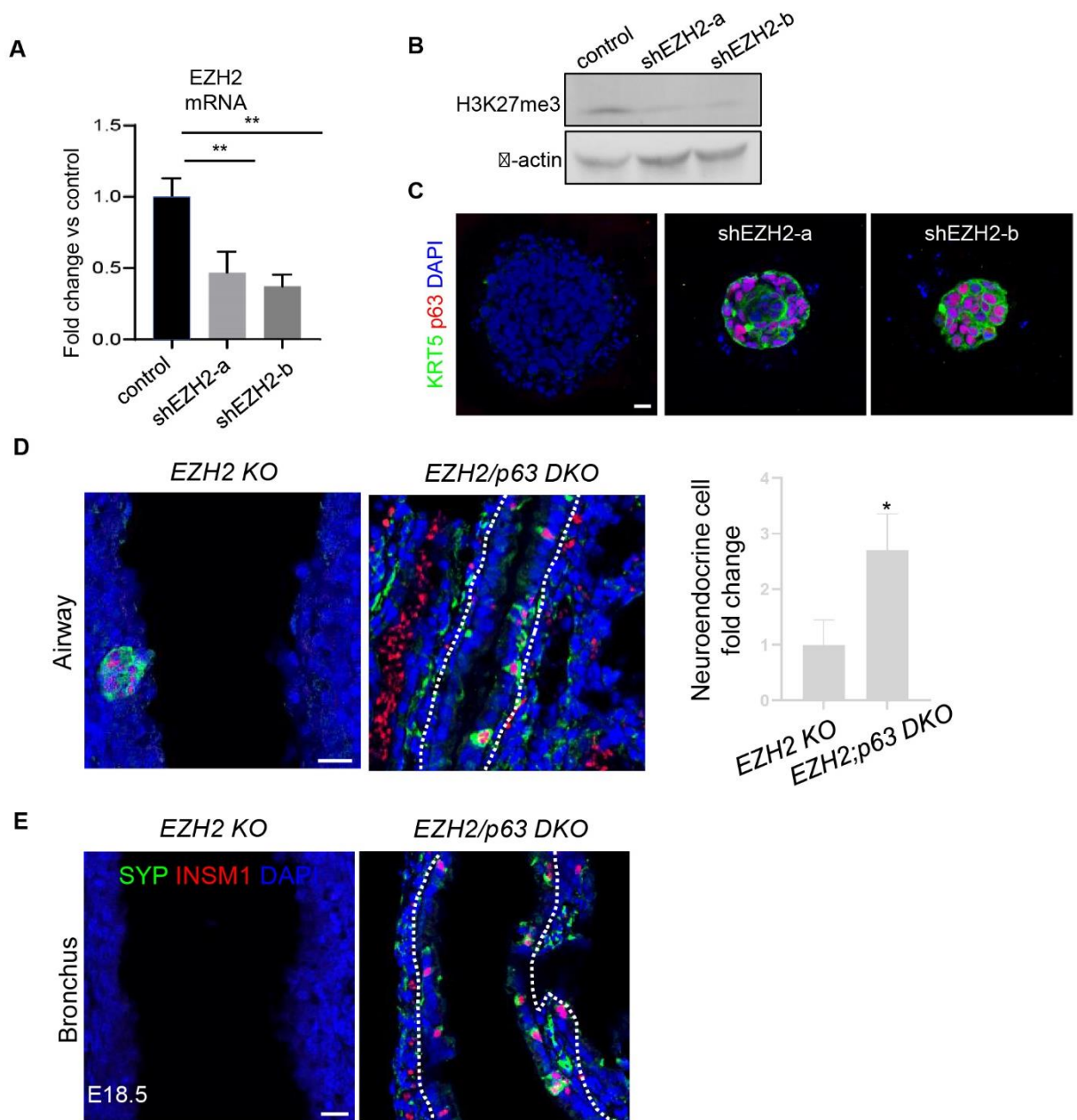
Figure 3.S6. Related to figure 3.6. (A) EZH2 transcript levels in TYUC-1 cells infected with lentivirus containing EZH2 shRNAs (shEZH2-a and shEZH2-b). ****p < 0.01. (B)** Protein levels of H3K27me3 decreased in TYUC-1 cells infected with EZH2 shRNAs. **(C)** IF staining of p63 and KRT5 in TYUC-1 organoids infected with EZH2 shRNAs. **(D-E)** Increased neuroendocrine cell differentiation in the airway (E) and bronchus (E) in Ezh2/p63 DKO mice compared to Ezh2 KO mice. *WT: Wildtype, EZH2 KO: Shh-Cre;Ezh2$^{loxp/loxp}$, EZH2/p63 DKO: Shh-Cre;Ezh2$^{loxp/loxp}$;p63$^{loxp/loxp}$.* Scale bars: 20 μm.

Conclusion

Precision oncology, the practice of identifying targetable alterations in cancer by molecular profiling to administer personalized treatment, is expanding ever more rapidly through the advancements in technology and biological understanding[1]. Study of chromatin in the context of targeted cancer therapy offers several advantages. Firstly, modulation of chromatin regulation can have multifaceted results, which can limit mechanisms of resistance. Secondly, there are currently several FDA-approved agents that target chromatin and are used for cancer treatment that can be repurposed. Thirdly, due to the complexity of chromatin regulatory processes there is space to deepen our knowledge and discover new therapeutic approaches.

In this dissertation, I explored the therapeutic potential of targeting chromatin in two specific cancer settings: metabolic reprogramming in LUAD with NRF2 activation and altered cell identity in NEC. Previous studies have shown that targeting chromatin in metabolically altered cancer can be beneficial for therapy. For example, HDAC inhibitor-mediated metabolic reprogramming reduced the growth of glioblastoma tumors and had a synergistic effect with inhibition of fatty acid oxidation[2]. In lung adenocarcinoma with *KRAS* mutation, tumors were sensitive to metabolic reprogramming induced by dual inhibition of the histone demethylases JMJD3 and UTX[3]. Similarly, chromatin-mediated targeting of cell identity has shown therapeutic efficacy in preclinical cancer settings. In pancreatic adenocarcinoma, BET protein inhibition decreased the expression of dedifferentiation markers and suppressed tumor growth[4]. In N-Myc driven neuroendocrine prostate cancer, downregulation of androgen-receptor (AR) signaling and increased tumor growth was suppressed by EZH2 inhibition[5]. My findings highlight new interactions of chromatin regulation with metabolism and cell identity that are relevant for cancer treatment.

The studies presented in my dissertation contribute to precision oncology in several aspects. Firstly, these two examples serve as proof of principle that precise targeting of regulatory processes of chromatin can be utilized to modulate specific gene expression programs and subsequently cellular processes. Specifically, we found that inhibition of histone deacetylation can result in rewiring of cellular metabolism and that inhibition of histone 3 lysine 27 methylation can result in de-repression of squamous cell identity. Modulation of metabolism and cell identity is an important element of many indirect and/or combinatorial therapeutic approaches, such as cancer cell differentiation therapy[6], sensitization of drug resistant tumors[7–9], and targeting of tumor-promoting cells of the tumor microenvironment[10]. Therefore, future studies can investigate the applicability of these findings in several therapeutic contexts.

Secondly, these studies reveal new insights into how remodeling of global chromatin landscape can impact expression of specific genes. In the LUAD study we found that global distribution of histone acetylation has a local and unexpected effect on the expression levels of genes that require high concentration of histone acetylation marks and readers at their promoters at basal state. These findings highlight how modulation of global histone modifications with pharmacologic means can be utilized to induce targeted gene expression changes for therapeutic benefit. Future studies could further investigate the influence of initial chromatin state on the outcome of epigenetic perturbation on gene expression. Improving our understanding of these mechanisms can overcome the challenge of therapeutic outcome prediction[11].

Finally, these studies highlight the potential for repurposing FDA-approved epigenetic drugs with rational biomarker-driven patient stratification. In LUAD, we show that Kras-active/p53-mutant tumors with NRF2 activation, such as by the frequently occurring *KEAP1* mutations, are more sensitive to HDAC inhibition by the FDA-approved drug Romidepsin. In

NEC, we show that the FDA-approved EZH2 inhibitor Tazemetostat can influence cancer cell lineage plasticity. Notably, further studies are needed to test the molecular background requirements of our findings. Specifically, Kras activation in LUAD has been associated with sensitivity to Romidepsin[12], which suggests that the Kras-active background is likely important for its efficacy in NRF2-active tumors. In NEC, study of additional cell lines with diverse NEC molecular subtypes would clarify whether there are any requirements for squamous identity restoration. Furthermore, it is not clear from these results if treatment with these agents alone would be sufficient for significant therapeutic benefit in patients, so future studies should consider alternative cancer models including orthotopic xenograft models and assessment of survival outcomes, combinatorial treatments such as glutaminase inhibition, and regimen optimization. In addition, these findings can be informative for future studies of epigenetic drugs in other cancer contexts with alterations in metabolism or cell fate.

Specifically, one future direction would be to assess efficacy of HDAC inhibitors in other NRF2-active cancers, such as *KEAP1/NRF2*-mutant squamous cell carcinomas of the lung[13] and head and neck[14], as well as pancreatic cancer[15,16]. Furthermore, HDAC inhibition could be effective in other contexts of metabolic reprogramming such as cancers with *KRAS* mutation[17] or c-Myc amplification[18,19]. Interestingly, cancer cells with such alterations have been reported to depend on glutamine for growth and survival[19,20], including in pancreatic cancer[21] and glioma[22,23]. On the other hand, epigenetic drugs that modulate p63 expression, such as EZH2, HDAC and BET inhibitors, could be utilized in cancers with aberrant gain or loss of squamous cell identity, such as squamous transdifferentiation in the pancreas and lung[24–26] and squamous-derived small cell cancer[27,28], respectively.

Overall, the purpose of this work is to demonstrate the value in targeting chromatin regulation for cancer treatment. Our findings contribute to our understanding of histone acetylation and methylation dynamics in the context of cancer metabolism and cell identity with epigenetic drugs and aim to set the basis for future studies on epigenetic therapy. Importantly, my work collectively suggests that beyond genetic alterations, the metabolic state and lineage identity of tumor cells can serve as robust biomarkers for guiding the application of epigenetic inhibitors.

References

1. Schwartzberg, L., Kim, E. S., Liu, D. & Schrag, D. Precision Oncology: Who, How, What, When, and When Not? *American Society of Clinical Oncology Educational Book* 160–169 (2017) doi:10.1200/EDBK_174176.
2. Nguyen, T. T. T. *et al.* HDAC inhibitors elicit metabolic reprogramming by targeting super-enhancers in glioblastoma models. *J Clin Invest* **130**, 3699–3716 (2020).
3. Hong, B.-J. *et al.* Oncogenic KRAS Sensitizes Lung Adenocarcinoma to GSK-J4–Induced Metabolic and Oxidative Stress. *Cancer Research* **79**, 5849–5859 (2019).
4. Roy, N. *et al.* Brg1 promotes both tumor-suppressive and oncogenic activities at distinct stages of pancreatic cancer formation. *Genes Dev.* **29**, 658–671 (2015).
5. Dardenne, E. *et al.* N-Myc Induces an EZH2-Mediated Transcriptional Program Driving Neuroendocrine Prostate Cancer. *Cancer Cell* **30**, 563–577 (2016).
6. Enane, F. O., Saunthararajah, Y. & Korc, M. Differentiation therapy and the mechanisms that terminate cancer cell proliferation without harming normal cells. *Cell Death Dis* **9**, 1–15 (2018).
7. Leary, M., Heerboth, S., Lapinska, K. & Sarkar, S. Sensitization of Drug Resistant Cancer Cells: A Matter of Combination Therapy. *Cancers (Basel)* **10**, 483 (2018).
8. Chen, X., Chen, S. & Yu, D. Metabolic Reprogramming of Chemoresistant Cancer Cells and the Potential Significance of Metabolic Regulation in the Reversal of Cancer Chemoresistance. *Metabolites* **10**, 289 (2020).
9. Boumahdi, S. & de Sauvage, F. J. The great escape: tumour cell plasticity in resistance to targeted therapy. *Nat Rev Drug Discov* **19**, 39–56 (2020).
10. Bejarano, L., Jordāo, M. J. C. & Joyce, J. A. Therapeutic Targeting of the Tumor Microenvironment. *Cancer Discovery* **11**, 933–959 (2021).
11. Berchialla, P., Lanera, C., Sciannameo, V., Gregori, D. & Baldi, I. Prediction of treatment outcome in clinical trials under a personalized medicine perspective. *Sci Rep* **12**, 4115 (2022).

12. Basseville, A. *et al.* A Histone Deacetylase Inhibitor Induces Acetyl-CoA Depletion Leading to Lethal Metabolic Stress in RAS-Pathway Activated Cells. *Cancers (Basel)* **14**, 2643 (2022).

13. Hammerman, P. S. *et al.* Comprehensive genomic characterization of squamous cell lung cancers. *Nature* **489**, 519–525 (2012).

14. Lawrence, M. S. *et al.* Comprehensive genomic characterization of head and neck squamous cell carcinomas. *Nature* **517**, 576–582 (2015).

15. Lister, A. *et al.* Nrf2 is overexpressed in pancreatic cancer: implications for cell proliferation and therapy. *Mol Cancer* **10**, 37 (2011).

16. Chio, I. I. C. *et al.* NRF2 Promotes Tumor Maintenance by Modulating mRNA Translation in Pancreatic Cancer. *Cell* **166**, 963–976 (2016).

17. Pupo, E., Avanzato, D., Middonti, E., Bussolino, F. & Lanzetti, L. KRAS-Driven Metabolic Rewiring Reveals Novel Actionable Targets in Cancer. *Front Oncol* **9**, 848 (2019).

18. Miller, D. M., Thomas, S. D., Islam, A., Muench, D. & Sedoris, K. c-Myc and Cancer Metabolism. *Clin Cancer Res* **18**, 5546–5553 (2012).

19. Dong, Y., Tu, R., Liu, H. & Qing, G. Regulation of cancer cell metabolism: oncogenic MYC in the driver's seat. *Sig Transduct Target Ther* **5**, 1–11 (2020).

20. Bernfeld, E. & Foster, D. A. Glutamine as an Essential Amino Acid for KRas-Driven Cancer Cells. *Trends in Endocrinology & Metabolism* **30**, 357–368 (2019).

21. Dash, S. *et al.* MYC/Glutamine Dependency Is a Therapeutic Vulnerability in Pancreatic Cancer with Deoxycytidine Kinase Inactivation-Induced Gemcitabine Resistance. *Molecular Cancer Research* **21**, 444–457 (2023).

22. Qing, G. *et al.* ATF4 regulates MYC-mediated neuroblastoma cell death upon glutamine deprivation. *Cancer Cell* **22**, 631–644 (2012).

23. Wise, D. R. *et al.* Myc regulates a transcriptional program that stimulates mitochondrial glutaminolysis and leads to glutamine addiction. *Proceedings of the National Academy of Sciences* **105**, 18782–18787 (2008).

24. Somerville, T. D. *et al.* Squamous trans-differentiation of pancreatic cancer cells promotes stromal inflammation. *eLife* **9**, e53381 (2020).

25. Han, X. *et al.* Transdifferentiation of lung adenocarcinoma in mice with Lkb1 deficiency to squamous cell carcinoma. *Nat Commun* **5**, 3261 (2014).

26. Hamdan, F. H. & Johnsen, S. A. DeltaNp63-dependent super enhancers define molecular identity in pancreatic cancer by an interconnected transcription factor network. *Proceedings of the National Academy of Sciences* **115**, E12343–E12352 (2018).

27. Kervarrec, T. *et al.* Merkel Cell Polyomavirus–Negative Merkel Cell Carcinoma Originating from In Situ Squamous Cell Carcinoma: A Keratinocytic Tumor with Neuroendocrine Differentiation. *Journal of Investigative Dermatology* **142**, 516–527 (2022).

28. Travis, W. D. Update on small cell carcinoma and its differentiation from squamous cell carcinoma and other non-small cell carcinomas. *Mod Pathol* **25**, S18–S30 (2012).